TÉCNICO LISBOA

Numerical simulation of Al_2O_3-isopropanol nanofluid flows in tubes of circular cross-section

Pedro Samuel Carvalho Romão

Thesis to obtain the Master of Science Degree in

Mechanical Engineering

Supervisor: Prof. Pedro Jorge Martins Coelho

Examination Committee

Chairperson: Prof. Carlos Frederico Neves Bettencourt da Silva
Supervisor: Prof. Pedro Jorge Martins Coelho
Member of the Committee: Prof. Sohel Murshed

July 2019

To my beloved parents,
for their unconditional love and support...

Acknowledgments

My first words are dedicated to Professor Pedro Coelho. For his guidance during the realization of this thesis, for all the knowledge shared without reservations, for all the clarifications, suggestions and patience, my deepest gratitude.

I also would like to express a word of thanks to Professor António Moreira and Doctor Artem Nikulin, from IN+, for all the experimental data kindly provided and for giving me the opportunity to have been in the laboratory understanding in more detail the experimental apparatus.

To my esteemed friends Rafael Lucas and Miguel Bigares, with whom I have shared many of my best moments throughout this journey at Técnico, for all the advices, brainstorms, simple chats and for the great memories that remain from these years that made possible the creation of this true friendship, a huge thanks! It was really a pleasure to have you by my side during these years, but is even better to know that our friendship will continue like that in the times to come.

To my parents, humble and honorable people who raised me the best way they could and passed me every single value that made me a better person today.

To my family, who demonstrated a continuous love and genuine interest during my whole life and education, and for whom I nourish a great consideration and affection.

To my closest friends, ”the family we chose”, for receiving me in their lives and for the entire collection of great moments and memories that I could experience alongside them during this time.

And to my dear Daniela, for her patience, continuous support and love, but principally for never giving up on me when I most needed her.

Several years ago, a friend told me that ”a man is not an island”. Thank you all for showing me the real meaning of that.

Resumo

O desenvolvimento de nova tecnologia de ponta com necessidades de arrefecimento acrescidas e a constante busca de soluções energéticas com melhores desempenhos tem vindo a motivar a comunidade científica dedicada ao estudo da transmissão de calor na procura de soluções de arrefecimento alternativas às já existentes. Essa incessante procura promoveu o desenvolvimento dos nanofluidos, uma nova classe de fluidos de arrefecimento que não são mais do que suspensões coloidais de nanopartículas sólidas num fluido de arrefecimento usual. A junção das nanopartículas ao fluido tem a particularidade de alterar as propriedades termofísicas dos fluidos base, em particular ao provocar um aumento na condutividade térmica, o que se pode refletir num possível melhoramento da capacidade de transmissão de calor do sistema.

O potencial exibido pelos nanofluidos motivou um estudo experimental relativamente à quantificação da capacidade de transferência de calor e das propriedades hidrodinâmicas de um escoamento de um nanofluido composto por nanopartículas de Al_2O_3 e isopropanol. Como suporte ao estudo experimental, propôs-se uma investigação numérica do escoamento baseada na hipótese de escoamento a uma fase, que acabou por dar origem ao presente trabalho. Este estudo consistia numa comparação direta entre valores medidos experimentalmente e valores previstos pelo modelo, que acaba por pressupor a validação das hipóteses adotadas ao considerar um nanofluido como um fluido homogéneo. Também uma análise paramétrica onde se pretendia testar a influência de cada um dos parâmetros que controlam a experiência foi levada a cabo, para no fim se mostrar e concluir sobre a influência que as diferentes bases de comparação têm na interpretação dos resultados.

O coeficiente de transmissão de calor e o fator de atrito foram calculados computacionalmente e, como conclusões principais, salienta-se o bom grau de concordância exibido entre os valores experimentais e os previstos, para regime laminar. Em condições de regime turbulento essa concordância não foi tão elevada quanto a para regime laminar, mas foi suficiente para não comprometer a validade das hipóteses em que se baseia este estudo. A análise paramétrica mostrou um ligeiro aumento do coeficiente de transmissão de calor com a adição de nanopartículas para regime laminar e uma considerável degradação do mesmo em regime turbulento, quando comparados através duma condição de caudal mássico constante. Esses mesmos resultados interpretados à luz duma condição de Re constante acabaram por produzir conclusões substancialmente diferentes, pelo que não se recomenda o seu uso.

Palavras-chave: Nanofluidos, Al_2O_3-isopropanol, Investigação numérica, Condição de escoamento a uma fase, Estudo comparativo

Abstract

The development of more advanced technology with increased cooling needs and the continuous search for solutions with better energetic performances has been motivating the heat transfer community to find alternatives to the cooling techniques employed until now. Such intensive search promoted the advent of nanofluids, a novel type of coolants which are no more than colloidal suspensions of solid nanoparticles into common cooling fluids. This nanoparticles addition has the particularity of modify the thermal properties of the base fluids, namely improve the thermal conductivity, what is reflected in terms of an possible enhancement of the system's heat transfer performance.

The potential exhibited by nanofluids motivated an experimental study regarding the evaluation of the heat transfer performance and the hydrodynamic characteristics of an Al_2O_3-isopropanol nanofluid flow. As a complement, a numerical investigation based on a single-phase conventional approach was proposed, which has resulted in the present work. This study consisted in a direct comparison of the measured data with their numerical predictions, which presumes a verification of the validity of the assumptions took to simulate a nanofluid behaving as a homogeneous fluid. Also a parametric analysis testing the influence of each controlling parameter considered in the experiments was conducted to, finally, show and conclude about the influence of the comparison basis on the interpretation of results.

Both heat transfer coefficient and friction factor were computationally computed and, as main conclusions, we can state the good agreement between experimental data and predictions for laminar flow. In turbulent flow conditions, the match between predictions and experiments for these two quantities was not so high as for laminar flow, still does not compromise the validity of the assumptions followed. The parametric analysis showed a small increase of the heat transfer coefficient with the addition of nanoparticles for laminar flow and a considerable deterioration in turbulent flow conditions, when compared under a constant mass flow rate condition. The same results interpreted in a constant Re basis produced significantly different conclusions, being then not recommended its use.

Keywords: Nanofluids, Al_2O_3-isopropanol, Numerical investigation, Single-phase conventional approach, Comparative study

Contents

Acknowledgments v
Resumo vii
Abstract ix
List of Tables xiii
List of Figures xv
Nomenclature xvii

1 Introduction **1**
1.1 World energetic situation: looking for more efficient energy solutions 1
1.2 Nanofluids: a general overview 3
1.2.1 Preparation methods and stability issues 4
1.2.2 Thermophysical properties and heat transfer performance 5
1.2.3 The need of numerical simulations and their different approaches 7
1.3 Early investigations 9
1.3.1 Experimental studies 10
1.3.2 Numerical studies 12
1.4 Main applications for nanofluids 14
1.4.1 Electronics cooling 14
1.4.2 Vehicle thermal management 16
1.4.3 Solar energy technology 17
1.5 Work description and objectives 18
1.6 Thesis outline 19

2 Mathematical modeling **21**
2.1 A nanofluid as a homogeneous fluid: the conventional approach 21
2.2 Governing equations for fluid flow with heat transfer 21
2.2.1 Mass conservation: the continuity equation 22
2.2.2 Momentum conservation: the Navier-Stokes equations 22
2.2.3 Energy conservation: the energy equation 23
2.2.4 Conservation equations for nanofluids: Boungiorno's formulation 25
2.3 Basic notions on internal flows 26

2.3.1 Fully developed flows: hydrodynamic considerations . . . 26
2.3.2 General approach for convection problems . . . 28
2.3.3 Thermal considerations . . . 30
2.4 Modeling turbulence . . . 31
2.4.1 The RANS equations . . . 32
2.4.2 Turbulence model . . . 33
2.5 Modeling thermophysical properties . . . 34

3 Numerical investigation **37**
3.1 The finite volume method . . . 37
3.1.1 Scalar's conservation in fluid flow problems . . . 37
3.1.2 Discretization schemes . . . 39
3.1.3 Discretizing momentum equations: SIMPLE and SIMPLEC algorithms . . . 41
3.2 The solver . . . 44
3.3 Boundary conditions . . . 45
3.3.1 Laminar case . . . 45
3.3.2 Turbulent case . . . 47
3.4 Mesh independence study . . . 48
3.5 Model validation . . . 52

4 Results and discussion **57**
4.1 Data acquisition and treatment . . . 57
4.2 Predictions vs. experiments . . . 57
4.2.1 Heat transfer coefficient . . . 58
4.2.2 Friction factor . . . 59
4.3 Parametric analysis . . . 62
4.3.1 Laminar flow . . . 62
4.3.2 Turbulent flow . . . 63
4.4 Influence of the comparison basis . . . 66
4.4.1 Mean velocity . . . 66
4.4.2 Reynolds number . . . 67
4.4.3 Pumping power . . . 69

5 Conclusions **73**
5.1 Main achievements . . . 73
5.2 Suggestions for future work . . . 75

Bibliography **77**

A Data and temperature plots for figures 4.1 and 4.2 **83**

List of Tables

2.1 Coefficients for the dynamic viscosity model 35

3.1 Conditions adopted in the mesh independence study 48
3.2 Grids considered in mesh independence study for laminar simulations 49
3.3 Grids considered in mesh independence study for turbulent simulations 51

A.1 Data used for the simulations presented in figure 4.1 (the color identifies each case in each image of figure 4.1). 85
A.2 Data used for the simulations presented in figure 4.2 (the color identifies each case in each image of figure 4.2). 85

List of Figures

1.1 Trends of change in world's energy demand 2
1.2 Schematics of the experiment 19

3.1 Cubic control volume and its surrounding nodes 39
3.2 SIMPLE flow chart for collocated grids 44
3.3 Pressure-based segregated solver flow chart 46
3.4 Schematics of the comptutational domain and boundary zones 48
3.5 Mesh independence study for laminar simulations 49
3.6 Mesh independence study for turbulent simulations 51
3.7 Detail of the meshes used 52
3.8 Isopropanol laminar predictions for validation purposes 53
3.9 Isopropanol turbulent predictions for validation purposes 54
3.10 Isopropanol friction factor predictions and experiments 56

4.1 Examples of predicted and experimental local heat transfer coefficients of Al_2O_3-isopropanol in laminar conditions, for several particle loadings and inlet temperatures 59
4.2 Examples of predicted and experimental local heat transfer coefficients of Al_2O_3-isopropanol in turbulent conditions, for several particle loadings and inlet temperatures 60
4.3 Comparison between numerical and experimental average heat transfer coefficients . . . 61
4.4 Al_2O_3-isopropanol friction factor predictions and experiments 61
4.5 Influence of mass flow rate and wall heat flux on average heat transfer coefficient, for laminar flow conditions 63
4.6 Influence of mass flow rate and wall heat flux on pressure drop, for laminar flow conditions 64
4.7 Influence of mass flow rate and wall heat flux on average heat transfer coefficient, for turbulent flow conditions 65
4.8 Radial profiles of turbulent kinetic energy and dissipation rate for several temperatures and particle loadings conserving the mass flow rate and heat flux 65
4.9 Influence of mass flow rate and wall heat flux on pressure drop, for turbulent flow conditions 67
4.10 Average heat transfer coefficient compared under constant mean velocity basis 68
4.11 Average heat transfer coefficient compared under constant Reynolds number basis 68
4.12 Pressure drop compared under constant Reynolds number basis 70

4.13 Average heat transfer coefficient compared under constant pumping power basis 71

A.1 Axial evolutions of T_m and T_w for the simulations presented in figure 4.1 83
A.2 Axial evolutions of T_m and T_w for the simulations presented in figure 4.2 84

Nomenclature

Abbreviations

BC	Boundary Condition
CFD	Computational Fluid Dynamics
CHTC	Convective Heat Transfer Coefficient
CV	Control Volume
EG	Ethylene-Glycol
FVM	Finite Volume Method
HX	Heat Exchanger
IEA	International Energy Agency
MUSCL	Monotonic Upwind Scheme for Conservation Laws
MWCNT	Multi-Walled Carbon Nanotubes
PDE	Partial Differential Equation
QUICK	Quadratic Upstream Interpolation for Convective Kinematics
RANS	Reynolds-Averaged Navier-Stokes equations
SIMPLE	Semi Implicit Method for Pressure Linked Equations
SST	Shear Stress Transport
UDF	User-Defined Function

Greek symbols

α	Thermal diffusivity [m^2/s]
$\boldsymbol{\tau}$	Shear stress [Pa]
δ	Boundary layer thickness [m]
κ	Turbulent kinetic energy [m^2/s^2]

μ Dynamic viscosity [Pa.s]

ν Kinematic viscosity [m^2/s]

ω Particle mass fraction [-]; Specific dissipation rate [1/s]

Φ Dissipation function [W/m^3]

ϕ Particle volume concentration [-]

ρ Density [kg/m^3]

Θ Mean generic transported property [various units]

θ Generic transported property [various units]

ε Dissipation rate [m^2/s^3]

Operators

Δ Variation [-]

$\frac{\partial}{\partial t}$ Partial time derivative [1/s]

$\frac{\partial}{\partial x}$ Partial spatial derivative [1/m]

$\frac{D}{Dt}$ Material derivative [1/s]

$\nabla\cdot$ Divergence [1/m]

∇ Gradient [1/m]

$\overline{(...)}$ Average; Linearly interpolated [-]

Roman symbols

A Area [m^2]; Matrix of coefficients resulting from the discretization process [various units]

a Coefficients of the discrete equations [various units]

b Vector of independent terms; Independent term of the discrete equations [various units]

C_f Skin friction coefficient [-]

c_p Specific heat at constant pressure [J/(kg.K)]

D Diameter [m]; Diffusion coefficient [m^2/s]; Diffusive mass flux arising from the discretization process [kg/s]

e Specific total energy [J/kg]; roughness [m]

F Convective mass flux arising from the discretization process [kg/s]

f Darcy friction factor [-]

$\mathbf{g}$	Gravity acceleration vector [m/s^2]
h	Convective heat transfer coefficient [W/(m^2.K)]; Specific enthalpy [J/kg]
$\mathbf{I}$	Identity tensor [-]
I	Turbulence intensity [-]
i	Specific internal energy [J/kg]
$\mathbf{j}$	Mass diffusive flux vector [kg/(m^2.s)]
k	Thermal conductivity [W/(m.K)]
ℓ	Turbulent integral length scale [m]
L	Characteristic length [m]
$\dot{m}$	Mass flow rate [kg/s]
M	Molar mass [kg/mol]
Nu	Nusselt number [-]
p	Pressure [Pa]
P_κ	Production of turbulent kinetic energy [kg/(m.s^3)]
Pr	Prandtl number [-]
$\mathbf{q}''$	Heat flux vector [W/m^2]
$\mathbf{r}$	Position vector [m]
R	Tube radius [m]
r	Radial coordinate [m]
Re	Reynolds number [-]
$\mathbf{S}$	Mean strain rate tensor [1/s]
S_θ	Source term associated to production/destruction of θ [various units/m^3]
S_P	Dependent term resulting from S_θ linearization [various units]
S_u	Independent term resulting from S_θ linearization [various units]
$\mathcal{T}$	Mean temperature [^{o}C]
T	Temperature [^{o}C]
t	Time [s]
$\mathbf{U}$	Mean velocity vector [m/s]

$\mathbf{u}$ Velocity vector [m/s]

U Characteristic velocity; Mean axial velocity [m/s]

u, v, w Velocity Cartesian components [m/s]

V Volume [m^3]

$\dot{W}_p$ Rate of work due to pressure forces [W/m^3]

$\dot{W}_v$ Rate of work due to viscous forces [W/m^3]

x, y, z Cartesian components [m]

y Particle molar fraction [-]

y^+ Non-dimensional vertical distance between the wall and the first grid point [-]

Subscripts

∞ Free-stream condition

avg Average mean

B Brownian motion; Bottom node

b Bottom face

bf Base fluid

c Cross-section

D Diameter; Downstream node

E East node

e East face

f Fluid; Generic face

i, j Computational indexes

in Inlet

m Mean

max Maximum mean

mix Mixture

N North node

n North face

nb Neighboring nodes

nf Nanofluid

np Nanoparticles

out Outlet

P Central node

rms Root mean square

S South node

s Surface; South face

T Thermophoresis; Top node

t Turbulent; Top face; Thermal

U Upstream node

W West node

w Wall; West face

Superscripts

$'$ Correction; Fluctuation

$*$ Guessed

n Constant positive exponent

R Reynolds

T Transpose

Chapter 1

Introduction

1.1 World energetic situation: looking for more efficient energy solutions

Energy is, was and will be part of our lives. We need energy for everything we can imagine, from cooking a simple meal to producing any kind of product in a factory, from watching television to propel a space rocket through the atmosphere. Even our vital functions are performed thanks to energy produced and stored in our cells through aerobic respiration, fermentation and digestion. Until now, scientific community did not achieve yet a universal and clear definition for energy, but one thing is for sure: it cannot be produced and it does not vanish, systems simply exchange energy in its many forms of existence. This, as one may notice, represents the well-known *first law of Thermodynamics*.

The previous paragraph illustrates in a simple way why energy is so important to mankind and we will see now why its management and rational use could be even more important. According to the *World Energy Outlook 2017* [1], International Energy Agency (IEA) predicts a world energy demand growth around 30% until 2040, although optimistic forecasts intend to show that it will go on at a smaller rate compared to what is currently happening. Figure 1.1 displays how such demand is divided, with countries like India and China placing themselves as leaders in energy requirements. It is an inevitable fact, once world's population is increasing and their energetic needs too. Also, the electrification and industrialization of such developing countries is a process that has been carried out over the last decades and also contributes to the substantial rise. Facing this problem, countries need to define strategies and new polices about how they can deal with such an increasing demand. Even with all the effort done by scientists, notorious people and environmental organizations trying to inspire nations and industry to a cleaner and more decarbonized world using renewable resources and more efficient techniques to produce electricity, the reality is that fossil fuels like coal, oil or natural gas still represent the major slice of the whole group of primary energy sources, as we can observe in the China's data [1].

Projections point that during next years renewables will increase and reinforce their marketplace in the power production sector, but coal and especially natural gas, will keep their throne as the most used resources. On the other hand, the case of oil is quite different, once its main usage now is the

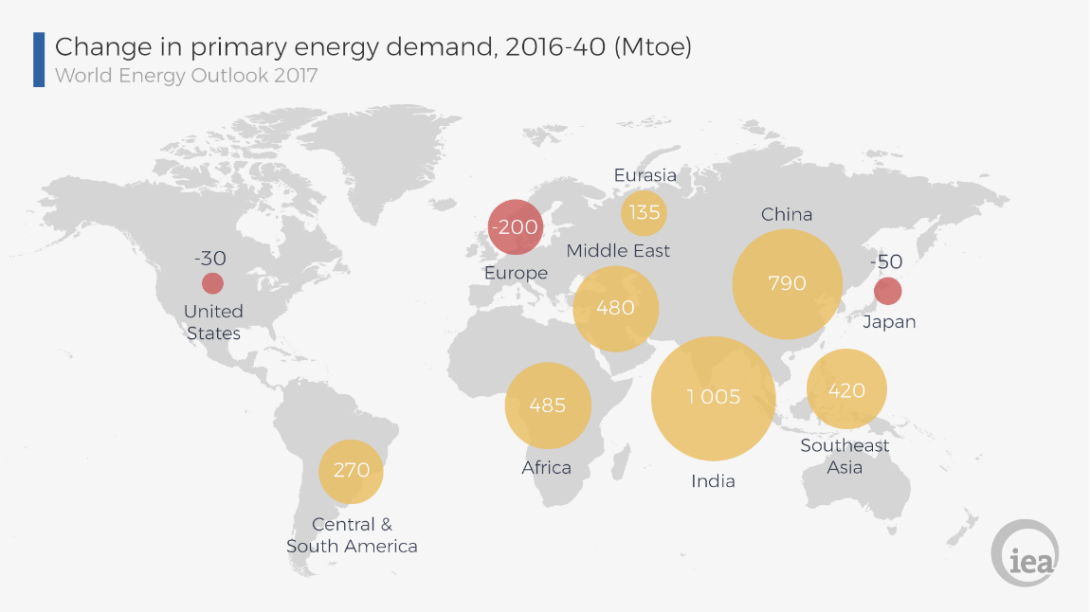

Figure 1.1: Trends of change in world's energy demand. Adapted from [1].

transportation sector. Due to development and globalization of hybrid and electric vehicles and the replacement of oil derivative combustibles by natural gas, producing less pollutant and CO_2, IEA predicts a future decrease in consumption during next years, but not enough to suppress oil totally [1].

Another way to face the problem of large pollutant emissions and, also, to reduce costs related to energy systems is the improvement of the process itself, by means of improving its global efficiency. Improving efficiency means reducing wasted resources or, in other words, a better usage of raw materials, taking more advantage of them and saving some money. According to IEA, without enhancement of efficiencies in energy sector, the consumption of final energy would be more than doubled compared to what is currently happening [1]. But acting on global efficiencies level is not so easy, once energy systems may be considerably complex sometimes. To work around this issue, engineers were forced to subdivide them, performing then detailed analyses that led to specified solutions. Taking as an example the energy production sector and a common power plant – fossil-fuel power plant – this subdivision can be done considering, for instance, sub-systems responsible for steam generation, electricity production or refrigeration. Each one with its own specific purpose, together they make possible the production of electrical energy in virtue of fossil fuel's combustion and acting on its solo efficiency, we are influencing the global efficiency of the plant.

Is the heat carried by the flue gases resulting from the combustion of fossil fuels that vaporizes the water present in the inner coils into high pressurized steam, which in its turn expands inside the turbine, producing the work that allows the electrical energy production through the coupled generator. However, heat is not only the heart of the process, it is also the main reason of verified low efficiencies in some thermal equipments, considering that a significant amount of heat is released when stack gases leave the boiler via exhaust pipes, or even lost through the enclosures. In fact, heat losses are a difficulty shared by every thermal machine facing temperature differences, due to the spontaneity of the heat transfer process. It is something we musk keep under control if we want to extract the maximum profit

from the equipment.

But not only in energy production sector thermal efficiencies are a key factor. Cooling solutions represent another large investigation area where thermal management has great importance to ensure either thermal comfort to people or appropriate working conditions to those devices that produce heat as result of their normal operation. Thermal engines, machining tools or electric and electronic equipments can be easily identified as belonging to a group of products with cooling needs. This kind of machinery sometimes dissipates so much heat that can even cause itself real damages if any type of cooling solution was not taken. Considering that, cooling systems are of extreme importance to industry and also for human lifestyle, once nowadays, people are much more addicted to technology and always looking for improved devices. As new electronic top-products generally have better specifications, faster processors and higher level of compactness, the amount of heat released is clearly denser than before, requiring improved cooling solutions as well.

Apparently, there is nothing in common between the two types of technology presented before, with exception that both deal with heat transfer inside *heat exchangers* (HXs). Due to their importance for real applications, HXs have received a lot of attention from the community along the years. Bergles [2], by the time he published his work, organized the various phases of HXs investigation into *generations of heat transfer technology*, each one characterized by a given step forward on the enhancement techniques. Besides the identification of the various types of HX, he have also classified all the techniques into *active* or *passive*, with the single difference of requiring extra power consumption, or not. From the passive ones, we would like to highlight the inclusion of additives to heat carrying agents to improve their heat transfer performance by modifying their thermal properties. Such technique can perfectly be the main reason behind the existence of this work.

1.2 Nanofluids: a general overview

Scientists and engineers have called *nanofluids* the colloidal suspensions of solid nanoparticles, generally with a diameter smaller than 100nm and in a low concentration range, into classic heat transfer fluids, the so-called *base fluids*. Examples of common base fluids are water, engine oils, lubricants or even alcohols. This solution, as many others in cooling science, came from the need of dealing with increasing thermal loads in industry and technological appliances and it is very appreciated by the community due to its promising results, while applicable to existing thermal systems, but also as a consequence of its great performance in experimental tests, indicating the possibility of developing new and more efficient technology based on nanofluids as a heat transfer medium. The term “nanofluid” first appeared in 1995 thanks to Choi and Eastman [3], in a research work where the improvement of thermal conductivity of liquids powered by suspended nanoparticles was addressed, although the authors indicated earlier studies noticing this fact.

Many specimens of nanoparticles were tested and reported during nearly the past twenty years, going from carbon-formed to magnetic particles, but a quick look into the literature shows that the most utilized nanoparticles are oxides, like Al_2O_3 (alumina), CuO (copper oxide II) or TiO_2 (titanium dioxide),

due to their large stage of oxidation [4]. Although they were recently created and studied, it is important to notice that, within typical low particle concentration ranges and for generally spherical particles, they behave much like to conventional Newtonian fluids, which represents another interesting feature about this new type of fluid [5].

1.2.1 Preparation methods and stability issues

Regarding the procedures taken with the objective of producing nanofluids with satisfactory quality, which should be the first main goal of anyone trying to do experiments on them, there are two well accepted methods of manufacturing such fluids. In contrast to what we might think, the preparation is of extreme importance for the overall nanofluid performance, once the method is directly responsible for achieving what researchers usually call a *stable* nanofluid. The stability of a colloidal suspension is measured in terms of its level of particle agglomerates created and the more clusters formed, the less stable the suspension is. In addition, a unstable nanofluid sees its properties be altered and deteriorated and do not demonstrate all the potential it has [6–8]. Stability turns itself into a key factor for all the experimental tests, findings and, posteriorly, future applications of this technology. Some proposed techniques to improve it will be addressed after we introduce the preparation methods.

A technique that has been extensively used over the last years, and probably the most intuitive one due to its simplicity, is the so-called *two-step method*. As the name states, it consists on the dispersion of separately produced nano-matter, for instance in the form of dry powders, into selected base fluids, suffering then a massive agitation process to well distribute the particles within the acceptor liquid. This method has as primary advantage its relatively low price, mainly thanks to well established chemical processes that reached the industrial level of production, capable of creating large quantities of powders and making cheaper the samples' production. However, and as a consequence of large particles' surface area together with their singular nature, agglomeration and sedimentation tend to appear and the nanofluid will certainly become unstable, which leads to a degradation of its unique characteristics. This is considered as the principal disadvantage of the presented method and, in order to overcome this major stability problem, another type of manufacture procedure was proposed later – the *one-step method*.

Although it involves higher complexity and lower production rates compared to their rival two-step, one-step methods offer advanced techniques that allow a narrow control over the nanoparticles size. It also promotes a more uniform distribution within the liquid while avoids nanoparticles' drying, storage, transportation and posterior artificial dispersion, resulting in suspensions with higher level of stability. The process, even with some different approaches and specific techniques, has a main general rule: it consists in the fabrication of a nanofluid in one single step, by means of producing and dispersing at the same time the formed particles into the host liquid. As any process, one-step technologies have some points against their use. The high price we need to pay in order to produce a small amount of nanofluid or the difficulty to produce it in industrial quantities are just two of them, but the possibility of remaining impurities inside the suspension seems to be other important issue. More detailed and

deeper information about these procedures is available on the consulted review papers [6–8].

In alternative to one-step techniques, cheaper “tricks” can be used in conjunction with a two-step technique to fight against the formation of clogs. A widely used simple technique is the addiction of a compound, called *surfactant*, to the suspension that will act on the surface of solid particles, preventing their linkage to other peers. Basically, when a surfactant meets a solid particle, its molecules will locate at the particle surface (the solid barrier between the two phases) and promote particles' *wettability*, which represent the capacity to attract or repulse liquid molecules. Consequently, solid particles will tend to be surrounded by liquid, placing surfactants as a simple and low-cost way combined with two-step methods to produce stable nanofluids. In fact it is, but with some reservations. The use of surfactants might degrade the heat transfer medium by two different factors: firstly, while promoting a good particle dispersion within the liquid, a surfactant layer will be formed around those particles, creating an extra resistance to heat flow; secondly, during heating/cooling cycles some undesirable compounds may be formed and what is expected to be a pure heat transfer medium becomes a contaminated one, which turns surfactants at the same time promoter compounds and pollutant agents [7]. Also, the typically not very high maximum temperatures where their use would guarantee a good particle dispersion level is a limitation for the combination of surfactants and nanofluids [6]. Until now, there is not yet an established production method that fits well all the most important features, say economic and productive.

1.2.2 Thermophysical properties and heat transfer performance

Nanofluids have superior interest in heat transfer field mainly because of their thermophysical properties. Through the addition of solid nanoparticles, we are influencing the fluid thermal conductivity and possibly promoting its heat transfer capacity, in comparison to the base fluid alone [4]. However, this evaluation may not be straightforward because, besides the thermal conductivity enhancement, other properties like density, specific heat and viscosity will also be affected, influencing the convective heat transfer coefficient (CHTC) in a way that may be different from the one verified in thermal conductivity [4, 9].

Thermal conductivity is by far the most studied and investigated property of a nanofluid. It is considered to be easily measured, essentially when compared to CHTC, and was seen as a good indicator to quantify the thermal performance of a nanofluid. In order to demystify this abnormal enhancement, several investigations were carried to analyze the influence of diverse mixture parameters and some conclusions could be taken about their trends of influence on thermal conductivity of a nanofluid [4, 10].

Still, its enhancement mechanisms represent a challenge for the community. Various processes were proposed to explain the verified increase in thermal conductivity, but no one has been generally accepted yet, revealing a lack in agreement within the heat transfer community. During the last decade, were essentially three the main proposed causes pointed to be the reason of such interesting increase, known as *particle random motion*, *liquid-layering* and *clustering* [10–13].

None of the proposed mechanisms was able to clearly explain the process behind these enhancements. Nevertheless, [10] presented some experimental evidence that clustering might be responsible for a conductivity increase. Still, it is important to refer the implications of clustering on stability of nanoflu-

ids. Random motion mechanisms were investigated by Buongiorno [14] who have identified *Brownian motion* and *thermophoresis* as the two possible mechanisms capable to promote slip velocities among particles. Unfortunately, neither Brownian motion nor thermophoresis were proven responsible for significant conductivity enhancement, and several explanations of this fact have been proposed, namely lower time scale of Brownian motion compared to heat's one [11], lower liquid diffusivity in relation to solid's one [10] and no influence of thermophoresis under experimentation [13]. [14] also computed some time scales and concluded that, under turbulent regime, only turbulent mixing matters.

Such disagreement is, consequently, transported to theoretical modeling of the thermal conductivity of a nanofluid. Maxwell's equation developed for dilute mixtures with suspended spherical particles can only reasonably predict conductivity values for very small concentrations, which is not suitable. A lot of effort has been put on developing new models, as the literature evidences [10, 12, 15, 16], but apparently none of them accomplishes its goal. While some under or over-predict experimental values, others are developed for specific conditions and unable to explain well the data produced, revealing the necessity of creating a general model which incorporates every contribution of the physics influencing thermal conductivity. For that reason, the only reliable way to characterize the thermal conductivity of a nanofluid is using experimental data measured under the intended work conditions [4, 17].

Nanofluid's density and specific heat can be accurately computed using expressions derived from the classic mixture rule because they seem to have no influence from the above cited solid-fluid interaction mechanisms. In its turn, dynamic viscosity, which is clearly powered by the addition of nanoparticles, suffers a strong influence from it. As a consequence, its prediction becomes an arduous task too, with Einstein's equation, the simplest model for a mixture's viscosity, becoming untrusted for viscosity computation. Similarly to thermal conductivity, no unifying model was created until now, which turns again experimentation the only precise way of having nanofluid's viscosity data [16, 17].

Despite the importance that thermal properties definitely have on the heat transfer mechanism, in fact what is going to quantify any improvement is the CHTC. For forced convective heat transfer, CHTC directly measures the amount of heat being convected and is clearly the key parameter for every cooling solution. For instance, some benefits of the CHTC enhancement is the reduction of equipment's size and weight, better efficiencies and improved capacity to deal with higher thermal loads [4]. However, this potential exhibited by nanofluids has a cost that must be paid, which is the penalty in pumping power due to the increase in pressure drop. The presence of suspended nanoparticles turns the nanofluid a more viscous fluid that needs additional power to flow inside the ducts and this may be a real problem. Hence, when energy resources are considered a limitation, these two parameters should stay side-by-side and the final goal must be one of the following options: find the highest CHTC for a fixed pumping power or find the lowest pumping power considering the same CHTC [17].

Comparison between thermal performances of nanofluids and their base fluids is what will dictate if the use of nanofluids is really valuable or not. Nevertheless, this comparison might not follow the traditional rules used when singe fluid are considered. For example, due to the dynamic similarity incorporated and dimensionless character, Reynolds number (Re) seems the perfect choice for a comparative basis for nanofluids too. This would be acceptable if the base fluid properties had remained unchanged

with the addition of nanoparticles, which is definitely not the case. Keeping Re constant, we are actually comparing two flows at different velocities and completely ignoring the penalty in pumping power due to logical differences in viscosity of the two fluids. We are mixing contributions from different velocities and thermal properties, so the physical conditions are not the same and they should not be compared. The same happens when computing the Nusselt number (Nu) to evaluate the thermal performance instead of the CHTC. A small Nu can be obtained due to an high thermal conductivity and not necessarily from a low CHTC. To solve such conflicts, pumping power appears to be the most conservative and clear choice for comparison basis, once they are made considering the same amount of power available to both fluids. Constant velocity can also be seen as a reliable basis when penalties are small [17].

The truth might be cruel but the doubts shared over the years still hold today without a clear answer. From our best knowledge, no general theory was yet proposed and consolidated, and actually may never be. Nowadays, the paradigm seems to have changed to a more pragmatic look into the potential benefits of nanofluids, as presented in the recent work of Buschmann et al. [18]. He and his team carried out a comparative study between experimental investigations performed under standard conditions to prove that a Newtonian nanofluid could be considered a homogeneous fluid. To ground their analysis, a similarity study was executed, where four conditions for a hypothetical nanofluid behaving as a homogeneous fluid were introduced. Similarity parameters were created and computed for every investigation with the intent to prove each one of the assumptions. In the end, they were able to conclude that a nanofluid can, effectively, be treated as a single-phase fluid with effective properties and classic fluid mechanics and heat transfer correlations are also applicable. They do not deny the existence of the intermolecular mechanisms already seen, but rather argue that they are of minor importance for the heat transfer process. About heat transfer enhancement, which has been stated to be higher than the thermal conductivity effect, [18] says they match perfectly since comparisons were made in identical hydro and thermodynamical bases.

1.2.3 The need of numerical simulations and their different approaches

Mathematical modeling of nanofluid flows has received much attention, due to the potential shown by *Computational Fluid Dynamics* (CFD) techniques on solving complex problems. They produce accurate results, but also gives flexibility to any project. *Computer Aided Design* (CAD) conjugated with CFD is something very appreciated in many engineering areas, once it offers a reliable way to model real problems, test several work conditions and introduce modifications with significant money savings, contrarily to a pure experimental design. Nevertheless, validation of a model does not occur without experimentation and it should never be put aside.

Almost all engineering problems are ruled by equations for which, until now, no analytical solution was discovered. However, it is part of engineer's mission to find solutions for complicated problems every day. It is precisely here that numerical simulation give its best contribution, providing the chance to solve complex problems using a software that could be developed in-house or is available somewhere. This, together with the development of more powerful processors, have placed CFD techniques on the

front line of the most used resources. Using CFD tools, researchers have the capacity of easily change the working conditions of the modeled problem, such as defining different materials and boundary conditions, which provides money savings or allow its redistribution to other important tasks. Also, by trying their new ideas in an artificial way, people are able to easily select the best design characteristics to reach a final decision in the end. Of course, computational time needs to be as short as possible and predictions must have a physical meaning. This implies not only a correct use of simulation tools but also a strong background knowledge about the solving methods and the physics itself.

Many papers can be found in the literature about CFD simulations with nanofluids, with almost all of them following one of the three next presented numerical approaches: *single-phase*, *two-phase* and more recently *lattice-Boltzmann* techniques [19, 20]. A brief and succinct description of the three different procedures is coming next.

Never forgetting that a nanofluid is a mixture of fluid and particles, the most used, simpler and, perhaps, more instinctive approach to model a nanofluid is to assume that, once the suspended particles' size is so small (order of nm), they can flow on the liquid without slip between them and fluid particles – becoming *easily fluidized*. Thus, considering also the existence of a *thermal equilibrium* among phases, the nanofluid behaves as a homogeneous fluid. The presence of nanoparticles, in this case, will be then reflected on the fluid properties, by means of computation of *effective* thermal properties, function of mixture parameters and mechanisms. This is the so-called *single-phase conventional method* and is the simplest approach applied to nanofluid simulation, considering that classic conservation equations are valid with altered properties [21]. Other option is to consider again one phase, but the existence of nanoparticles with chaotic and disorganized movements will promote energy exchanges inside the fluid – the *thermal dispersion* effect. This concept was firstly introduced by Xuan and Roetzel [21] who intended to explain the augmentation of the heat transfer rate thanks to fluctuations in both velocity and temperature fields. Those were induced by random particle movements, increasing the temperature gradient between wall and fluid and promoting the exchange of heat.

The main reason of modeling a nanofluid as a two-phase mixture is to try to understand in detail how the interaction between fluid and solid particles takes place and how thermal properties and heat transfer performance is influenced by them. Thus, researchers thought that dealing separately with each phase would be a more realistic way to treat the problem, producing clearer results about fluid-particle interaction mechanisms. This type of approach can be mainly divided into two major groups: *Eulerian-Eulerian* and *Eulerian-Lagrangian*. The principal distinction between them is how particles are treated, whether from the Eulerian or Lagrangian points of view. The fluid is always treated as a *continuum* and classic transport equations rules the dynamics – the Eulerian way.

Eulerian-Eulerian approach considers both fluid and particles as being part of an *interpenetrating continua*, i.e., the total domain is composed by the two phases, where no volume occupied by one phase can be shared with the other one. After that, phasic volume fractions are created, with their summation equal to the unity and similar conservation equations are obtained for the two phases. The problem closed recurring to constitutive laws or empirical models [22]. Eulerian-Eulerian approaches are divided into three different methods: *mixture model*, *volume of fluid* (VOF) and *eulerian*. The differences

between them are out of the scope of this work, but the main reasons of selecting one instead of another consist on the problem itself, due to specific flow considerations and co-existing conditions of all phases (please see [22] for more information).

Alternatively, the Eulerian-Lagrangian method, also known as *discrete phase model*, considers particles as a disperse phase, tracking then the trajectories of a considerable number of particles which are capable of exchanging mass, momentum and energy with the fluid phase at discriminated time steps, while the flow field is being computed [22]. This method, although its available applicability, is often unappropriated to nanofluids simulations thanks to the small particle's size, which involves a great number of particles to be tracked and an enormous consumption of computational time [19].

Following a totally different procedure, the lattice-Boltzmann method (LBM) appears as a disruptive method to analyze the dynamics of a nanofluid flow. It looks for the transport processes and particles interaction from a microscopic point of view. This means that the nanofluid is considered to be a set of fluid and solid particles, where all of them are allowed to interact with their neighbors, independently the phase. The responsible mechanisms for such interactions, like Brownian force or gravity, are considered at a molecular level, leading to a deeper understanding about how these mechanisms influence transport conditions. The method received its name thanks to the way it interprets and builds the problem: it is assumed that the mixture is composed by particles *mesoscopically* placed in series of 2D or 3D lattices and their distribution obeys to the Boltzmann equation. Then, internal and external particle forces are taken into account on the light of a particle collision model [23]. LBM provides velocity and temperature fields that, macroscopically, are proven to be solutions of Navier-Stokes equations [23], showing the feasibility of such methods to fill the gap between micro and macroscopic worlds. Simulations using LBM are becoming a reality in the nanofluids area and specific LBM applications can be seen in review papers such as [19, 20], but not enough yet, they say.

1.3 Early investigations

Many different specimens of nanofluids, in as many other operative conditions, were tested all over the world by a community whose main concern was an appropriate explanation of the abnormal phenomena observed. A lot of published works can be found in the literature referring to both experimental and numerical investigations where nanofluids were tested, in order to acquire relevant information about their performance. Therefore, after the considerable overview done, a look over some investigations will be presented now, to illustrate what has been done until this moment. Such information can also be seen, logically, as a comparative and inspirational source of knowledge, allowing us to know what we might expect at the end.

Since single-phase forced convection in horizontal circular pipes submitted to a constant heat flux is an extremely popular setup, we will focus our review in studies addressing such configuration.

1.3.1 Experimental studies

There are a few papers about nanofluids that can be considered pioneers and inspirational, and the case of the work presented by Pak and Cho [24] in 1998 can be easily defined as one of them. Motivated by their potential, authors proposed an experimental apparatus composed by a closed loop with a circular pipe as test section, a set of thermocouples connected to a data acquisition system and all the auxiliary equipments needed (e.g., pumps, cooling unit, etc.), where the fluid would flow and its heat performance would be characterized. The intention was to submit the nanofluid, flowing in turbulent fully developed conditions, to a constant heat flux and evaluate how effectively heat convection occurred and how friction losses were affected. For this purpose, γ-Al_2O_3 and TiO_2 nanoparticles were separately dispersed into water and nanofluids were in-loco prepared. Their viscosity was experimentally measured and proved to be significantly higher compared to water's alone. Available data for thermal conductivity was used and both density and specific heat were computed using two-phase mixture equations. Having the fluid characterized, the authors did some measurements of the friction factor and CHTC, both as function of Re, and were able to observe two main conclusions: friction factor was correctly predicted through the Kays' correlation, showing a clear linear decrease with Re and a penalty in pumping power was verified of approximately 30%; both CHTC and Nu were found to have a linear growth with Re with largest enhancements of about 75% verified for γ-Al_2O_3 nanofluids at maximum loading, but under constant velocity condition, a 12% reduction in heat transfer performance was found, with authors advising for a proper selection of nanoparticles.

The promising findings of Pak and Cho [24] inspired many other similar works where researchers tried different combinations of nanoparticles, base fluids, particle concentrations and other possible and interesting factors in turbulent flow conditions. Works like those of Xuan and Li [25], Kim et al. [26], Azmi et al. [27] or, more recently, Martínez-Cuenca et al. [28] are a perfect example of the replication of the major conclusions presented in [24], although in different proportions. [25] tested Cu-water nanofluids and found improvements of the CHTC within a range of 6 to 39% compared to pure water, while [26] used Al_2O_3 and amorphous carbonic nanoparticles separately suspended in water and was only able to verify a significant augmentation of 20% in the CHTC when Al_2O_3 nanofluids were being tested. [27] mixed nanoparticles of SiO_2 and TiO_2 with water and achieved enhancements in CHTC of 33% and 26%, respectively. Finally, [28] studied the heat transfer performance of Al_2O_3 and SiO_2 nanoparticles and multi-walled carbon nanotubes (MWCNTs) individually suspended in water and came up with the best results in terms of CHTC enhancement, with authors reporting augmentations of 65%, 84% and 48% for the three studied nanofluids, respectively. All the four studies have also in common the fact that each one presents the same kind of behavior of the friction factor, which decreases almost linearly with Re for any nanofluid and the intensification of the CHTC when the particle concentration is higher, at least for the range of concentrations evaluated (less or equal than 5 vol.%).

Besides some conclusions presented in common, authors have not agreed in all other aspects. In fact, no great agreement was found between predicted and experimental values in these analyzed papers. This disagreement might be attributed to the way thermal properties were computed, like if they were experimentally measured or not and what procedure was followed, or just acquired from

other literary sources. Mansour et al. [29] investigated the influence of uncertainty in thermophysical properties and concluded that the final design parameters were strongly influenced by those properties and, of course, by their method of computation. Also, Duangthongsuk and Wongwises [30] investigated how the model selected to compute thermophysical properties would affect the CHTC in TiO_2 nanofluids flows and end up saying that the model was not responsible for the biggest discrepancies, but the experimental apparatus itself and its calibration. The way we obtain such important variables clearly influences the final results and, although all authors claimed they had done experimental measurements for their own studies, only [28] were able to say that Gnielinski equation for Nu could predict their experimental values with an average correlation coefficient of 0.89 for Nu greater than 150, followed by the Dittus-Boelter equation with 0.8 and also the friction factor could be well predicted using the famous Colebrook equation. Based on their findings, they were able to conclude that correlations developed for single-phase flows are also valid for nanofluids, but only with carefully and properly measured thermal properties, which they claim they have done in an earlier investigation.

A look at laminar flow regime publications about nanofluids allows us to make a similar analysis to the previous one for turbulent flow experiments. Wen and Ding [31], Lai et al. [32] and Hwang et al. [33] tested Al_2O_3-water nanofluids, in volume concentrations always smaller than 2%, and every investigation came up with some shared conclusions. All of them were able to notice that heat transfer was enhanced by the addition of nanoparticles to the base fluid and, for a prescribed Re, the CHTC was particularly high at the entrance region, becoming then smaller and stabilizing in the fully developed region of the flow. They also mentioned the positive effects of particle volume concentration and Re in the CHTC enhancement, which was something expected once it was already observed in turbulent experiments. To quantify those augmentations, [31] estimated a 47% higher CHTC near to tube's entrance and 14% higher in fully developed region, [32] measured an 8% increased Nu and Hwang et al. [33] an 8% enhanced CHTC as well. All these observations were also proved by Kim et al. [26], who reported an increase in CHTC of 15% for Al_2O_3 nanofluids and 8% for amorphous carbonic nanofluids. Later, and with the aim of testing a new type of nanofluids that could improve their thermal conductivity in a greater fraction than viscosity, Ilhan and Ertürk [34] mixed hexagonal boron nitride nanoparticles with water, in a particle volume concentration range below than 1%, and achieved a maximum improvement of 15% in CHTC over water's alone. The previously mentioned conclusions about the CHTC were also reported, with authors revealing the preservation of nanofluid properties after the end of the experiments and alerting to a stable and suitable new nanofluid for heat transfer applications.

Shah's equation is a well-known and widely used correlation to estimate Nu in laminar flows inside ducts and can be valuable as a comparative source of theoretical information. To evaluate the quality of their own experiments, scientists usually compare their results with those predicted by Shah's equation and check the agreement between them. Two attempts were done by [31] and [33] and both conclude that this classic correlation was not able to satisfactorily predict the enhanced Nu. [31] proposed a main reason to this failure, which was the fact that this correlation has been developed for larger ducts than the one used in their work, but without any strong certainties.

About the friction factor, from the set of analyzed papers, only [33] dedicated some of their attention

to know how this parameter behaves. It is perceptive the reduced quantity of references to friction factor investigations in laminar regime, comparatively to turbulent regime, due to characteristic small velocities and, consequently, small friction losses. Still, from the Hagen-Poiseuille analytical solution for laminar and fully developed flows in circular ducts, it is possible to derive an exact equation for friction factor as a function of the Re. The comparison performed showed a good agreement between predicted and experimental data which, together with the fact that these authors also verified a higher enhancement in CHTC than in thermal conductivity, represent strong implications of the possibility of considering these nanofluids with low particle loadings as homogeneous fluids with altered properties resulting of solid-fluid particles interactions within the flow.

Although the great majority of experimental investigations reported enhancements using nanofluids, there are also some researchers who were not able to verify any or significant intensification of the heat transfer process. Two examples are the study of Williams et al. [35] and, more recently, the one of Piratheepan and Anderson [36]. [35] suspended Al_2O_3 and ZrO_2 nanoparticles in water, separately, with the aim of evaluate their heat transfer performance in turbulent flow conditions and measure the pressure losses promoted by the increase in viscosity. To attain that, they have measured all thermal properties as a function of temperature and particle concentration before the execution of the experiments and their main conclusions were the good agreement of predicted and measured results, which they claim to be a consequence of the computation of dimensionless numbers using effective properties evaluated by the team. Besides that, no significant heat transfer increase was noted. The study of [36] was similar but they chose to test MWCNT-water nanofluids, also in turbulent regime. They end up saying that the heat transfer process was not improved using MWCNT-water nanofluids in turbulent flow conditions and, instead, a significant reduction was detected, proving that such nanofluids are not suitable for forced convective turbulent flows.

1.3.2 Numerical studies

The two studies of Maïga et al. [37, 38] can be seen as pioneers investigations on the topic. In [37], Maïga and his team proposed a numerical investigation of Al_2O_3-water and Al_2O_3-EG nanofluids flowing in a circular and uniformly heated tube, in both laminar and turbulent conditions, with the assumption of homogeneous fluid. In order to achieve their purposes, a computational model was created where conservation equations were numerically solved employing the finite volume method, a technique extensively used in CFD calculations. As turbulent regime was considered, the time averaged Navier-Stokes equations were employed and the standard κ-ε was selected to model turbulence. In fact, this numerical treatment is a procedure followed in all the analyzed investigations. For the laminar case, their simulations revealed a heat transfer promotion, with a maximum temperature difference of 17 K when compared to base fluid's, for nanofluids loaded at 10 vol.%. In both flow regimes, the addition of nanoparticles promoted the CHTC and the wall friction, while Re was kept constant. This type of conclusion is consistent with those observed for experimental investigations and despite no quantitative comparison was done, this agreement is always a good indicator of the feasibility of numerical predictions.

[38] can be considered a sequel of the previous work, where the influence of Re in the heat transfer process was one of the aims, although only for laminar flow conditions. Enhancements of 2.73 times in CHTC and of 6.81 in wall friction were predicted for EG nanofluids loaded at the maximum concentration considered. The generated data was then used to create new correlations for Nu that end up being used in other posterior similar works.

Following the steps of Maïga et al., Namburu et al. [39] published a paper where the same type of problem was addressed. The chosen nanofluids were CuO, Al_2O_3 and SiO_2 nanoparticles independently dispersed into a mixture of water-EG. Turbulent flow conditions were ensured throughout the whole set of simulations. As main conclusions, can be pointed out that both CHTC and Nu showed enhancements in all tested nanofluids, compared to their base fluids, when particle concentration and Re increased. Additionally, it was noted the augmentation of the shear stresses when more CuO nanoparticles were added, reaching for 6 vol.% loading nearly the double of those predicted for the base fluid. As final appointment, they concluded showing the best performance of CuO nanofluids over the two others, confirmed by the computation of CHTC and Nu, this last one showing a great agreement with Gnielinski correlation.

During the same year, two very interesting papers were released with the objective of carrying out a comparative study between two different numerical approaches: conventional hypothesis and discrete phase model. He et al. [40] simulated the heat transfer performance of TiO_2-water nanofluids and were able to prove again the trend that CHTC has to decrease axially and increase with particle concentration and Re, for laminar flow conditions. With respect to the results produced by the two different models, it can be seen that both approaches predict in a very similar way the heat transfer mechanism, through the computation of the CHTC.

In its turn, Bianco et al. [41], reproduced the flow of Al_2O_3-water nanofluids in laminar regime following both single and two-phase approaches. Moreover, they went a bit further investigating the influence of temperature-dependent thermal properties on the CHTC and found that it always yields higher values when compared to those generated using properties only function of the particle concentration. Observing the predictions, the evolution of CHTC with the flow parameters was not qualitatively different from what was described before, with both models producing closer results. Only 11% difference was found, with two-phase one having the tendency to produce slightly larger results.

The same team proposed another study in 2011 with the same nanofluid but in turbulent flow conditions and aiming a comparison between single-phase hypothesis and two-phase mixture model [42]. Analyzing the axial evolution of the CHTC, they were able to notice a sharper decrease to its fully developed and almost constant value. Enhancements in the CHTC were also noticed, with a nearly 30% higher coefficients found for particle loading of 6 vol.% and, for these conditions, shear stresses almost tripled in relation to the base fluid only. Regarding the comparison of the two numerical approaches, the trend shown by the conventional method in the previous works of predicting with relatively good agreement when compared to the more complex two-phase formulations was again verified.

More recently, two investigations following the homogeneous fluid assumption and turbulent flow conditions were reported. Saha and Paul [43] present us a comparative study where two distinct nanofluids

have been tested. They observed the enhancement of both heat transfer performance and viscous dissipation when higher Re and particle concentrations were chosen, however these two features have a tendency to decrease when bigger particles were used in the nanofluid samples. Through the computation of a parameter called "thermal performance factor", which is an indicator that relates the heat transfer enhancement with the adverse pressure drop increase, in order to decide whether the heat transfer augmentation is valuable or not, authors end up saying no significant penalties were detected. Globally, alumina nanofluids presented better thermal indicators, but since titania is more environmental-friendly, authors have recommended its use.

A novel type of nanofluid was tested by Sadeghinezhad et al. [44] who proposed an experimental and numerical investigation over the thermal performance of graphene nanoplatelets (GNP) dispersed into water. Wall temperatures were found to be slightly numerically over-predicted, but in terms of Nu, good agreement among experimental and numerical investigations was found, exhibiting the expected rising behavior while Re, particle concentration and heat flux increased. Maximum enhancements of 83% reported for Nu surely represent a good indicator for this new colloid and opens the door to more research in new types of nano-matter.

1.4 Main applications for nanofluids

Since the revelation of its great potential, scientists and engineers have tried to find the best practical applications where nanofluids can become an added value when performing a particular task. The use of nanofluids in the energy sector seeks the improvement of efficiencies and a reduction in energy consumptions, with a major goal of contribute to a cleaner and sustainable world. Currently, there are no commercial applications using nanofluids yet, but the experiments reported in specialized literature show some auspicious results that, once suppressed the problems found in production and stabilization methods, will absolutely end up in better solutions than those used nowadays. If we look at some review articles, like [7, 45, 46], it can be seen that a considerable number of different practical applications have been studied along the previous years, but, despite the great diversity of published work, not all of them received the same amount of effort. Thus, this sub-chapter intents to illustrate the most prominent applications where nanofluids have been being tested, trying also to prove their potential when applied to real technology.

1.4.1 Electronics cooling

To face the advent of tinier and more powerful processors capable of dealing with more information, achieving faster processing speeds and, consequently, dissipating higher amounts of heat, cooling techniques must be effective enough to allow a perfect and reliable performance of such equipments, preventing them to suffer crucial damages in their normal operation and supporting a trustworthy work-life. Innovative solutions have, thus, to be found and applied successfully, or cooling performance will become rapidly the bottleneck of the entire design in electronics components. To add still more restrictions

to the problem, reductions in total volume of an electrical equipment are achieved not just thanks to smaller components but also as a result of an increase in compactness, which reduce the space available among hardware. So, the idea of increasing the size (by means of its contact area) of a cooling system should stay aside of designer's thoughts and a more effective approach must be encountered to deal with increasing thermal loads in small spaces. Nanofluids fit well in that suit with their special characteristics and seems to be a solution to take into account in this field.

Typical new cooling solutions used in electronics appliances with higher thermal dissipation are systems based in *heat pipes* or *microchannels* technology (figures), although Murshed and de Castro [47] refer other emerging ones in their review on electronics cooling. A heat pipe is a technology that uses coolant's phase change inside a closed structure (for instance a metallic pipe) to remove heat from a specific location. An experimental study by Qu et al. [48] where an Al_2O_3-water nanofluid was used in an oscillating heat pipe was performed, in order to evaluate its thermal performance when confronted to pure water. They conclude saying that heat pipe's thermal performance was improved by the use of alumina nanofluids, suggesting as possible enhancement reason the surface condition affected by settlement in evaporator. Do et al. [49] performed a similar study where they used the same type of nanofluid, in a 1 to 3 vol.% range and base fluid, but in a different type of heat pipe – a circular screen mesh wick heat pipe. Authors were able to conclude that using alumina nanofluids, the thermal performance was improved when compared to water. They also found that as particle concentration increases, evaporator temperature tends to decrease, reaching its lowest value when 3 vol.% of Al_2O_3 nanoparticles were dispersed in water. The responsible mechanism for these reported results was the formation of a thin coating layer around the wick in the evaporation zone, they said.

Microchannels technologies are essentially from two types: microchannel HXs or microchannel heat sinks. Their working principle is pretty much like a regular HX, except the size and heat transfer performance, which is far better. These are two specialized solutions on dealing with high heat fluxes generated in compact equipments, as the case of the new chips with large integration of components [47]. To evaluate the performance of a microchannel heat sink working with a nanofluid, Escher et al. [50] added silica nanoparticles to water, in concentrations from 5 to 31 vol.% and tested it into three heat sinks, with different channel widths. The measured Nu increased with the particle concentration, for a given Re. Predictions were done too, with experimentally measured Nu remaining in a $\pm$10% range of predicted ones, which led authors to admit no great enhancement using nanofluids. Another experimental and numerical study was performed by Kalteh et al. [51] where an alumina-water nanofluid was used inside a rectangular heat sink. They showed an average Nu increasing with both Re and volume concentration for both numerical and experimental investigations. In addition, numerical predictions show the augmentation of average Nu when particles are smaller. The numerical study also revealed accurate predictions from the two-phase Eulerian-Eulerian simulation than from the homogeneous model, when compared to experiments.

A different electronic cooling approach was followed by Nguyen et al. [52] who cooled a heated block, used to simulate the generated heat of an electronic equipment, with a closed system where an alumina-water nanofluid was responsible to remove the heat. The experiments were conducted in turbulent

regime and within a loading range of 1 to 6.8 vol.%. Authors could show a considerable enhancement, compared to simple water as cooling fluid, namely achieving a heat transfer coefficient augmentation of 40%, for 6.8 vol.% loaded samples. To conclude, the same experiments were conducted with particles of different diameters and was clearly demonstrated that for higher CHTCs, small particles must be used. Some years after, Rafati et al. [53] tested three types of nanoparticles, namely Al_2O_3, TiO_2 and SiO_2, into a mixture of water and ethylene-glycol (EG) in different volume concentrations, to cool a processor with a commercial set. All nanofluids enhanced heat performance of the system, but higher heat transfer coefficients were obtained for Al_2O_3 nanofluid with 1 vol.%, allowing the processor temperature to a temperature decrease of 5.5ºC for maximum flow rate conditions.

1.4.2 Vehicle thermal management

Another widely investigated area where nanofluids could play an important and innovative role is the thermal management of vehicles. Cars, trucks, or any other vehicle possessing a thermal engine with effective cooling needs can be considered an acceptor of such improvements. Thermal efficiencies of most internal combustion engines are low and limited once a significant part of the chemical energy is lost during the conversion process as heat for the closest structures. Therefore, keeping engine components (cylinder, piston, head, block, etc.) in perfect working conditions becomes a crucial task that needs to be accessed and cooling them correctly is essential for an excellent performance. Otherwise, engines will be prone to suffer structural problems that could cause their failure in advance.

Looking to a common cooling system used in road vehicles, the *radiator* is responsible to promote the contact between the incoming air flow with a finned structured heated by the liquid coolant after it left the engine, rejecting the excessive heat. Generally placed in the front line of the vehicle, a radiator must have a sufficient contact area, in order to dissipate the correct amount of heat, but designers should be aware that the greater the frontal area, the higher the undesired drag force. Also, a high frontal area generally represents a large cooling system, adding extra weight to the vehicle and extra power consumption. Those are just obvious reasons why engineers are on the way to find more efficient radiators, but one of the biggest challenges faced are the poor thermal properties, especially thermal conductivity, exhibited by common liquid coolants, such as mixtures of water and EG [54]. It is precisely to overcome this obstacle that researchers have started to test nanofluids in existing systems like radiators.

Heris et al. [55] studied the performance of CuO nanoparticles suspended in a base fluid composed of water and EG, for different particle loadings, flow rates and inlet temperatures. The experimental setup simulates a typical cooling system present in every common vehicle. They reported enhancements in heat transfer at radiator, expressed by a higher Nu compared to base fluid, reaching 55% of augmentation, at maximum particle loading used. Authors also found that Nu is influenced by Re and inlet temperature, achieving higher values when both Re and inlet temperature are at their top values. Hussein et al. [56], in their turn, present a work where TiO_2 and SiO_2 were separately suspended in pure water, varying the flow rate, inlet temperature and particle concentration, with the objective of studying the heat performance of a car radiator under laminar flow. Forced convective enhancements were ob-

served in both cases, relatively to the base fluid solely, with SiO_2 nanofluids showing a Nu 22.5% higher, although it have increased with the three considered parameters.

Different from the previously presented case studies and applicable to vehicles and machinery in general, is the case where nanoparticles are added to engine or lubrication oils with the objective of increase their thermal performance. This will remove and spread heat in a more effective way, promoting a lower temperature distribution along the entire structure. An illustration of this approach was proposed by Tzeng et al. [57] in a study of a real four-wheel vehicle transmission system. Al_2O_3, CuO and antifoam were separately added to engine oil, with the goal of measure the temperature profile in the rotary blade coupling (part of the transmission system which needs to be protected from thermal stresses) for different rotation speeds. Authors could conclude that both oxide nanofluids were able to reduce the temperature measured for all range of speeds, with CuO revealing itself as the best additive. They also reported the cooling performance deterioration when antifoam-nanofluids were tested.

1.4.3 Solar energy technology

Solar energy conversion technology is clearly an up-to-date research subject all over the world. During the last decades and mainly because of the growing sense of environmental awareness, scientists have changed their focus to alternative sources of energy capable of reducing our dependence in fossil-fuel combustibles, in which solar energy is one of the most promising ones. With the purpose of collect and use/transform the incoming solar radiation, some equipments were developed, such as solar collectors or photovoltaic panels (PV) that nowadays are easily seen in many habitations, mainly thanks to the already mentioned environmental care from the population, but also due to welcomed government incentive programs. But knowledge and, consequently technology, are not steadily processes and research in those systems still represent an important slice of the whole effort put into solar energy field, with people always looking to possible enhancements even to well-established technologies like this.

One of the pointed aspects to improve is the poor absorptive properties exhibited by commonly used liquids in solar collectors, proven by a study in which Otanicar et al. [58] evaluated the optical properties of different liquids used in solar thermal energy systems. They concluded that water is the best absorbing fluid, but only capable of accumulating 13% of the incident radiation. This work has motivated another one in which Otanicar et al. [59] performed an experimental study using carbon nanotubes and nanoparticles of graphite and silver suspended in water, as a direct absorption solar collector (a simplification of the classic solar thermal collector), where the energy is directly absorbed by the fluid volume. As a complement, the same experiment was then numerically modeled with the model being used as a comparative source of data that generally matched well with experiments. Their findings were interesting, with improvements in collector's efficiency of around 5% when silver-nanofluid was used, especially for very small particle loadings. They also suggested some benefits of using nanofluids to directly absorb solar energy apart from the increase in absorption capacity, saying that this solution promotes a more uniform temperature profile which prevents some heat losses at the boundaries and that the collector's design could be improved by removing the black hot surface, no needed with this technique.

The performance of nanofluids in solar energy technology and some other examples of application can be consulted in specialized reviews, such as the one done by Mahian et al. [60], where a vast number of technological applications of nanofluids in solar energy was summarized. They report studies in common collectors for purposes of water heating, thermal energy storage or solar cells, but they also present some suggestions of future work in solar technology, as the case of PV panels or thermoelectric cells. Furthermore, difficulties in real applications are discussed, as well as the high costs in nanofluids production, which are pointed as a possible disadvantage.

1.5 Work description and objectives

Sections 1.2 to 1.4 can be seen as a *state-of-the-art* regarding nanofluids and we can extract interesting information while reading them. One fact clearly implied there is the controversy around nanofluids be, or not, heat transfer enhancement agents. This mainly occurs because some researchers have reported great improvements, while others showed deteriorations of the heat transfer process. We have already proved that thermal properties are sources of error and comparison basis can lead to misleading conclusions, still no final decision on nanofluid's topic seemed to be attained.

With the aim of help on the clarification of the effects that nanoparticles have on the CHTC of liquid coolants, researchers from Instituto Superior Técnico conceived and produced an experimental setup where an Al_2O_3-isopropanol nanofluid was tested [61]. The selection of such nanofluid, which they report to be stable and Newtonian under all the tested working conditions, intends to enlarge the options of non-water based nanofluids available on the literature [61].

The experimental setup consists in a closed duct circuit inside which the nanofluid flows, being then submitted to a constant heat flux supplied at the test section, a 2.4 m long circular tube, horizontally placed and with an internal diameter of 3.5 mm. A simple schematics of the experiment is available in figure 1.2. The setup was also equipped with a pump, a cooling unit to control the inlet temperature, a vacuum system to prevent ambient heat losses, a power supply and several measurement equipments, including those necessary to measure the needed thermophysical properties. Besides the setup validation, the set of tests consisted on measuring the pressure drop and wall and fluid temperatures along the tube to posteriorly calculate the friction factor and CHTC. Several samples loaded in different proportions were tested, as well as distinct inlet temperatures, mass flow rates and heat fluxes were contemplated. The experiments considered both laminar and turbulent fully developed conditions and were conducted under steady state [61].

In order to complement the described study, the present work reports a numerical simulation through the use of the commercial CFD code ANSYS-Fluent®. Our main goal is the application of a computational model based on the single-phase conventional approach which is able to correctly predict the experimental measurements or, at least, estimate them within a small range of error. To attain that, a mesh is built and checked its independence and, finally, the governing equations are numerically solved. Then, the produced results are compared with experimental ones and a proper analysis will be done, in order to conclude about the reliability of the model.

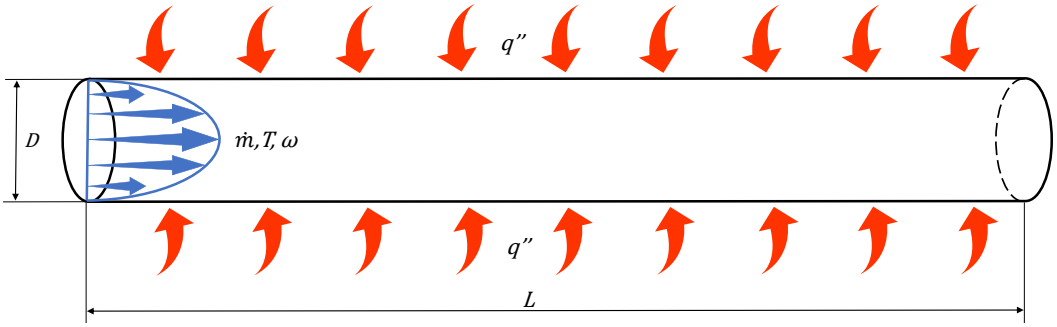

Figure 1.2: Schematics of the experiment.

Additionally, thermal properties effectively measured under the same working conditions are available in [61], allowing us to use them in the computational model and investigate the statements of Buschmann et al. [18] about consider a nanofluid as a homogeneous fluid. It is our intention to verify, or not, the validity of such considerations. We will also provide results on the comparison bases proposed by [17] and infer whether conclusions about the possible enhancement using nanofluids are in fact real, or just a fallacy.

To attain that, a thorough investigation of the numerical details of the solution methods of the governing equations has been done. Careful selection of available tools and their parameters is totally necessary for an accurate and trustworthy solution. Thus mesh, discretization schemes, empirical models or even solution algorithms were exploited to understand their role on the computational process, with substantial information provided, including official informations available on solver's manuals. Justifications were presented whenever necessary to demystify any possible doubt. In the end, we intend to have created a useful tool, capable to produce solid information on the topic, throughout which we expect to reach our proposed aims. If conclusions turn out to be contrary to those expectable, at least we have in mind to conclude about the inefficacy of the assumptions followed.

1.6 Thesis outline

The body of this document is divided into five main chapters, each one with sub-divisions where related topics are addressed. A brief description of what is discussed there is coming next.

Introduction: is in the present chapter we introduce the main topics about nanofluids in general. It starts by giving a view of the global energetic panorama, then goes through nanofluids' preparation methods, concerns, special abilities and review some of the investigation done on the field, ending with a presentation of some of the possible applications to such fluids. Based on some inconsistencies pointed during this exercise, the description and objectives of the present work receive a pride of place in this chapter.

Matemathical modeling: this chapter is where the mathematical formulation, in which this work is supported, is presented. There, one can find every single equation describing the involved physical processes.

Numerical investigation: is where the all information about the numerical solving procedure is avail-

able. Several aspects of the solution method including numerical methods, information about the solver and the boundary conditions employed are available here. It is then complemented with a sub-chapter dedicated to mesh independence and other to model validation.

Results and discussion: as the name states, this chapter is dedicated to the presentation of the obtained results with respective interpretation and discussion.

Conclusions: is in the last chapter where the main conclusions are gathered and listed, finishing with some suggestions for future work.

Chapter 2

Mathematical modeling

2.1 A nanofluid as a homogeneous fluid: the conventional approach

As described along the previous chapter, one of the aims of this thesis is to investigate how accurate is modeling a nanofluid as it behaves like a common fluid. With this assumption, it is desired to simplify the complexity of having to deal with a two-phase flow. It means all the special treatment we need to have to correctly reproduce what is physically happening and also the additional computational effort required to perform such numerical simulations. If a nanofluid could be, with satisfactory accuracy, modeled as an ordinary liquid with altered properties, therefore a set of simple, well-established and no excessive time-consuming tools are already available and might be of great utility.

Considering a nanofluid like a pure fluid does not ignore that it is actually a mixture of solid and fluid particles. In fact, such influence will be accounted by the computation of new thermal properties, called *effective properties*, that will consider their presence, either beneficial or not. This basically represents the main idea of the single-phase conventional approach, which is supported by two main assumptions. First, as the particles are usually very tiny ($<$100nm) and in very low concentrations, we can presume they mix efficiently with the surrounding fluid. This holds up the first assumption, which says that no slip velocity exists among solid and fluid particles within the flow. The other assumption is to consider that both phases co-exist in such a way that the condition of thermal equilibrium is verified [21].

So, if a nanofluid can be considered a pure fluid with altered properties, would it be governed through the same laws? It makes sense to assume that, so we dedicate this chapter to present of all the theoretical background needed to support this hypothesis.

2.2 Governing equations for fluid flow with heat transfer

Before writing any equation, it is important to briefly explain an assumption where all the upcoming theory is based. To derive those equations, it was admitted that the fluid could be treated as a *continuum*, and

this means that, macroscopically, the fluid is considered to be continuous, even if in a microscopic scale it is composed by separate molecules. This assumption allows to split the domain into several *elements of fluid* so small that all macroscopic properties (function of space and time) are there defined as representing the mean value of a set of molecules enclosed by the imaginary boundaries of a *control volume* larger than the molecular scale, giving us the possibility to neglect any molecular effect.

Based on the assumption described above, let us consider an infinitesimal and fixed control volume where, instantaneously, an element of fluid was located. Then, employing mass, momentum and energy balances, we will reach the governing equations for fluid flow. All the following reasoning is available in books like [62] or [63].

2.2.1 Mass conservation: the continuity equation

Every conservation law is characterized by the equality among the variation rate of the property itself and the net value resulting from the balance between the amount of property that enters, leaves or is generated inside the control volume. As expected, mass conservation law obeys to this generic rule and may be expressed as the equality among the temporal rate of increase of mass and the net mass that cross the boundaries of the control volume. This is the mathematical description of the physical principle which says that any mass can be lost. So, balancing all the mass flows crossing the boundaries and matching to the temporal variation of mass in the volume, after some math we end up reaching what is called the *continuity equation* in its more general vectorial form of

$$\frac{\partial \rho}{\partial t} + \nabla \cdot (\rho \mathbf{u}) = \mathbf{0} \tag{2.1}$$

in which ρ means the fluid *density* (or mass per unit volume) and $\mathbf{u}$ represents the velocity vector. This equation can be easily simplified if we adapt it to our problem, by means of including physical considerations. Regarding our case study represented by a liquid flowing in a pipe, the condition of *incompressible flow* may be used. It basically states that the changes in fluid density are almost null or negligible with respect not only to time but also to space, turning density as a constant property all over the flow. This assumption is particularly true for liquid flows once the velocities involved are in general really small compared to the speed of sound. This eliminates all the partial derivatives where ρ appears and equation 2.1 reaches the following form for incompressible flows.

$$\nabla \cdot \mathbf{u} = \mathbf{0} \tag{2.2}$$

2.2.2 Momentum conservation: the Navier-Stokes equations

Momentum conservation reflects the well-known *Newton's second law of motion* which states that the rate of change of momentum in a body is equal to the summation of all forces acting on it. Forces acting in a fluid particle can be of two types: *body forces* and *surface forces*. The first group represent forces that the whole mass would "feel" due to external force fields present in the environment. In our case only gravitational field matters. The second one is related to stresses occurring on the surfaces of the

fluid elements originated by distortions as a result of the interaction between neighboring fluid elements while flowing, or from a *hydrostatic* pressure field, p.

Contrasting with the hydrostatic pressure field which is easily characterized by a diagonal tridimensional tensor, the *viscous stress* (or *deviatoric stress*) tensor, $\boldsymbol{\tau}$, has six independent and unknown stresses beforehand. However, ignoring how these stresses would be evaluated, is possible to balance them because we know where they act and how many they are. So, while flowing, elements of fluid are subjected to gravity acceleration, $\mathbf{g}$, and to pressure and viscous effects, appearing the vectorial momentum balance equation as

$$\rho \frac{D\mathbf{u}}{Dt} = \rho\mathbf{g} - \nabla p + \nabla \cdot \boldsymbol{\tau} \tag{2.3}$$

Equation 2.3 is valid without restrictions and $D\mathbf{u}/Dt$ represents the element of fluid acceleration written into its *material derivative* form, where the convective contribution are already included. The remaining contributions appear in the right hand side, all dimensionally classified as forces per unit volume (N/m^3).

Apparently, no relation exists among viscous stresses and the velocity vector, the primary variable of equation 2.3. However, for many fluids, it was noted the existence of a linear relationship between the components of the deviatoric tensor and the spatial gradients of the velocity vector. Such fluids are referred to as *Newtonian* and the constant of proportionality of this model is the well-known *dynamic viscosity*, μ. Thus, considering an isotropic fluid, the six independent viscous stresses are computed by means of

$$\boldsymbol{\tau} = \mu\left(\nabla\mathbf{u} + (\nabla\mathbf{u})^T\right) - \frac{2}{3}\mu\left(\nabla \cdot \mathbf{u}\right)\mathbf{I} \tag{2.4}$$

in which $\mathbf{I}$ the *Identity tensor*. Note that the second term of the right-hand side represents the effect of volumetric deformations, being null for incompressible fluids.

The introduction of this model into equation 2.3 allows the replacement of the viscous stress terms by their dependence on the spatial velocity gradients. We are now in presence of the *Naver-Stokes equations*, the governing equations for Newtonian fluid flow.

$$\rho \frac{D\mathbf{u}}{Dt} = \rho\mathbf{g} - \nabla p + \nabla \cdot \left[\mu\left(\nabla\mathbf{u} + (\nabla\mathbf{u})^T\right)\right] \tag{2.5}$$

2.2.3 Energy conservation: the energy equation

There are several forms of expressing the first law of Thermodynamics but its general meaning remains unchanged. This widely known law states that, given a system, its energy variation must equalize the amount of heat that crosses its borders, plus the amount of work delivered by or to the system, during a time interval. In other words, no energy is generated or lost during any process, on the contrary, the variation of the total energy of a system reflects only the heat and work exchanges with its neighborhood.

Considering again the same infinitesimal element of fluid and neglecting radiative contributions, only the thermal gradients may induce heat fluxes across the element boundaries. These are well described by the *Fourier's law* for heat conduction, expressed as

$$\mathbf{q}'' = -k\nabla T \tag{2.6}$$

where T is the temperature and k means the *thermal conductivity*. The negative sign on the gradient reflects that heat flows from high to low temperatures.

For an element of fluid subjected to pressure and viscous forces while flowing, the rate of work done assumes the form of the divergence of the dot product between the components of the hydrostatic and deviatoric stress tensor with the velocity vector, with units of [W/m^3]. Thus, the contribution from the shear forces for the total work done is

$$\dot{W}_v = \nabla \cdot (\mathbf{u} \cdot \boldsymbol{\tau}) = \mathbf{u} \cdot (\nabla \cdot \boldsymbol{\tau}) + \Phi \tag{2.7}$$

where Φ represents the *dissipation function*, equal to

$$\Phi = \mu \left[2\left(\frac{\partial u}{\partial x}\right)^2 + 2\left(\frac{\partial v}{\partial y}\right)^2 + 2\left(\frac{\partial w}{\partial z}\right)^2 + \left(\frac{\partial u}{\partial y} + \frac{\partial v}{\partial x}\right)^2 + \left(\frac{\partial u}{\partial z} + \frac{\partial w}{\partial x}\right)^2 + \left(\frac{\partial v}{\partial z} + \frac{\partial w}{\partial y}\right)^2 \right] \tag{2.8}$$

Note that the equality 2.7 is only valid for Newtonian fluids and symmetric tensors, like the deviatoric one, where the condition of static equilibrium needs to be satisfied. The work done by the pressure forces can be computed similarly, although due to the simpler nature of the hydrostatic field compared to viscous stresses, it is resumed to

$$\dot{W}_p = \nabla \cdot (p\mathbf{u}) \tag{2.9}$$

By now we have presented all the relations needed for the energy balance we want to perform, but understanding if such quantities are entering or leaving the system is crucial. We will adopt the convention of setting as positive the heat that is transferred into the system and as negative the work done on the system. If we consider heat as entering, the pressure forces performing work on the element of fluid and viscous forces delivering work to the surroundings, dissipating energy, the differential *energy equation* of a Newtonian fluid is

$$\rho \frac{De}{Dt} = -\nabla \cdot \mathbf{q}'' - p(\nabla \cdot \mathbf{u}) + \mathbf{u} \cdot (\nabla \cdot \boldsymbol{\tau}) + \Phi \tag{2.10}$$

where $e = i + \frac{1}{2}(u^2 + v^2 + w^2) + g\Delta z$ is the specific *total energy* of the system, the summation of the specific *internal energy*, i, plus the kinetic and potential energies.

Intensive properties like specific enthalpy are more often object of interest than total energy, so it has become usual to rearrange equation 2.10 as a function of those quantities. Still, it is the temperature that gives the most valuable contribution to this study, since temperature profiles are important sources of information. From equation 2.10, it is possible to derive a similar transport equation for i, which can be related to the specific enthalpy applying a convenient thermodynamic relation. Considering the fluid as an incompressible liquid, a relationship between specific enthalpy and temperatureis is also known from the thermodynamics, by means of the *specific heat* at constant pressure, c_p. Condensing all this information into equation 2.10 and rearranging, we finally obtain

$$\rho c_p \frac{DT}{Dt} = \nabla \cdot (k \nabla T) + \Phi \tag{2.11}$$

2.2.4 Conservation equations for nanofluids: Boungiorno's formulation

The presence of nanoparticles whitin a fluid flow greatly complicates its modeling due to additional phenomena that needs to be accounted. Faced with this problem, Buongiorno [14] created a model including several aspects of this interaction, but in a simplified process, once he complemented the conservation equations for pure fluid with contributions from the real two-phase flow. The result was a non-homogeneous model with modified transport equations, plus a continuity equation for nanoparticles.

As stated in section 1.2.2, the two mechanisms responsible to promote slip among liquid and solid particles have been identified to be Brownian motion and thermophoresis. Following this idea is logical that if a diffusive flux of particles relatively to fluid exists, it would be governed by these two mechanisms, in the absence of turbulence. Thus, such mass flux would be equal to

$$\mathbf{j} = \mathbf{j}_B + \mathbf{j}_T = -\rho_{np} \left(D_B \nabla \phi + D_T \frac{\nabla T}{T} \right) \tag{2.12}$$

where ϕ represents the *particle volume concentration* and D_B and D_T the diffusive coefficients regarding Browninan motion and thermophoresis, respectively. Particles can now be balanced by matching its temporal rate of change of their concentration to respective convective and diffusive transport, once we are not in presence of chemical reactions. The resultant transport equation is then

$$\frac{D\phi}{Dt} = \nabla \cdot \left(D_B \nabla \phi + D_T \frac{\nabla T}{T} \right) \tag{2.13}$$

As one may know, mass fluxes have associated the transport of thermal energy carried by the particles while moving. Then, there is an extra heat flux that must be added to the heat flux vector, $\mathbf{q}''$, representing the energetic contribution of the mass income. The modified heat flux vector is

$$\mathbf{q}'' = -k_{nf} \nabla T + h_{np}\, \mathbf{j} \tag{2.14}$$

where h_{np} represents the specific enthalpy of the solid nanoparticles. The same mass fluxes origin a new term into the energy equation, accounting for the rate of variation of energy due to nanoparticles diffusion. Assuming as valid the derivation of equation 2.11, the new energy equation for a nanofluid is

$$\rho c_{p,nf} \frac{DT}{Dt} = -\nabla \cdot \mathbf{q}'' + h_{np} \nabla \cdot \mathbf{j} + \Phi \tag{2.15}$$

which, after the incorporation of equation 2.14 and some algebra, turns into

$$\rho c_{p,nf} \frac{DT}{Dt} = \nabla \cdot (k_{nf} \nabla T) + (\rho c_p)_{np} \left(D_B \nabla \phi + D_T \frac{\nabla T}{T} \right) \nabla T + \Phi \tag{2.16}$$

Equation 2.16 represents the energy balance applied to a Newtonian, incompressible and non-reactive nanofluid.

Mass and momentum balances are quite simple to consider. Due to the homogeneous movement of solid and fluid particles, the velocity field is shared among phases, which implies that continuity and

Navier-Stokes equations (equations 2.2 and 2.5) are suited for the purpose, although with effective properties. Joining them with equations 2.13 and 2.16 is enough to describe a dilute nanofluid flow.

This model has served as basis to several studies along the previous years, including the two recent works of Buschmann et al. [18] and Myers et al. [64], which present useful information to simplify our problem. Their results for dilute mixtures strongly support the idea of the role played by Brownian motion and thermophoresis to be considerably small when compared to traditional diffusion mechanisms. So, at least as first hypothesis, they can be neglected without considerable loss of information. Moreover, during our simulations we intend to keep constant the particle concentration, assuming a perfect homogeneity inside the nanofluid flow. Therefore, there is no need to solve equation 2.13.

Equations 2.2, 2.5 and 2.11 represent a system of five equations for five unknowns (u, v, w, p and T) that allow us to solve a pure fluid flow. Based on what was discussed above, one can justify its usage to model a dilute nanofluid flow, where the only modification resides on the altered thermal properties.

2.3 Basic notions on internal flows

Introduced the governing equations for general fluid flow with heat transfer, we will focus now on the real problem treated in this study, a fluid flow inside a heated circular tube. All the following mathematical treatment is available in [65], but few local referred cases.

2.3.1 Fully developed flows: hydrodynamic considerations

Before any discussion, let us first introduce one of the most valuable and widely used dimensionless parameters – the *Reynolds number*. It is defined as

$$Re = \frac{\rho U L}{\mu} = \frac{U L}{\nu} \tag{2.17}$$

where L is a characteristic length (usually the diameter D in pipe flows), U a characteristic velocity and ν is the *kinematic viscosity*. It is an essential parameter to characterize the flow regime, with $Re = 2300$ being usually the frontier between laminar and transition to turbulent regime for pipe flows. It can also be seen as the ratio of inertia to viscous forces and evolutions of flow quantities as its function are quite popular among the heat transfer and fluid dynamics community.

The *mean velocity*, u_m, is defined as a velocity that multiplied by the density and the cross-sectional area of the tube, A_c, yields the *mass flow rate*. In its turn, the mass flow rate can be given by the two subsequent expressions

$$\dot{m} = \rho u_m A_c = \int_{A_c} \rho u \, dA_c \tag{2.18}$$

in which u represents the the axial velocity. This flow has the particularity of having an analytical solution for the velocity profile, being one of the few known solutions of the Navier-Stokes equations. For those reasons, it is recognized and usually called by *Hagen-Poiseuille flow* and its velocity profile is

represented by

$$\frac{u}{u_m} = 2\left[1 - \left(\frac{r}{R}\right)^2\right] \tag{2.19}$$

While flowing inside a duct, due to friction effects, the fluid is subjected to a diminution of its energy reflected in terms of a *pressure drop*. This quantity is usually a required parameter in internal flow problems, once it is related to the energy we need to supply to the fluid to guarantee its continuous movement. It is possible to compute this pressure loss using directly the *Bernoulli equation*, however it may become advantageous calculate it adopting other type of procedure that involves another dimensionless parameter – the *Darcy friction factor*. It may be seen as a non-dimensional pressure drop, with the definition of

$$f \equiv \frac{-(dp/dx)D}{\rho u_m^2/2} \tag{2.20}$$

In the case of fully developed laminar flows, this leads to

$$f = \frac{64}{Re_D} \tag{2.21}$$

and should not be mislead with the *skin friction coefficient*, C_f, given by

$$C_f = \frac{\tau_w}{\rho u_m^2/2} \tag{2.22}$$

It is perceptible the existence of a close relationship between the pressure drop and the friction factor, and this leads us to assume that knowing one, the other can be computed as well. Thus, the pressure drop of the flow is given by the integration over the total length of the pressure gradient and, logically, results in

$$\Delta p = \int_{x_1}^{x_2} f \frac{\rho u_m^2}{2D}\, dx \tag{2.23}$$

Regarding fully developed turbulent flow, the role played by turbulence turns the problem much more complicated from the mathematical point of view. It will be seen in chapter 2.4 that, when dealing with turbulence, the instantaneous velocity field will be replaced by a mean velocity field, U, a more appropriate quantity for calculation purposes, plus a fluctuating contribution. No analytical solution is known for this mean field, instead, experimentation shows that it is accurately approximated by

$$\frac{U}{U_{max}} = \left(1 - \frac{r}{R}\right)^n \tag{2.24}$$

where $n = 1/7$ works fairly well [62]. Equation 2.24 reproduces the typical flatter profile exhibited in turbulent pipe flows, a direct result of an increased mixing capacity verified inside the turbulent boundary layer. Similarly to laminar case, it is possible to associate the *average mean velocity*, U_{avg} (computed from $\dot{m}$), with the *maximum mean velocity*, U_{max}, using the definition of mass flow rate presented in equation 2.18 and equation 2.24, like [62]

$$\frac{U_{avg}}{U_{max}} = \frac{2}{(n+1)(n+2)} \tag{2.25}$$

With respect to pressure drop, the only difference resides on the friction factor computation, once in turbulent flow there is no exact equation for it. It was discovered that this parameter not only depends on the Re, but also on the surface roughness, e. Experimentation gave then origin to the *Moody diagram*, a chart where the friction factor is plotted as a function of the Re and the dimensionless roughness, for diverse flow and surface conditions. An alternative is to use the *Colebrook equation*, an implicit equation that accurately correlates data from the Moody diagram as follows

$$\frac{1}{\sqrt{f}} = -2\log\left(\frac{e/D}{3.7} + \frac{2.51}{Re_D\sqrt{f}}\right) \tag{2.26}$$

2.3.2 General approach for convection problems

Introduced the basic principles of the fluid mechanics of internal flows, it is now time to focus on the heat transfer process and its particularities. As in the majority of heat transfer problems involving fluid organized motion, *convection* is the responsible mechanism for the heat flow that occurs in the presence of a temperature gradient due to, for instance, a heated wall. On flows near solid walls, it is known from the fluid mechanics the formation of a *hydrodynamic boundary layer* closer the solid-fluid interface, however when this phenomenon is conjugated with a temperature gradient, a *thermal boundary layer* starts to be developed as well. This thermal layer, although might co-exist with the hydrodynamic one, does not have necessarily to grow at the same rate, since besides the obvious velocity effect, its growing rate is also influenced by the rates of energy and momentum diffusion. It is what is behind the following empiric equation

$$\frac{\delta}{\delta_t} \approx Pr^n \tag{2.27}$$

where δ and δ_t are, respectively, the hydrodynamic and thermal boundary layers thicknesses, n a positive exponent and Pr the *Prandtl number*, defined as

$$Pr = \frac{\nu}{\alpha} = \frac{c_p\,\mu}{k} \tag{2.28}$$

where α is the *thermal diffusivity*. This dimensionless number relates the diffusion coefficients of momentum and energy, evaluating the effectiveness of both transports inside their respective boundary layers. It is assessed using exclusively properties of the fluid, which made it a property as well.

The heat transferred by convection is intimately linked to bulk fluid motion in the upper zones of the thermal boundary layer and is ruled by random movements of molecules near the solid zones where the velocity is very small, due to the no-slip condition. At the wall the velocity is null, so the heat flow is exclusive ruled by the *conduction* mechanism, a diffusive process. Convection has, in fact, a contribution from heat diffusion, however it is possible to macroscopically define the convective process employing the following equation

$$q'' = h(T_s - T_\infty) \tag{2.29}$$

where q'' is the convective heat flux, T_s the surface temperature and T_∞ the fluid temperature. This equation is widely known as *Newton's cooling law* and incorporates a vital parameter when dealing

with convection – the *convective heat transfer coefficient*, h. This very important quantity resumes in its computation many convection problems and is many times object of optimization in thermal equipments, once it is directly related to the transferred heat rate. Nevertheless, it represents sometimes a difficult quantity to find, as this empirical coefficient depends on many variables like the geometry of the flow and the properties of the fluid, and evaluating all the contributions may become a hard task to complete.

Due to the nature of the thermal transport in the solid-fluid interface, conduction rules the heat transfer process and the Fourier's law can be employed. Considering no losses, r as the radial direction and the tube wall placed at $r = R$, the heat conducted to the fluid is given by

$$q'' = -k_f \left.\frac{\partial T}{\partial r}\right|_{r=R} \tag{2.30}$$

in which k_f is the fluid's thermal conductivity. This amount of heat must equalize the one transferred into the boundary layer, expressed by equation 2.29, so combining these two equations we achieve to an expression for h equal to

$$h = \frac{-k_f \partial T/\partial r|_{r=R}}{T_s - T_\infty} \tag{2.31}$$

From equation 2.31 we can see the influence that the thermal boundary layer has on h and, consequently, on the amount of heat transferred. The radial temperature gradient changes with the axial direction since heat transfer is occurring and this dependence on the axial position within the thermal boundary layers lead us to introduce the concept of *local convection coefficient*. If we intend only to consider global values over an entire surface of area A_s, it is possible to define an *average convection coefficient* as

$$\overline{h} = \frac{1}{A_s} \int_{A_s} h \, dA_s \tag{2.32}$$

We have now, by means of equation 2.31, a possible methodology to achieve our goal of estimating h. Still, is not the usual way to do that, and we should understand why. First, dealing with temperature derivatives presume a beforehand known temperature profile, which in most cases does not happen. Then, the great number of parameters influencing h suggests a creation of an alternative method, obtained introducing non-dimensional variables into the respective transport equations and normalizing them. This mathematical operation gives rise to the appearance of a dimensionless energy equation, simplified on the light of boundary layer theory, that has as *similarity parameters* the already mentioned Re and Pr. It has revealed to be a smart modification, once it gives us the possibility of extrapolating results to other *geometrically similar surfaces* experiencing different velocities, length scales and fluids, as long as similarity parameters and dimensionless boundary conditions are the same. Thanks to these normalized variables, is possible to define a non-dimensional thermal gradient over the solid-fluid interface using equation 2.31 which will be of great utility. The *Nusselt number*

$$Nu = \frac{hL}{k_f} \tag{2.33}$$

where L means again a characteristic length, can be seen as the ratio of convection to pure conduction heat transfer and, once known for a given geometry, make possible the computation of h. The knowledge

of Nu provides a solution for the convection problem based on a much less dependent procedure, because it only depends on position, Re and Pr. A similar expression to equation 2.32 may be interesting when the position dependence is not considered and only an *average Nusselt number* is required.

2.3.3 Thermal considerations

Internal flows, due to their nature, have from the analysis point of view the incapacity of defining a reference velocity, like the free stream one, and this represents the major necessity of defining a mean velocity. The same happens when temperature is the object of interest, so a *mean temperature*, T_m, needs to be defined as well. Equivalently to the hydrodynamic case, is possible to compute an average temperature that multiplied by the mass flow rate and specific heat can give the rate of sensible energy carried by the fluid. Considering this, the definition of T_m is

$$T_m = \frac{\int_{A_c} \rho c_p u T \, dA_c}{\dot{m} c_p} \tag{2.34}$$

It has a major importance when using, for instance, equation 2.29 for h computation. As no reference temperature can be defined for internal flows, the mean temperature overcomes this problem providing a reliable value that reflects the whole radial profile into one single value.

As said in section 2.3.2, the assessment of Nu is a key factor when dealing with convective heat transfer. Due to the geometry dependency, many types of different flows started to be analyzed with the goal of obtaining their own Nu functions. The laminar fully developed flow inside an uniformly heated circular tube was one of the first to be addressed and, as the exact velocity profile is known, it could be analytically investigated using a proper non-dimensional form of the energy equation.

The introduction of the concept of *thermally fully developed flow* can lead to interesting conclusions. Contrarily to the hydrodynamic case, this definition does not imply a constant temperature profile, since as long as convection exists, both $T(r)$ and its longitudinal gradient are always changing with the axial position, x. What actually remains unchangeable is the difference between wall and mean temperatures, revealing an axially independent h characteristic of a thermal developed flow. The previous conclusion can be corroborated with the analytical result obtained for Nu considering both hydro and thermal developed conditions. Skipping the math, it can be proven that for a constant-property and fully developed laminar flow, the Nu is constant and equal to

$$Nu_D = 4.364 \tag{2.35}$$

However, for laminar flows with fluids less permeable to heat diffusion (large Pr), the thermal entry length revels to be a significant fraction of the entire length and its presence cannot be neglected. Accounting with this entrance region turns the problem a generalization of the previous formulation and more complex from the mathematical point of view. Once solved the non-dimensional partial differential energy equation, their analytical solutions are in form of infinite series, including the solution for the local Nu, as seen in [66]. Nevertheless, it is not practical to work with infinite series, reason why those results

were correlated for a constant heat flux boundary condition via [67]

$$Nu_D = \begin{cases} 1.302x_*^{-1/3} - 1 & \text{for } x_* \leq 0.00005 \\ 1.302x_*^{-1/3} - 0.5 & \text{for } 0.00005 < x_* \leq 0.0015 \\ 4.364 + 8.68(1000x_*)^{-0.506}\exp(-41x_*) & \text{for } x_* > 0.0015 \end{cases} \tag{2.36}$$

where $x_* = (x/D)/(Re_D Pr)$ is a dimensionless axial distance. Note that when $x_* \to \infty$, equation 2.36 logically degenerates into equation 2.35.

Regarding turbulent flow, a correlation initially developed for smooth pipes seems to work fairly well also for rough ones since f was computed from equation 2.26. The *Gnielinski equation* is expressed as

$$Nu_D = \frac{(f/8)(Re_D - 1000)Pr}{1 + 12.7(f/8)^{1/2}(Pr^{2/3} - 1)} \tag{2.37}$$

and applicable for $0.5 \leq Pr \leq 2000$ and $2.3 \times 10^3 \leq Re_D \leq 5 \times 10^6$, including thus the transition region [67]. It is embracing enough to contemplate either constant wall temperature and constant wall heat flux cases. For the use of equation 2.37, thermal properties must be evaluated at T_m.

2.4 Modeling turbulence

It is known among the community that the majority of the flows in engineering are, in fact, turbulent, but while laminar flows can be correctly predicted using the Navier-Stokes equations presented in chapter 2.2, turbulent flows do not. They are characterized by a random and chaotic movement of fluid particles triggered by the amplification of small disturbances within the flow that gave rise to the appearance of typical rotational structures called *eddies*. Such disorganized movements provides always a three-dimensional aspect and an increased transport and mixing capacity to turbulent flows.

The *transition to turbulent regime* is an unclear process yet but, for pipe flows, experiments have shown that transition occurs for Re_D among 2000 and 10^5. However, it was noticed that exterior factors like pressure gradient and wall roughness influence the way transition occurs.

The energy spectrum of turbulent flows reveals important features about them as well. It shows that most of the energy content is placed within the largest eddies, which means they are the entities that rule the dynamics of the flow. A dissipative nature is associated to the smallest eddies, once their tiny dimensions and velocities (and consequently Re) reveals more accentuated viscous effects.

But how does this kinetic energy go from the larger to the smaller eddies? The presence of velocity gradients in the mean flow (concept introduced in a shorter time) promotes distortions on the larger eddies, in a process of deformation called *vortex stretching*, which is also responsible to supply the energy needed to maintain turbulence. As these eddies are predominantly inviscid, its angular momentum is conserved, which forces the surrounding smaller eddies to rotate faster and increase their kinetic energy. The *energy cascade* goes on until the smaller scales are reached and viscous dissipation became relevant, where the remaining kinetic energy is converted into internal energy (heat).

The materials presented during this chapter can be consulted in [68], as well as further information.

2.4.1 The RANS equations

The totally chaotic and disorganized movement of fluid particles induced by turbulence produces a set of fluctuations that makes an instantaneous measurement of a flow quantity (say velocity, pressure, etc.) an extremely complex signal, where fluctuations are strongly present. So, it is usual to start by decomposing all instantaneous flow quantities into their mean value, plus a fluctuating component, like

$$\theta(\mathbf{r},t) = \Theta(\mathbf{r}) + \theta'(\mathbf{r},t) \tag{2.38}$$

where θ represents a generic quantity, either a scalar or a vector. This statistical procedure, valid for statistically stationary turbulent flows, is known as *Reynolds decomposition*. The *mean value* is computed as

$$\Theta(\mathbf{r}) = \frac{1}{\Delta t}\int_0^{\Delta t} \theta(\mathbf{r},t)dt \tag{2.39}$$

where Δt is a large enough time interval (to include the slowest variations from the largest eddies). By definition, the mean value of a fluctuation θ' is zero. Other two valuable statistical operators are the *variance* of a fluctuation around its mean value, expressed by

$$\overline{(\theta')^2}(\mathbf{r},t) = \frac{1}{\Delta t}\int_0^{\Delta t} (\theta')^2(\mathbf{r},t)\ dt \tag{2.40}$$

and its *root mean square* (rms) value, defined as

$$\theta'_{rms} = \sqrt{\overline{(\theta')^2}(\mathbf{r},t)} \tag{2.41}$$

Supposing that $\theta = \mathbf{u}$, the first one gives a measure of the energy carried by the fluctuations and makes possible the definition of a quantity very useful in engineering calculations called *turbulent kinetic energy* (per unit mass), like

$$\kappa = \frac{1}{2}\left(\overline{u'^2} + \overline{v'^2} + \overline{w'^2}\right) \tag{2.42}$$

The second one represents the average magnitude of velocity fluctuations and is valuable for the computation of the *turbulence intensity*, an important quantity in turbulent flows equal to

$$I = \frac{u'_{rms}}{U_{avg}} \tag{2.43}$$

Navier-Stokes equations rule any kind of Newtonian fluid flow, however the Reynolds decomposition introduces some additional terms that come from the mathematical treatment of replacing the instantaneous vectorial quantities by their Reynolds decomposition. After some considerable algebra, we finally achieve to what are commonly called the *Reynolds-averaged Navier-Stokes (RANS) equations*.

$$\nabla \cdot \mathbf{U} = 0 \tag{2.44a}$$

$$\rho\frac{D\mathbf{U}}{Dt} = \rho\mathbf{g} - \nabla P + \nabla\cdot\left[\mu\left(\nabla\mathbf{U} + (\nabla\mathbf{U})^T\right) - \rho\overline{\mathbf{u}'\mathbf{u}'}\right] \tag{2.44b}$$

These are the governing equations of turbulent flows, in which six new unknowns dimensionally equivalent to stresses appear, called the *Reynolds stresses*. The transportable property is now the mean velocity vector, so these apparent stresses can be seen as the fluctuations' influence on the mean flow.

Regarding the energy equation 2.11, where the transportable property is the temperature, T, if we follow the same procedure, the *time-averaged energy equation* appears as

$$\rho\frac{D\mathcal{T}}{Dt} = \nabla\cdot\left(\frac{k}{c_p}\nabla\mathcal{T} - \rho\overline{\mathbf{u}'T'}\right) + \frac{\Phi}{c_p} \tag{2.45}$$

2.4.2 Turbulence model

The arising of the *Reynolds stress tensor*, $\boldsymbol{\tau}^R$, originated six new quantities, totally unknown a priori, that must be estimated in order to close the problem. Such necessity promoted the advent of turbulence models, being two-equation models like $\kappa-\omega$ and $\kappa-\varepsilon$ popular methods to close the RANS equations system. Despite the solution for the mean flow only, their sufficiently accurate results and low computational requirements make them the most used worldwide.

In a flow with straight geometry and without adverse pressure gradient, swirl, recirculating zones or compressibility effects, any two-equation model should be able to reproduce turbulence effects with satisfactory quality. Still, we have to select one, but which one is better for our purposes? We believe there is no correct answer for that due to the simple character of our flow. There are quite a few available models and some of them are more suited for some conditions than others, but there is nothing specifically in our problem that points to one model and discards another.

Due to its popularity, standard $\kappa-\varepsilon$ model would be seen as a strong hypothesis. It uses the turbulent kinetic energy, κ, to set a characteristic velocity and the *dissipation rate* (destruction of kinetic energy per unit mass), ε to define a length scale. Its good performance is properly documented for numerous industrial flows and its robustness and economy are very appreciated [22]. As weakest points, standard $\kappa-\varepsilon$ model assumes fully developed turbulence and is not valid in the near-wall region, which is a strong drawback. Instead, it offers the possibility to use *wall functions* to make the bridge between wall and turbulent core zones, but this treatment is only valid at high Re. Despite this, the application of those wall functions or even a two-layer approach to resolve the entire near-wall zone is strongly dependent on the *non-dimensional wall distance*, y^+, to produce coherent results, which turns the model greatly dependent on the mesh too [22].

Such y^+ dependence can be extinguished if we consider the *specific dissipation rate* (or turbulence frequency), ω, instead of ε, using a $\kappa-\omega$ model. Since $\omega=\varepsilon/\kappa$ and at a smooth wall we have $\kappa=0$, then $\omega\to\infty$ there. In practice, and accounting for possible rough walls, specific numerical values of κ and ω are imposed to allow the resolution of the entire boundary layer [22]. This is a special feature of all $\kappa-\omega$ models, but standard in particular is very sensitive to κ and ω on the far field, motivating researchers to try some improvements on it. Thus, and recognizing that such dependency was not verified in standard $\kappa-\varepsilon$, *Shear Stress Transport (SST)* appears as the most successful variation of the initial $\kappa-\omega$ model. Basically, SST $\kappa-\omega$ is a hybrid model that incorporates the good near-wall performance of its ancestor and gradually changes to standard $\kappa-\varepsilon$ in fully turbulent region, adopting its good performance there.

Based on this, we believe it is the right model for our purposes.

Coming back to what triggered this discussion, the Reynolds stresses appearance, within this class of two-equation models there is a simplistic but very popular way to model them. Recognizing the limited complexity involved, the simplest way to compute Reynolds stresses is assuming, like in laminar flow, they are proportional to the strain rate. This is known as the *Boussinesq hypothesis* and states that

$$\boldsymbol{\tau}^R = -\rho\overline{\mathbf{u}'\mathbf{u}'} = 2\mu_t\mathbf{S}\cdot\mathbf{S} - \frac{2}{3}\rho\kappa\mathbf{I} \tag{2.46}$$

where $\mathbf{S} = \frac{1}{2}\left(\nabla\mathbf{U} + (\nabla\mathbf{U}^T)\right)$ is the *mean strain rate* and μ_t is the *turbulent* (or *eddy*) *viscosity*, concept created assuming that Reynolds stresses affect flow quantities in such a way it can be described by an additional viscosity, larger and property of the flow, in analogy with molecular viscosity. However, this hypothesis considers an isotropic eddy viscosity and, consequently, isotropic Reynolds stresses, which for most of the flows is not true. Still, it works nicely for a great number of studied flows [22].

SST $\kappa-\omega$ model provides two extra transport equations plus a turbulent viscosity formulation to close RANS system. With a hybrid nature, κ-equation comes directly from the standard $\kappa-\omega$ model while ω-equation is obtained transforming the ε-equation of $\kappa-\varepsilon$ model. Such equations are

$$\frac{D(\rho\kappa)}{Dt} = \nabla\cdot\left[\left(\mu + \frac{\mu_t}{\sigma_\kappa}\right)\nabla\kappa\right] + \underbrace{2\mu_t\mathbf{S}\cdot\mathbf{S} - \frac{2}{3}\rho\kappa(\nabla\mathbf{U})\mathbf{I}}_{P_\kappa} - \beta^*\rho\kappa\omega \tag{2.47a}$$

$$\frac{D(\rho\omega)}{Dt} = \nabla\cdot\left[\left(\mu + \frac{\mu_t}{\sigma_{\omega,1}}\right)\nabla\omega\right] + \gamma_2\frac{\omega}{\kappa}P_\kappa - \beta_2\rho\omega^2 + 2\frac{\rho}{\sigma_{\omega,2}\,\omega}\nabla\kappa\nabla\omega \tag{2.47b}$$

where P_κ represents κ production and $\sigma_\kappa = 1$, $\beta^* = 0.09$, $\sigma_{\omega,1} = 2$, $\gamma_2 = 0.44$, $\beta_2 = 0.083$ and $\sigma_{\omega,2} = 1.17$ are model constants. Left hand side of equations 2.47 gathers the combination of property's rate of change plus the net income by convection. The right hand side contains, respectively, the diffusive transport, production and destruction terms due to turbulence, although in ω-equation the last term arises from the ε-equation transformation process, being known as the cross-diffusion term.

What is new in the SST version is the accounting of the principal shear stress in eddy viscosity formulation in order to better predict possible separation bubbles and improve, for instance, the performance under adverse pressure gradients [22]. This is done limiting the eddy viscosity so that it became

$$\mu_t = \frac{a_1\rho\kappa}{max\left(a_1\omega, \sqrt{2\mathbf{S}\cdot\mathbf{S}}F_2\right)} \tag{2.48}$$

in which a_1 is a constant and F_2 a blending function. Also, a limiter is introduced on P_κ to prevent extra formation of κ surrounding stagnation points, a undesired aspect seen in $\kappa-\varepsilon$ models.

2.5 Modeling thermophysical properties

The importance of thermophysical properties on heat transfer performance of nanofluids was clearly exposed in section 1.2.2 and their influence on possible conclusions was highlighted in section 1.3.1.

Such evidences reveal, without any doubt, the importance of having reliable models to account for thermal properties into numerical simulations.

There is no more accurate method to determine thermal properties than experimental measurements. Following this idea, [61] investigated in loco both density and dynamic viscosity, while thermal conductivity and specific heat were adopted from dedicated publications regarding Al_2O_3-isopropanol nanofluid (please see [61] for more details). Posteriorly, the obtained measurements were validated against other correlations and available data, in order to reinforce their veracity. Finally, for the range of temperatures and mass fractions considered, data were fitted into mathematical models that reflect the properties' dependency on the two aforementioned variables.

For the nanofluid in question, the measured values for density can be adequately predicted employing the following equation [69]

$$\rho_{nf} = 808.7697 - 0.9508T + 6.4576\omega \tag{2.49}$$

where ρ_{nf} means the density in [kg/m^3], T the temperature in [ºC] and ω the *particle mass fraction* in [%]. One should not confuse ω with particle volume concentration, ϕ, since they are different. It is possible to relate them via

$$\phi = \left(1 + \frac{1-\omega}{\omega}\frac{\rho_{np}}{\rho_{bf}}\right)^{-1} \tag{2.50}$$

Dynamic viscosity exhibit different non-linear behavior with T and ω and, contrarily to density, fitting a single equation to predict its values within the entire variation range of the parameters was not possible. For that reason, an equation for each ω [%] studied was proposed, in the form of [69]

$$\mu_{nf} = \begin{cases} (a+bT)^{-1} & \text{for } \omega = \{0; 0.387; 0.992; 3.12\} \\ (a-b/T^2)^{-1} & \text{for } \omega = \{4.71\} \end{cases} \tag{2.51}$$

in which μ_{nf} is the dynamic viscosity in [Pa.s] and a and b are constants with values given in table 2.1.

Table 2.1: Coefficients for the dynamic viscosity model.

ω [%]	0	0.387	0.992	3.12	4.71
a	175.5004	126.2533	137.8122	142.4812	355.8237
b	12.9337	12.5972	11.2665	7.8454	36462.5170

The case of thermal conductivity is quite similar to density, since it was possible to express the influence of the two parameters into one single model equation. Such equation is then equal to [69]

$$k_{nf} = 0.09545 + 0.00128\omega + \frac{13.1182}{T} \tag{2.52}$$

where k_{nf} is expressed in [W/(m.K)], ω in [%] and T in [K].

Finally, the model for specific heat at constant pressure is quite different and requires more auxiliary math than the others. It is approximately given by [69]

$$c_{p,nf} = \frac{a + bT^2 + cT^4}{M_{mix}} \tag{2.53}$$

where $c_{p,nf}$ appears in [J/(kg.K)], T in [K], a, b, and c are constants and M_{mix} [kg/mol] is the *mixture molar mass* equal to

$$M_{mix} = M_{bf}(1 - y) + M_{np}y \tag{2.54}$$

with $M_{bf} = 0.060095$ and $M_{np} = 0.101961$ [kg/mol] being the substances' molar mass and y the *particle molar fraction* given by

$$y = \left[1 + \frac{M_{np}}{M_{bf}}\left(\frac{1}{\omega} - 1\right)\right]^{-1}, \quad y > 0 \tag{2.55}$$

Note that in equation 2.55, ω appears in [kg/kg] to generate y in [mol/mol]. Constants a, b, and c are computed through the following set of equations, this time with y being used in [%].

$$a = 105.93 - 0.532y \tag{2.56a}$$

$$b = -1.43 \times 10^{-4} - 4.01 \times 10^{-6}y \tag{2.56b}$$

$$c = 7.89 \times 10^{-9} + 1.1 \times 10^{-11}y \tag{2.56c}$$

These are the models in which the computation of the respective thermal properties are based, for each simulation ran. Thanks to the solver's customization capacity, these equations are coupled through the writing of appropriate *user-defined functions* (UDFs) [70].

Chapter 3

Numerical investigation

3.1 The finite volume method

The *finite volume method (FVM)* is a numerical technique widely used to solve partial differential equations (PDEs) representative of a general conservative process or law, providing approximations for the real solutions of those equations.

FVM is greatly appreciated by the scientific community especially when applied to fluid flow and heat transfer problems. It is based on a domain division into several aggregated *control volumes* (CVs), for which the PDE will be integrated over the CV boundaries and each one including a mesh (or grid) point. This integration results in an algebraic equation that, once extended this procedure to the remaining CVs, will produce a system of algebraic equations whose solution represents the dependent variable value in each point of the domain. To this procedure we give the name of *discretization*.

It is important to say that this happens without loss of information, since doing the discretization like this, we are ensuring the integral conservation of mass, momentum, or any other variable conservative, for the entire computational domain. This represents the fundamental reason of choosing FVM instead of other well-known numerical methods, like finite element methods, largely used in structural mechanics and not so commonly employed for fluid flow problems [71].

The information presented during this chapter can be consulted in books like [63] or [68].

3.1.1 Scalar's conservation in fluid flow problems

What was said during the previous paragraphs can be in an easier way illustrated using an example. Going through section 2.2 one may have noticed that all the derived transport equations seem to have some similarities between them and, for sure, they have. All of them have a temporal derivative, plus a convective and diffusive terms. What cannot be included into one of these three terms goes to a source term that, obviously, is different for each of the conservation laws. The exception is the pressure gradient term present in equations 2.5, which is responsible for the special treatment given to them available in section 3.1.3.

Thus, for a generic scalar property θ, in a convection-diffusion problem we have

$$\frac{\partial(\rho\theta)}{\partial t} + \nabla \cdot (\rho \mathbf{u}\theta) = \nabla \cdot (\Gamma \, \nabla\theta) + S_\theta \tag{3.1}$$

where Γ is a generic diffusion coefficient and S_θ is the source term associated to production/destruction of θ inside the CV. Note that the total derivative is written like this for a better identification of the respective terms. The integration of equation 3.1 over the CV and for a prescribed time step Δt, conjugated with the application of the divergence theorem yields

$$\int_{\Delta t} \left(\int_{CV} \frac{\partial(\rho\theta)}{\partial t} \, dV \right) dt + \int_{\Delta t} \int_S (\rho \mathbf{u}\theta) \cdot \mathbf{n} \, dS \, dt = \int_{\Delta t} \int_S (\Gamma \nabla\theta) \cdot \mathbf{n} \, dS \, dt + \int_{\Delta t} \int_{CV} S_\theta \, dV \, dt \tag{3.2}$$

Equation 3.2 represents the integral balance of θ within a CV. Clarifying, on the left-hand side is the term associated to the rate of change of θ plus the net rate of θ flowing out of the CV due to convection, while the right-hand side represents the net income of θ due to diffusion plus the source term.

Let us consider a generic three-dimensional CV with a rectangular shape in Cartesian coordinates, as illustrated in figure 3.1, where equation 3.2 is going to be employed. Subscripts e, w, n, s, t and b mean, respectively, *East*, *West*, *North*, *South*, *Top* and *Bottom*, identifying every one of the six faces of the CV. The upper letters are representative of the grid nodes in neighboring CVs.

Considering only stationary problems, every integration of the type $\int_{\Delta t} dt$ disappears, together with the transient term. The derivative terms on the border faces, here generically denoted as f, can be approximated assuming a linear variation of θ over the surrounding nodes, like

$$\left(\frac{\partial\theta}{\partial x_i} \right)_f \approx \frac{\theta_D - \theta_U}{\Delta x_i} \tag{3.3}$$

where θ_D and θ_U are the values of θ at the immediately next downstream and upstream grid points to the face f, over direction x_i. Equation 3.2 can now be presented in the following form of

$$\begin{aligned} &F_e\theta_e - F_w\theta_w + F_n\theta_n - F_s\theta_s + F_t\theta_t - F_b\theta_b = \\ &D_e(\theta_E - \theta_P) - D_w(\theta_P - \theta_W) + D_n(\theta_N - \theta_P) - D_s(\theta_P - \theta_S) + D_t(\theta_T - \theta_P) - D_b(\theta_B - \theta_P) + \bar{S}V \end{aligned} \tag{3.4}$$

where $F_i = (\rho u A)_i$ and $D_i = \left(\frac{\Gamma}{\Delta x} A\right)_i$ are variables introduced for simplification and $\bar{S}V = S_u + S_P\theta_P$ the linearized source term. A special case is when $\theta = 1$ and equation 3.1 turns into the continuity equation. The integral mass balance written in this notation is

$$F_e - F_w + F_n - F_s + F_t - F_b = 0 \tag{3.5}$$

Note that both equation 3.4 and 3.5 are also valid for reduced-dimensional problems, by setting the corresponding node values and length as null and unitary, respectively, when computing face area, A_i, and cell volume, V.

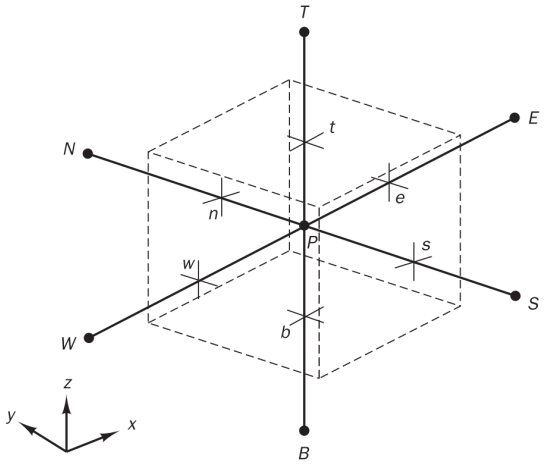

Figure 3.1: Cubic control volume and its surrounding nodes. Adapted from [68].

3.1.2 Discretization schemes

A *discretization scheme* is, basically, a mathematical formulation used to express θ face values as a combination of their closer node values. There are plenty of them reported on the literature, but the selection of a proper scheme should be done carefully, because they have a strong influence on the final solution quality, as we will see next.

An important feature is the order of the scheme. From the development in Taylor series of θ, the order of the scheme is the power at which the grid spacing is elevated on the first neglected term. It is important since it quantifies the error reduction rate as long as mesh is refined, showing how important is mesh refinement on discretization error reduction. Based on that, higher order schemes should always produce more accurate results compared to first order ones, since their discretization error is smaller. This is true, still, not straightforward, since there are additional conditions that must be satisfied to ensure the best quality possible for the respective numerical solution. *Conservativeness*, *boundedness* and *transportiveness* are the three more important [68].

Conservativeness states that θ needs be conserved allover the computational domain. This implies that a flux leaving a CV face must be equal to that entering an adjacent CV through the same shared face, ensuring its *consistent* computation.

The boundedness criterion simply states that, for any CV without a source term, the nodal value of θ must be within its border values. This property has important consequences on the solution of the system of algebraic linear equations, which can be written in the matrix form of

$$A_{ij}\theta_j = b_i \tag{3.6}$$

where A_{ij} is the coefficients' matrix and θ_j and b_i vectors of unknown nodal values and independent terms, respectively. Due to generally large dimensions of A_{ij} and location of the non-zero coefficients, the system 3.6 is usually solved adopting iterative methods. A sufficient condition for such methods to be convergent is to ensure that the coefficients of A_{ij} fulfill the *Scarborough criterion*, so A_{ij} could be considered as *diagonally dominant*. One may think what this has to do with discretization schemes,

but bounded schemes are suitable to yield diagonally dominant matrices. This also requires S_p to be always negative after the source term linearization. The other condition is ensure that every discretized equation contain coefficients sharing the same sign among them. Unbounded schemes promote the creation of oscillatory solutions which, sometimes, may not converge.

Transportiveness is the capacity of the scheme to "identify" the flow direction in convective problems. For a problem ruled by convection where fluid motion is always present, given a transport direction it means that a grid node value should suffer a greater influence from the upstream node than from the downstream one. Schemes which do not retain this property are then unsuited for convective problems.

The selection of the best discretization scheme is obviously confined to those available in the solver. Since the *central difference* scheme does not posses the transportiveness property, the role of options are resumed to the *upwind*-based, namely *first order upwind*, FROOM (named as *second order upwind* in [72]), QUICK and MUSCL [72]. The first one is unconditionally stable but its first order truncation error is not enough for our purposes. Both QUICK and MUSCL are third order schemes but significant improvements over second order ones might only be noticed in rotating or swirling flows, which is not our case [72]. Thus, we end up adopting FROOM scheme to discretize all the transport equations numerically solved during this study, even knowing it might be unbounded sometimes. However, the solver has strategies to prevent this behavior (please see section 3.2).

In FROMM scheme, the spatial gradient is computed using both upstream and downstream node values, assuming the same linear variation among the central node and the face values [63]. For a Cartesian mesh, it means

$$\theta_f = \theta_P + \frac{1}{4}\left(\theta_D - \theta_U\right) \tag{3.7}$$

where subscripts D, P and U represent the downstream, central and upstream nodes regarding f, respectively. The incorporation of the discretization scheme into the face values of equation 3.4 leads to the *discretization equation* for a generic CV with nb as neighboring nodes.

$$a_P\theta_P = \sum_{nb} a_{nb}\theta_{nb} + b \tag{3.8}$$

For FROOM scheme, the respective coefficients are given by [63]

$$a_W = D_w + \beta_p\left(F_w + \frac{1}{4}F_e\right) + \frac{1}{4}\beta_n F_w \quad \text{(3.9a)} \qquad a_E = D_e - \beta_n\left(F_e + \frac{1}{4}F_w\right) - \frac{1}{4}\beta_p F_e \quad \text{(3.9b)}$$

$$a_S = D_s + \beta_p\left(F_s + \frac{1}{4}F_n\right) + \frac{1}{4}\beta_n F_s \quad \text{(3.9c)} \qquad a_N = D_n - \beta_n\left(F_n + \frac{1}{4}F_s\right) - \frac{1}{4}\beta_p F_n \quad \text{(3.9d)}$$

$$a_B = D_b + \beta_p\left(F_b + \frac{1}{4}F_t\right) + \frac{1}{4}\beta_n F_b \quad \text{(3.9e)} \qquad a_T = D_t - \beta_n\left(F_t + \frac{1}{4}F_b\right) - \frac{1}{4}\beta_p F_t \quad \text{(3.9f)}$$

$$a_{WW} = -\frac{1}{4}\beta_p F_w \quad \text{(3.9g)} \qquad a_{EE} = \frac{1}{4}\beta_n F_e \quad \text{(3.9h)} \qquad a_{SS} = -\frac{1}{4}\beta_p F_s \quad \text{(3.9i)}$$

$$a_{NN} = \frac{1}{4}\beta_n F_n \quad \text{(3.9j)} \qquad a_{BB} = -\frac{1}{4}\beta_p F_b \quad \text{(3.9k)} \qquad a_{TT} = \frac{1}{4}\beta_n F_t \quad \text{(3.9l)}$$

$$a_P = \sum a_{nb} + F_e - F_w + F_n - F_s + F_t - F_b - S_p \quad \text{(3.9m)} \qquad b = S_u \quad \text{(3.9n)}$$

where β_p and β_n are two auxiliary variables with unitary value when velocity vector is align with the positive or negative axis direction, respectively.

The question of *numerical diffusion* of certain schemes is another problem researchers are faced with. It appears in cases where the flow is oblique to the grid lines due to unidimensional flow treatment at the CV faces, which causes a non-physical diffusion in zones where gradients are intense. It is, therefore, a multidimensional problem, mitigated with a higher grid resolution for such zones. Still, our methodology presume a mesh aligned with the flow, so we should not be worried about it [71].

3.1.3 Discretizing momentum equations: SIMPLE and SIMPLEC algorithms

The Navier-Stokes equations (momentum balance for a newtonian fluid) need special care when they are going to be discretized. A simple comparison between equations 2.5 and 3.1 illustrates the presence of a pressure gradient that needs to be accounted for and for which there is no transport equation (or equation of state, considering incompressible flow). Both velocity and pressure terms appear in all directional momentum balances and, if the pressure field was known a priori, the discretization procedure presented before was sufficient to treat this problem. However, it is often unknown, leading to the *pressure-velocity coupling* problem. For a better understanding of the problem itself, let us first present the example of the discretized x-momentum equation for a grid node in a Cartesian mesh

$$u_P = \left(\frac{\sum_{nb} a^u_{nb} u_{nb}}{a^u_P}\right)_P + \left(\frac{b^u}{a^u_P}\right)_P - \left(\frac{V}{a^u_P}\right)_P \left(\frac{\partial p}{\partial x}\right)_P \tag{3.10}$$

with a^u_P and a^u_{nb} coefficients being computed through any scheme, including FROMM presented in 3.1.2, and ΔV the volume around the node. If we consider a traditional interpolation to compute $\partial p/\partial x$ face values, it might lead to an incorrect interpretation of the real pressure distribution, since it never considers p_P contribution - the checkerboard problem. So, the *staggered grid* concept was developed, where different locations were considered to store velocities and pressures: velocities on cell faces and pressures and other scalars on cell nodes. This staggered grid would avoid an incorrect perception of the pressure field whereas it would compute it where no interpolation is needed in the momentum equations and velocities where no interpolation is necessary for the continuity equation.

Although some benefits were brought to the procedure, the staggered pattern has some disadvantages, like increased memory requirements and, mostly, considerable rigidity when applied in non-Cartesian or unstructured meshes. Knowing that robustness and a wide range of applicability are important features in a CFD commercial code, the *collocated* arrangement appears as a better alternative to deal with any type of problems in a singular way. It consists in grids where all the data are stored on the grid nodes. Based on this collocated concept, we will introduce the *SIMPLE algorithm* (Semi Implicit Method for Pressure Linked Equations), a method developed to find a pressure field such that the velocity field satisfies the continuity equation. The book [63] supports the following explanation.

Considering the non existence of face nodes in contrast to staggered arrangement, in collocated grids velocity should be interpolated at the CV faces, to compute the respective mass fluxes. Linear

interpolation is the simplest choice and keeps the second order error. We have then

$$u_e = \overline{\left(\frac{\sum_{nb} a^u_{nb} u_{nb}}{a^u_P}\right)}_e + \overline{\left(\frac{b^u}{a^u_p}\right)}_e - \overline{\left(\frac{V}{a^u_P}\right)}_e \left(\frac{\partial p}{\partial x}\right)_e \tag{3.11}$$

with $\overline{(...)}$ denoting interpolated terms. Expressing the first term of the right-hand side of equation 3.11 employing equation 3.10 to nodes P and E, and introducing the result into equation 3.11, we achieve to

$$u_e = \overline{u_e} - \overline{\left(\frac{V}{a^u_P}\right)}_e \left[\left(\frac{\partial p}{\partial x}\right) - \overline{\left(\frac{\partial p}{\partial x}\right)}\right]_e \tag{3.12}$$

This is the so-called *Rhie-Chow interpolation*, which corrects the linearly interpolated face velocity with a contribution from the difference between the computed and the interpolated pressure gradients at the face. Equation 3.12 is applicable to the other velocity components and to other coordinates.

The SIMPLE method starts by defining a pressure field, p^*, usually from a previous iteration, that, once solved the momentum equation 3.10, is capable of generate a velocity vector, $\mathbf{u}^*$, which verifies

$$u^*_P = \left(\frac{\sum_{nb} a^u_{nb} u^*_{nb}}{a^u_P}\right)_P + \left(\frac{b^u}{a^u_P}\right)_P - \left(\frac{V}{a^u_P}\right)_P \left(\frac{\partial p^*}{\partial x}\right)_P \tag{3.13}$$

This new velocity must verify the momentum balance but does not need to satisfy the mass balance, once it is based on previous pressure values. In order to verify continuity, corrections are added to the pressure and velocity fields, like

$$p = p^* + p' \tag{3.14a}$$

$$\mathbf{u} = \mathbf{u}^* + \mathbf{u}' \tag{3.14b}$$

and, subtracting equation 3.13 to 3.10, is possible to derive a velocity correction equation such as

$$u'_P = \left(\frac{\sum_{nb} a^u_{nb} u'_{nb}}{a^u_P}\right)_P - \left(\frac{V}{a^u_P}\right)_P \left(\frac{\partial p'}{\partial x}\right)_P \tag{3.15}$$

Since each one of the three momentum equations has a velocity component as primary variable, it makes sense the use of the remaining equation to deal with the pressure field. So, the continuity equation is used to find the pressure correction, without which it would be impossible to calculate the velocity correction. Considering the integral mass balance over a CV and adopting velocity notation of equation 3.14b, it leads to

$$\sum_f \left[\rho(\mathbf{u}' \cdot \mathbf{n})A\right]_f = -\sum_f \left[\rho(\mathbf{u}^* \cdot \mathbf{n})A\right]_f \tag{3.16}$$

Face velocity correction $\mathbf{u'}_f$ can be written using the Rhie-Chow interpolation, equation 3.12. The resulting $\overline{\mathbf{u'}_f}$, in its turn, can be found interpolating the velocity's correction, equation 3.15, at downstream and upstream nodes. Combining these two results into equation 3.16, yields

$$\sum_f \left[-\rho\overline{\left(\frac{V}{a^{\mathbf{u}}_P}\right)}(\nabla p')A\right]_f = -\sum_f \left[\rho(\mathbf{u}^* \cdot \mathbf{n})A\right]_f - \sum_f \left[\rho\overline{\left(\frac{\sum_{nb} a^{\mathbf{u}}_{nb} \mathbf{u}'_{nb}}{a^{\mathbf{u}}_P}\right)}A\right]_f \tag{3.17}$$

This is the denominated *pressure correction equation* and allows us to find the pressure correction all over the mesh. The last term of the right-hand side represents the influence of the surrounding nodes on central node's velocity correction, but in SIMPLE it is simply neglected, once at this point no correction is known. As all corrections tend to zero while convergence process is going on, this simplification only affects the rate of convergence of the solution, and not the solution quality.

Hence, to completely solve equation 3.17, it is necessary to define a scheme that discretize the pressure gradient. Like in staggered arrangements, pressure gradient is approximated using the second order face centered scheme represented by equation 3.3, which allow us to write a discretization equation for pressure correction like

$$a_P^{p'} p'_P = \sum_{nb} a_{nb}^{p'} p'_{nb} + b^{p'} \tag{3.18}$$

where, after some algebra, it is possible to find the following expressions for the coefficients $a^{p'}$ and $b^{p'}$.

$$a_E^{p'} = \rho_e \overline{\left(\frac{A^2}{a_P^u}\right)}_e \quad (3.19a) \qquad a_W^{p'} = \rho_w \overline{\left(\frac{A^2}{a_P^u}\right)}_w \quad (3.19b) \qquad a_N^{p'} = \rho_n \overline{\left(\frac{A^2}{a_P^v}\right)}_n \quad (3.19c)$$

$$a_S^{p'} = \rho_s \overline{\left(\frac{A^2}{a_P^v}\right)}_s \quad (3.19d) \qquad a_T^{p'} = \rho_t \overline{\left(\frac{A^2}{a_P^w}\right)}_t \quad (3.19e) \qquad a_B^{p'} = \rho_b \overline{\left(\frac{A^2}{a_P^w}\right)}_b \quad (3.19f)$$

$$a_P^{p'} = \sum_{nb} a_{nb}^{p'} \tag{3.19g}$$

$$b^{p'} = (\rho u^* A)_w - (\rho u^* A)_e + (\rho v^* A)_s - (\rho v^* A)_n + (\rho w^* A)_b - (\rho w^* A)_t \tag{3.19h}$$

Once solved equation 3.18 for pressure correction, we are in conditions to also correct velocity using equations 3.14b and 3.15. Figure 3.2 illustrates how this iterative algorithm works.

Some improvements were thought for SIMPLE algorithm, especially due to its modest rate of convergence. One very appreciated is the *SIMPLE-Consistent* (SIMPLEC) in which the the neighbors' velocity corrections, discarded in the original method, are instead approximated via

$$\sum_{nb} a_{nb}^{\mathbf{u}} \mathbf{u}'_{nb} \approx \mathbf{u}'_P \sum_{nb} a_{nb} \tag{3.20}$$

Introducing it in equation 3.15 for two consecutive grid nodes, the velocity correction on a face f can be given by

$$\mathbf{u}_f = -\overline{\left(\frac{V}{a_P^{\mathbf{u}} - \sum_{nb} a_{nb}^{\mathbf{u}}}\right)}_f (\nabla p)_f \tag{3.21}$$

which, when included in the mass imbalance equation 3.16, generates a discretized equation all the way analogous to 3.18 despite the coefficients $a_F^{p'}$, this time equal to

$$a_F^{p'} = \rho_f \overline{\left(\frac{A^2}{a_P^{\mathbf{u}} - \sum_{nb} a_{nb}^{\mathbf{u}}}\right)}_f \tag{3.22}$$

for a generic grid node F and respective face f. All the remaining reasoning stands valid among the two

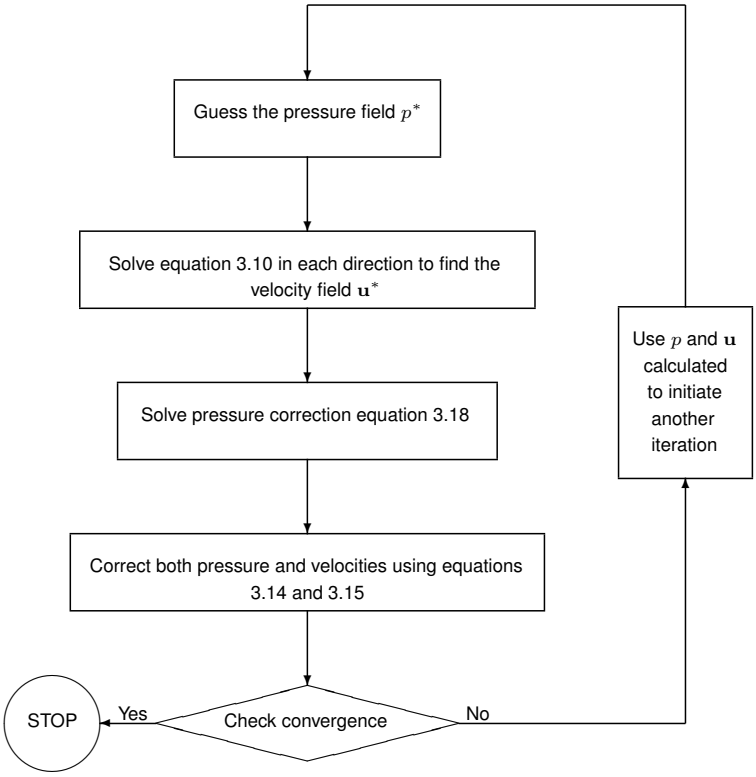

Figure 3.2: SIMPLE flow chart for collocated grids

algorithms. SIMPLEC is preferable over its ancestor because, while performing the approximation 3.20, we are actually neglecting a smaller contribution than what is discarded in SIMPLE, which improves the convergence rate exhibited by SIMPLEC, at least for laminar flows [63, 72]. This reason is what stands behind the choice of SIMPLEC over regular SIMPLE.

3.2 The solver

Fluent® is a commercial CFD code widely used to run any type of fluid flow simulations. It can handle several flow configurations and simulate many working conditions, including more complex cases such as flows inside turbomachinery or multiphase flows. It incorporates, as well, a bunch of mathematical models to deal with phenomena of radiation, combustion or turbulence and supports customization through the creation of UDFs [70].

Fluent® offers two different solving strategies [72]. The pressure-based solver is the option followed when incompressible flows are simulated, while density-based solver is dedicated to flows where compressible effects are present. Due to the coupling between pressure and density in compressible flows, plus the already discussed coupling for pressure and velocity, this approach is based in a solution technique that treats all the discretized transport equations in a coupled fashion, solving them together.

The pressure-based solver also provides a coupled way to solve the flow equations (energy equation is left out of this procedure), but is the segregated method that represents the chosen approach during this work. There, every momentum equation is separately solved, following the SIMPLE algorithm described in section 3.1.3, being then energy, turbulence and other equations solved one each time too.

This technique requires less memory, although the convergence may not be so fast [22, 72].

Based on this segregated approach, figure 3.3 illustrates all the steps taken on a solution process, showing also the order by which they occur inside each loop. The iterative process starts by setting user-defined data first, such as boundary conditions or thermal properties. Only then the numerical calculation process effectively starts, with pressure-velocity coupling being the first addressed point, following the SIMPLE algorithm. With the pressure and velocity fields already calculated, energy and other scalars' transport equations are solved and properties depending on flow quantities are updated with their new values, in order to check the convergence of the solution. This iterative process goes on until the established convergence criteria is verified.

There is a lot of theory supporting the solution process used by Fluent® so it could be adapted and solve the whole range of problems treated by this commercial solver. Still, we would like to refer a few techniques used to achieve a solution in Fluent®, without going into much detail. During the discretization process, the FROOM scheme does not possess the boundedness property, which might lead to an oscillatory solution. Fluent® ensures that new extrema are not created by limiting the *reconstruction gradient* (gradient which origins equation 3.7), in a process called *linear reconstruction*. In its turn, this gradient is calculated using a *Least Squares method*, a method designed for every type of mesh. Finally, after the discretization process, the resultant system of equations is effectively solved applying the iterative *Gauss-Seidel method* incorporated in an *Algebraic Multigrid* approach. The use of iterative methods grants the convergence of the solution for diagonally dominant matrices, while the multigrid technique improves the solution convergence rate. For more details, more information about the solver can be consulted in [22, 72].

3.3 Boundary conditions

This section is dedicated to the explanation of the boundary conditions considered in this study. Laminar and turbulent cases will be treated separately since they require particular considerations.

3.3.1 Laminar case

To correctly model the real problem, we must specify what physically is known and controls the experiment. For that, inlet BCs can be created to define in which circumstances the flow reach the inlets of the computational domain. From the beginning we have stated that the study will run over fully developed conditions, which implies no longer development of hydrodynamic boundary layers in the heated section of the tube. It means that the velocity profile is fixed at the entrance section and can be correctly predicted by equation 2.19, which was imposed in the solver writing a proper UDF. Temperature is another flow variable whose inlet distribution needs to be established. From the experiments, we know that the fluid enters the heated section with a constant and known temperature and replicate this situation is easily achieved assigning such temperature to the fluid at the inlet. Information about the pressure is not necessary, once it appears directly from the provided velocity field as a consequence of

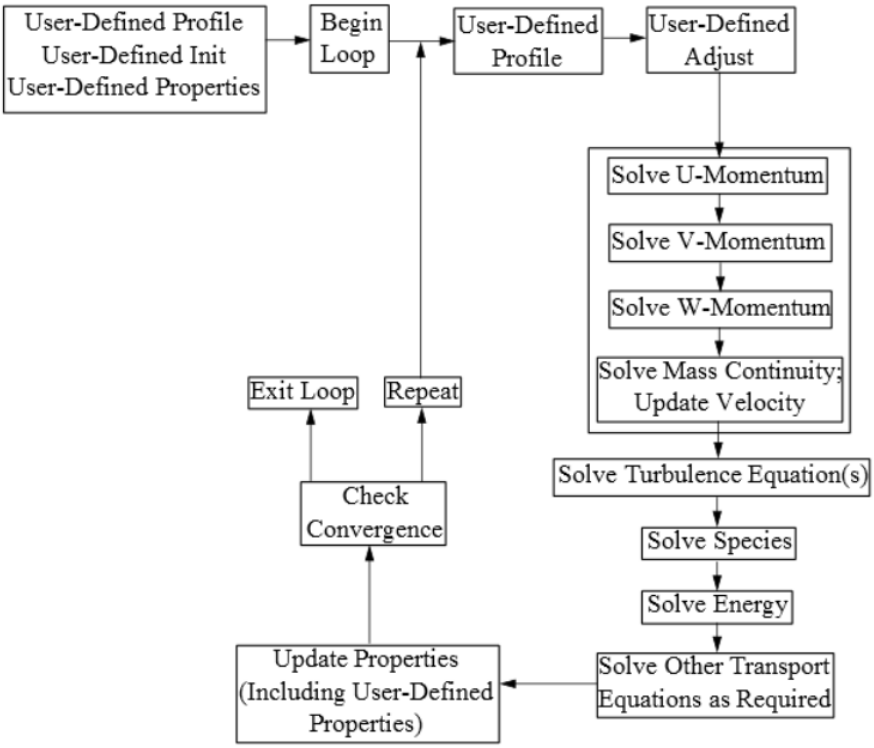

Figure 3.3: Pressure-based segregated solver flow chart. Adapted from [70].

the pressure-velocity coupling.

Similarly, exits need also to be characterized, but generally not much information is available. In such cases, we need to ensure the flow evolves over the domain with no interference from the exterior. This can be achieved using a *Pressure Outlet* BC and setting the gauge pressure at the exit to zero. Physically, we are defining a flow exit at atmospheric pressure, which allows us to correctly compute the static pressure drop and revealed to have better performance against the *Outflow* BC.

The presence of a wall always affects the flow development and its effect on the flow can be accounted using a *Wall* BC. In the present case, a static wall where the no-slip condition have been considered, ensuring a null velocity over the CV near-wall border faces. The condition of constant heat flux supplied at the wall is also defined at this point. As the heat flux is a parameter in study, likewise the inlet temperature, it is known a priori and it is set constant during every simulation.

Geometry can be used as a helpful source of information which, sometimes, provides a great contribution to computation process optimization. When analyzing the geometry of the real problem, the presence of any type of symmetry should be checked, as it grants a significant computational domain's reduction, reflected in less time consuming simulations. *Symmetry* BC is characterized by the definition symmetry planes through which the solution can be mirrored to the remaining domain. The beauty of our cylindrical geometry is that it is not only symmetric, but it is also axisymmetric, which means symmetry along the symmetry axis. This allows a large reduction in our computation domain, transforming a 3D problem into a 2D one, where only a no-thickness fluid sheet is going to serve as computational domain. Besides this enormous simplification, it turns possible the use without restrictions of the discretization relations introduced in chapter 3.1 for structured Cartesian meshes, since we consider the

x-coordinate as the axial direction and the y-coordinate as the radial one. The use of this BC has also implicit the same type of symmetry reflected in the flow variable fields, like velocity. In fact, such axisymmetric velocity profile is obtained when no swirl is present inside the flow and can be checked looking to equation 2.19, noting no spatial dependence besides the radial coordinate. Due to its specificity, this BC is distinguished in Fluent® from the classic Symmetry one, and receives the name of *Axis* BC.

Figure 3.4 illustrates the computational domain which will be used to run the simulations. The blue line indicates the inlet face, where BCs are implemented. Similarly, the outlet BCs must be applied on the face represented by the green line, as well as wall BCs in the face here defined in red. The axis is, logically, expressed by the yellow line and receives the axis BC, while the interior domain is symbolized by the grey squared pattern.

3.3.2 Turbulent case

The introduction of the new PDEs to model turbulence quantities requires, logically, an extra set of BCs to them. In our case, the SST $\kappa - \omega$ was the chosen turbulence model and two extra transport equations were added to the problem. Like momentum and energy, these two equations also need estimations for κ and ω at the inlets of the computational domain.

Contrarily to velocity or temperature, it is not usual to have turbulent kinetic energy or dissipation rate measurements available, which have forced researchers to resort on academic similar experiments or in rough estimations based on turbulence theory. A common method to estimate κ and ω at the entrance of a fully developed turbulent pipe flow used by Fluent® is available in [72]. Based on the concept of turbulence intensity, expressed by equation 2.43, it is stated that for such flows, turbulence intensity can be given by

$$I = 0.16(Re_{D_h})^{-1/8} \tag{3.23}$$

where D_h is the *hydraulic diameter* of the tube (in a cylinder, it corresponds to the geometrical diameter, D). Considering isotropic turbulence, where fluctuations have the same magnitude in all directions, it is possible to transform equation 2.43 into the following one, obtaining then a feasible estimation for κ.

$$\kappa = \frac{3}{2}(U_{avg}I)^2 \tag{3.24}$$

The prediction of ω requires the computation of the *turbulence integral length scale*, ℓ, a parameter related to the dimensions of the largest eddies in the flow. For the case under consideration, it can be estimated as

$$\ell = \frac{0.07D_h}{C_\mu^{3/4}} \tag{3.25}$$

where $C_\mu = 0.09$ is an empirical constant. Once both κ and ℓ are known, it is possible to relate them with the specific dissipation rate using the definition of length scale considered in $\kappa - \omega$ models that, solving for ω, is given by

$$\omega = \frac{\kappa^{1/2}}{C_\mu \ell} \tag{3.26}$$

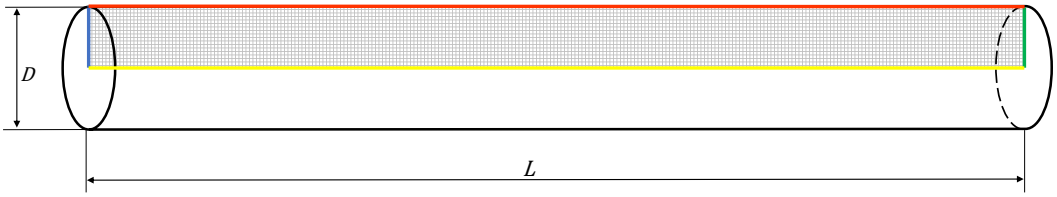

Figure 3.4: Schematics of the comptutational domain and boundary zones.

The remaining BCs can be left as if laminar simulations were performed, despite the more complex treatment executed by the solver for turbulent BCs, especially in the presence of a wall. Still, no modifications are required from the user. The only exception is the inlet velocity profile. The previous laminar profile is no longer valid for turbulent flow, being now described with good approximation through equations 2.24 and 2.25.

3.4 Mesh independence study

Due to the strong influence that the mesh has on the solution process, seen in section 3.1.2, one should investigate when the results become independent from the mesh used. It means the point when the solution becomes insensible to mesh refinement, and can be attained while computing the same features using consecutive finer grids and evaluating the convergence of those predictions.

The axisymmetric character of the geometry turned this a 2D study with a Cartesian mesh fitting perfectly. These type of grids should be used whenever possible, once they minimize the problem of numerical diffusion, as said in the end of section 3.1.2. Simulations for laminar flow were considered converged at the moment that continuity's scaled residual was inferior to 10^{-8}, while for turbulent flow, predictions were accepted converged when continuity's scaled residual became smaller than 10^{-8} or κ's and ω's smaller than 10^{-7}. This criteria is valid during the entire work.

For reasons related to near-wall flow in the presence of turbulence, distinct grids will be used for laminar and turbulent predictions, each one requiring a separate study. Still, the tests will be identical, consisting on the computation for consecutive finer grids of temperature and axial velocity profiles in two different sections of the domain ($x = L/2$ and $r = 0$) and, additionally, C_f and h for turbulent flow only. Homogeneous fluid was considered and the controlling conditions, listed in table 3.1, were kept constant during the simulations. The grid selected will be the one where the improvement in solution quality does not justify the augmented time consumption.

Results for the laminar case can be seen in figure 3.5, as well as the different grids tested in table

Table 3.1: Conditions adopted in the mesh independence study.

$Regime$	T_{in} [^oC]	$\dot{m}$ $[kg/s]$	q'' $[W/m^2]$	ω [%]	u/U $profile$	I [%]
Laminar	15	0.00767	1000	0	Parabolic	-
Turbulent	15	0.0767	10000	0	Constant	5

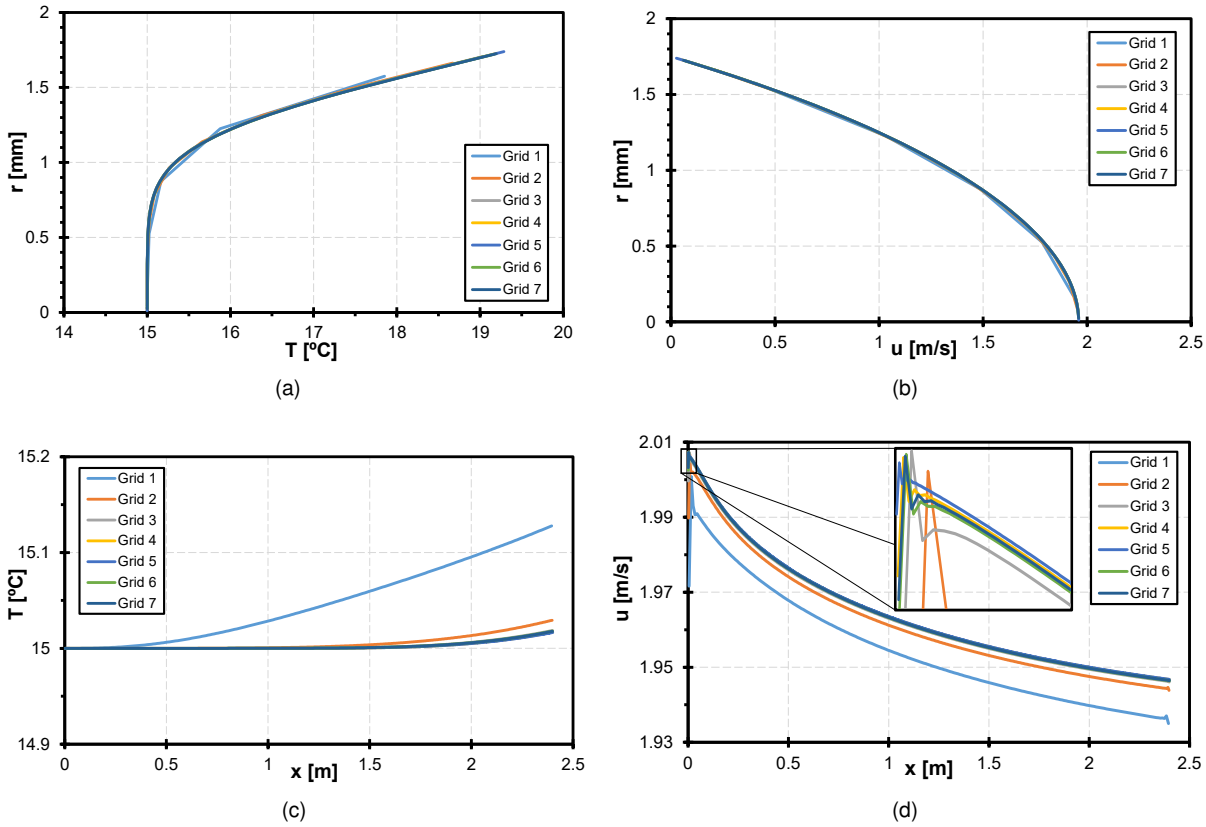

Figure 3.5: Mesh independence study for laminar simulations. (a) temperature radial profile and (b) velocity radial profile, at $x = L/2$. (c) temperature axial evolution and (d) velocity axial evolution, at $r = 0$.

Table 3.2: Grids considered in mesh independence study for laminar simulations.

$Grid$	1	2	3	4	5	6	7
$n^oCVx \times n^oCVr$	240x5	480x10	960x20	1920x40	3860x80	1440x30	1600x35

3.2. For this study, Cartesian uniform grids were adopted and, from grid 1 to 5, the refinement was attained by doubling the number of CVs in both directions.

The radial predictions of figure 3.5 hardly change throughout the refinement process, with the coarser grids showing good results. The same does not happen axially and a more delayed convergence was verified, clearly proving grids 1 and 2 are too coarse. A closer inspection of the axial velocity at the centerline indicates a potential improvement from grid 3 to grid 4 which, considering the computation time (around 5 minutes), definitely worths a search for an optimal mesh. The solution computed for grids 4 and 5 is very close to each other and therefore the former was preferred, since the better yields additional time consumption.

Grids 6 and 7 have then been proposed, revealing closer results to grid 4, as detailed in figure 3.5 (d). The oscillations in the axial velocity close to the inlet can be seen as an adaptation of the flow to the imposed fully developed velocity profile at the inlet. In that zone some non-zero radial velocities were observed that, by continuity, are responsible for those oscillations. Despite this, which has negligible effects in practice and can be mitigated via mesh refinement, we end up adopting grid 6 (see figure 3.7) in the laminar simulations.

The turbulent case was treated in a similar fashion but adding the complementary quantities of C_f and h. The first one is a classic quantity many times analyzed in boundary layer research, which is of great utility evaluating the velocity profile, namely through its gradient at the wall. h, in its turn, is the major object of interest of this work and we want to see the mesh impact on it. Also, it provides a good estimation for the process of $T_m(x)$ computation, which is explained in section 4.1.

In virtue of the large temperature and velocity gradients at the wall, of vital importance for h computation (thermal) and C_f (friction), it was considered that equally spaced meshes might not be able to capture them with high resolution, so a new strategy of grid construction had to be tested too. Biased meshes, identified as "bf", keep the same number of CVs but redistribute them in a specific direction to capture in more detail the desired zone, the wall in this case. Using the ratio between the largest and the shortest CV, named as *bias factor*, the algorithm allocates more and smaller CVs to the wall region, leaving the central zone of the tube to the remaining CVs with larger dimensions.

Another aspect that might influence turbulent simulations is the Re range experimentally considered, which belongs to the transition region and implies non-developed turbulence. Since it is possible to conjugate SST $\kappa-\omega$ with the *Intermittency transition model*, the influence of the transition detection was tested as well.

Figure 3.6 presents the results obtained for the mesh convergence study in turbulent flow regime. Using the know-how acquired in laminar case, only three grids were considered this time, as indicated in table 3.3, and the procedure adopted was identical in terms of convergence and control, despite new appropriate numerical values. The aforementioned variations of each grid were tested and the first conclusion got was the insensitivity to the transition model coupling evidenced on the results. For every case, we could check that predictions from grids with transition model were always superposed with those of equally spaced grids, showing turbulence model alone is enough to capture all the details.

Consequently, the question sums up to the impact of wall zone refinement on the computed quantities. Like in laminar case, temperature and velocity radial profiles do not show any major difference among grids, as well as temperature at centerline. It was on the axial velocity plot (figure 3.6 (d)) that such influence has started to be noted, being also more significant in C_f and h cases (figures 3.6 (e) and (f) respectively). These plots clearly show the effect of the biased arrangement, but especially on C_f plot that more than doubled from the grid 1 to any biased one. None of the grids but the biased ones could capture this shape, with grid 3 (the more refined of the equally spaced group) yielding results almost 20% lower than those of the biased grids. Not much difference was found in C_f curves among biased grids, so predictions can be considered as converged.

If the biased approach is justified via C_f computation, the best grid for turbulent simulations can be chosen complementing with a look to h plot. Figure 3.6 (f) shows a variation among biased grids 1 and 2 that is not seen from 2 to 3, indicating an already mesh independent result. This time, equally spaced grid 3 reveals a good performance while predicting h, showing that the T_m computation procedure (explained in section 4.1) is more dependent on the number of CVs than on y^+, contrarily to hydrodynamic quantities. The initial depression verified in h curves has simply to do with the developing length of the flow (around 0.1m based on figure 3.6 (d)), in response to an inlet constant velocity profile. Once

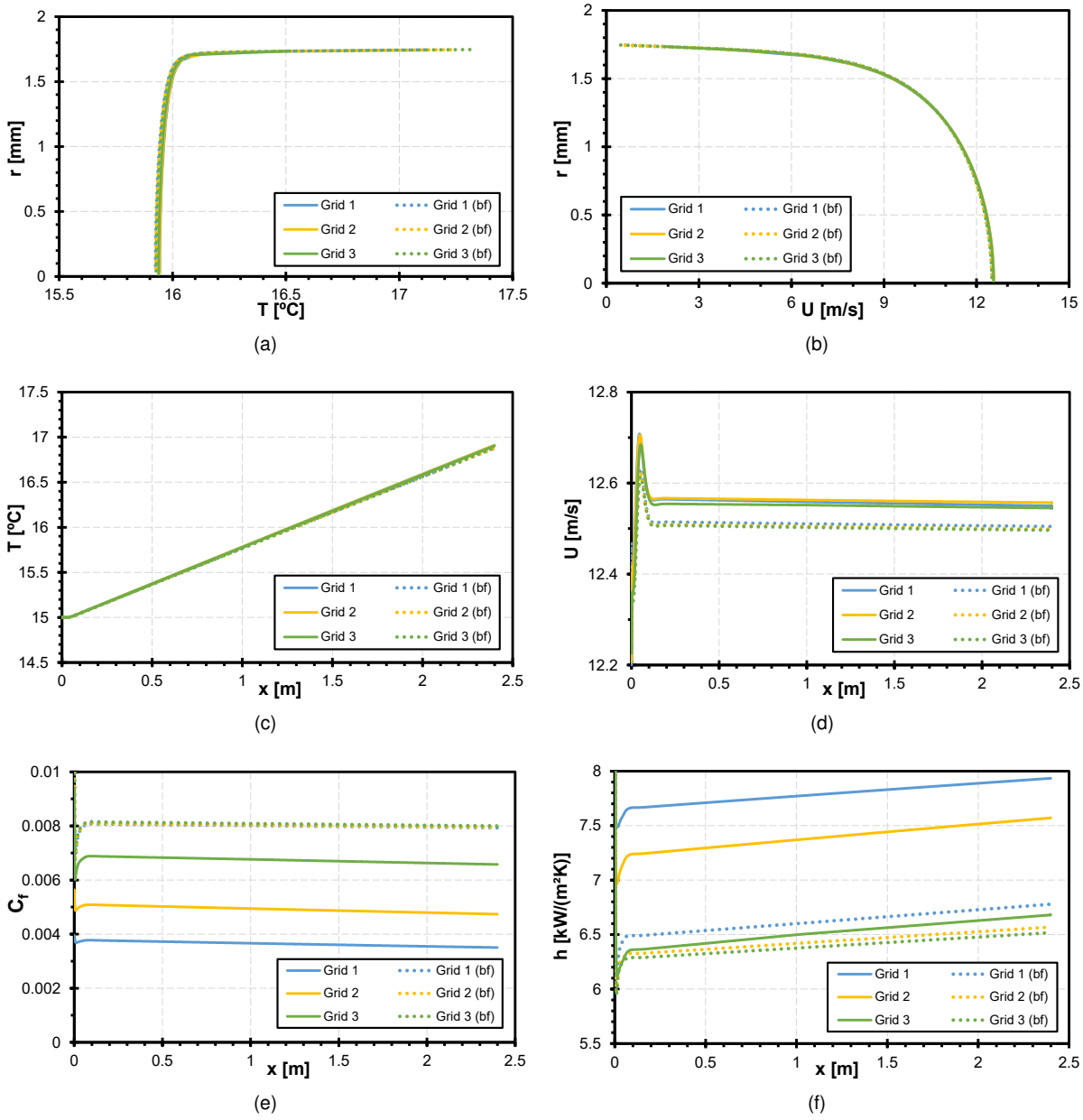

Figure 3.6: Mesh independence study for turbulent simulations. Axial evolution of (a) and (c) T, (b) and (d) u, at $x = L/2$ and $r = 0$, respectively, and (e) C_f and (f) h.

Table 3.3: Grids considered in mesh independence study for turbulent simulations.

$Grid$	1	2	3
$n^oCVx \times n^oCVr$	1440x30	1920x40	2880x60

developed, h reveals the expected trend of growing almost linearly with the axial position, effect of the Re augmentation along the tube. Finally, we are in conditions to conclude and say that biased grid 2 (see figure 3.7) is the one that better serves our purposes, proving also that despite the SST $\kappa - \omega$ model independence from y^+, quantities like C_f and h are strongly influenced by its magnitude within the boundary layer zone, proving that grids having y^+ nearby unity at the wall are more suited for such predictions.

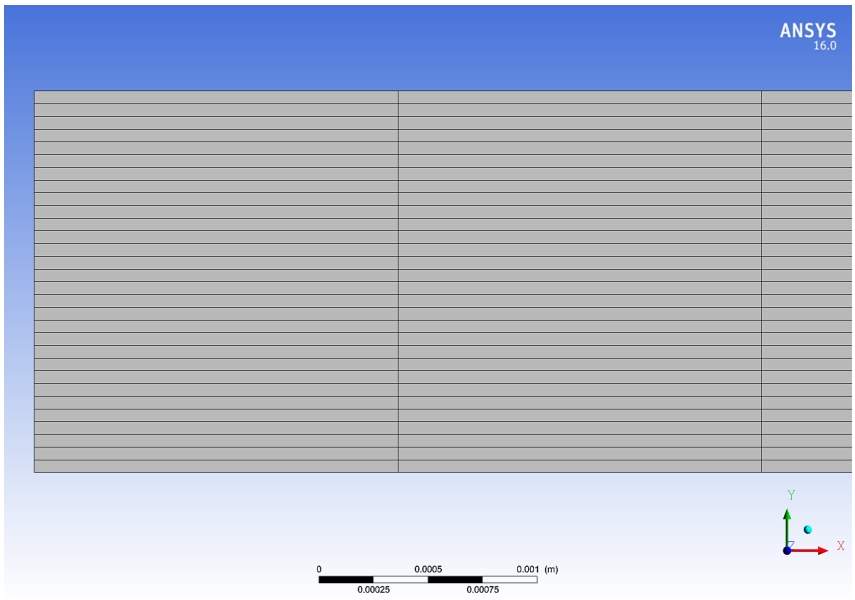

(a)

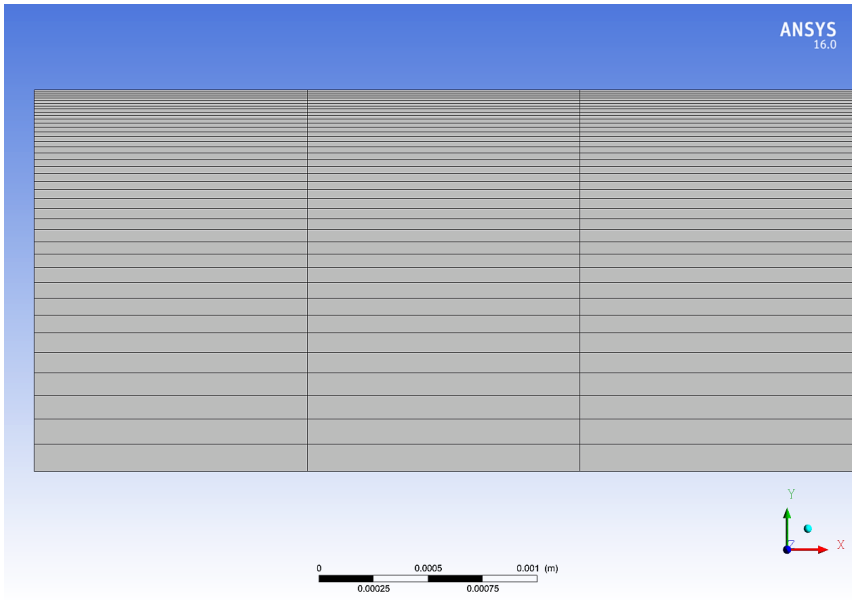

(b)

Figure 3.7: Detail of the mesh used in (a) laminar simulations and (b) in turbulent simulations.

3.5 Model validation

Once found an appropriate mesh, this validation procedure intends to estimate the accuracy of the model by comparing measurements on the base fluid alone with their predictions, and with theory whenever possible. Thus, Nu, T_m and wall temperature, T_w, were tracked in non-isothermal tests, while f was the object of interest of isothermal replications. The reason we chose to analyze these quantities is simple, since this temperature difference $T_w - T_m$ is what supports the experimental h, while empirical correlations for Nu and f are widely known for this geometry in both flow regimes. Such approach was then followed in laminar and turbulent cases.

Figure 3.8 (a) allow us to compare temperature predictions with experimental measurements, for

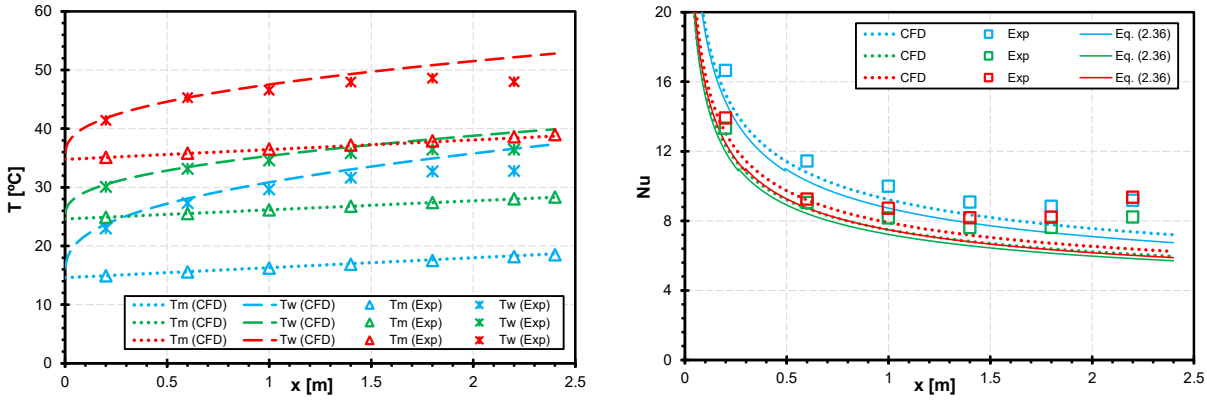

(a) (b)

Figure 3.8: Isopropanol laminar predictions for validation purposes. (a) axial evolution of T_m and T_w and (b) axial evolution of Nu. Conditions $\Rightarrow$ $T_{in} = 14.6^oC,\ q'' = 5397.6\ W/m^2,\ \dot{m} = 0.01467\ kg/s$ (Blue) • $T_{in} = 24.6^oC,\ q'' = 2742.5\ W/m^2,\ \dot{m} = 0.00742\ kg/s$ (Green) • $T_{in} = 34.8^oC,\ q'' = 3452.7\ W/m^2,\ \dot{m} = 0.00787\ kg/s$ (Red).

laminar flow conditions. Regarding T_m, one can see that experiments match perfectly the CFD line for each one of the studied inlet temperatures, in a clear agreement with energy conservation principle, but the same does not happen with T_w. In fact, experiments until the fourth point ($x = 1.4m$) agree very well with the predicted dashed line, but this trend is lost, especially in the last point ($x = 2.2m$). Such difference has certainly a reason to be, and we believe it is purely related to experimental errors.

Although the real temperature increasing rate might be slower than the predicted, as evidenced when comparing fourth and fifth experimental points, it is known from the theory that the condition of constant heat flux at the wall of a laminar, hydrodynamically developed flow, implies a continuous axial increase of T_w that is not present from the fifth to the sixth experimental points. Actually, for every case, temperature measurements at $x = 2.2m$ are lower than in the previous location, which is not physically possible. Still, the predicted T_w is supported by the experimental evidence for every inlet temperature in more than half tube length, so we believe to have enough reasons to rely on the calculated temperature profiles.

The results for Nu are plotted in figure 3.8 (b), where the predictions were no more than 10% higher compared to theoretical results (equation 2.36), but at the same time where experiments are directly affected by the abnormal T_w observed before. Logically, both theory and predictions depart from experiments on the critical points already identified. One can examine the influence of T_w on Nu doing the simple exercise of understanding first its influence on h. Since experimental ΔT is smaller than the predicted one, equation 2.29 shows that the expected h is higher in the experimental case. As Nu is directly related to h, we can conclude that the experimental Nu on those points is larger than predictions, as shown in the respective plot. Once we have mentioned before the non-physical meaning of those T_w values, results based on them are unreliable as well, and should not be taken into account. The remaining experimental points of the three tests are all within 15% of the theoretical curve, confirming the good performance of the present model regarding laminar simulations.

A similar study was conducted for turbulent regime and the results are given in figure 3.9. Again, both T_m and T_w were axially matched against experimental measurements and Nu compared with ex-

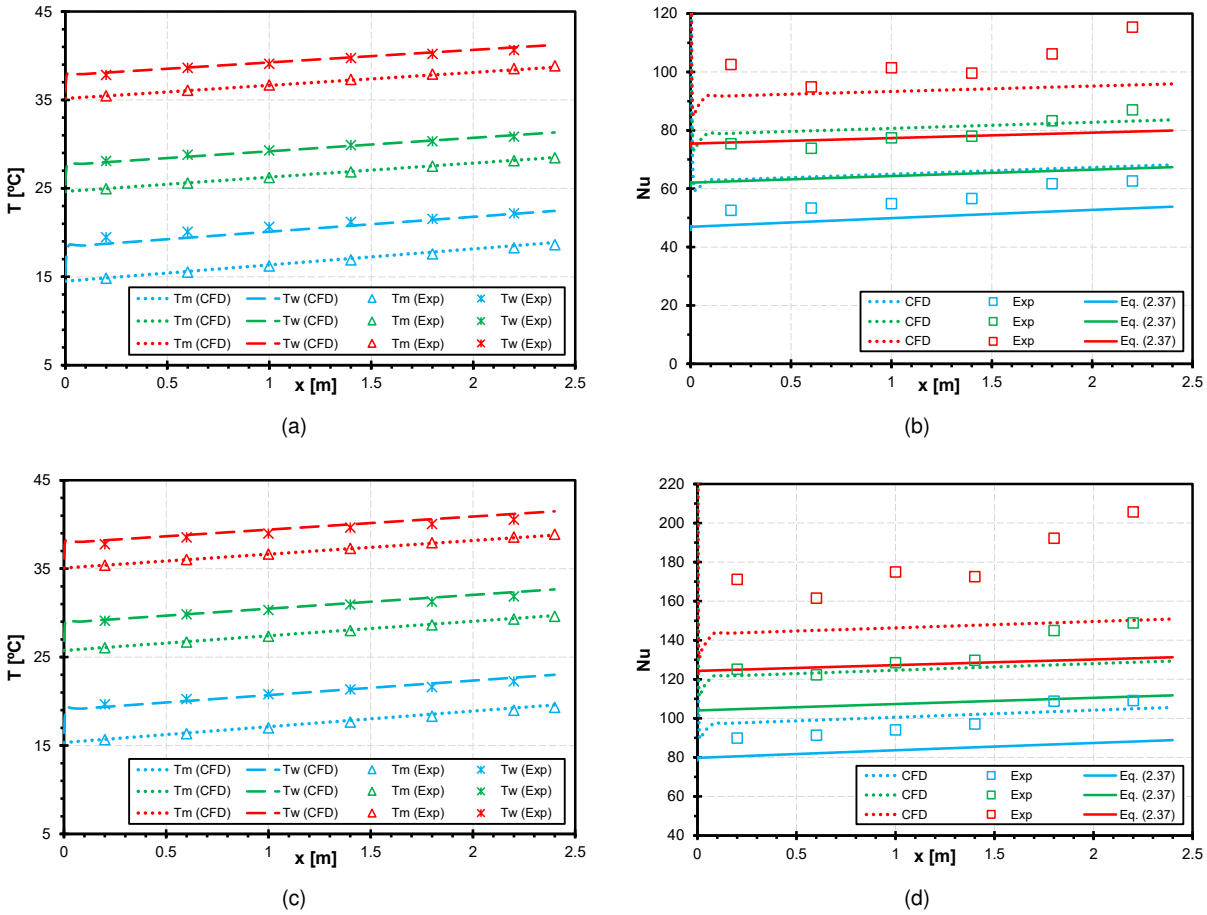

Figure 3.9: Isopropanol turbulent predictions for validation purposes. (a) and (c) axial evolution of T_m and T_w and (b) and (d) axial evolution of Nu. Conditions (a)/(b) $\Rightarrow$ $T_{in} = 14.5^oC$, $q'' = 9809.2\ W/m^2$, $0.02517\ kg/s$ (Blue) • $T_{in} = 24.7^oC$, $q'' = 9399.2\ W/m^2$, $0.025\ kg/s$ (Green) • $T_{in} = 35.2^oC$, $q'' = 9533\ W/m^2$, $0.02477\ kg/s$ (Red); (c)/(d) $\Rightarrow$ $T_{in} = 15.3^oC$, $q'' = 14416.1\ W/m^2$, $0.03837\ kg/s$ (Blue) • $T_{in} = 25.8^oC$, $q'' = 15171.2\ W/m^2$, $0.03942\ kg/s$ (Green) • $T_{in} = 35.1^oC$, $q'' = 15962.9\ W/m^2$, $0.04018\ kg/s$ (Red).

periments and with the results given by Gnielinski equation (2.37) combined with Colebrook equation (2.26) for f computation. One more time, predictions and measurements for T_m exhibit a better agreement than T_w. Still, the trends of evolution are very close and the absolute deviations are no more than 0.75ºC for the six cases considered, which we consider totally acceptable.

In terms of Nu, the agreement between predictions and experiments can be considered very good whenever the numerical and experimental ΔT are very close, but any small difference in ΔT is highly amplified in terms of Nu. The worst case is plotted in figures 3.9 (c) and (d) and occurs for the inlet temperature of 35^oC. Looking at T_w curves, one can see that predicted values are slightly higher than real ones, implying a larger numerical ΔT. Considering the values of heat flux imposed in turbulent flow, using equation 2.29 it is easy to find that a small reduction in ΔT produces a great augmentation in h and consequently in Nu. This is the main explanation for the observed results, since when no difference was noted on measured and predicted ΔT, experimental and computational Nu agree very well. Even though, and neglecting the last two experimental points, all the local predicted Nu are within 20% of the measured ones.

On the other hand, the Gnielinski equation was not able to correctly predict the local Nu, despite being valid in the range of studied Re. Such behavior has already been noticed in [28], [39] or [42], and we accept it as expected, since we are dealing with heat transfer in developing turbulence. However, a decreasing tendency on the relative error has been identified when higher mass flow rates (Re), for the three temperatures considered. Another important aspect is the fact that both numerical and Gnielinski line slopes are similar. This ends up supporting the rising trend shown in Nu predictions along the tube and not the oscillatory behavior of the experimental data, possibly related with small errors in temperature measurements.

We finally conclude this validation study by performing isothermal simulations to evaluate the precision in the prediction of the friction factor. As the experimental length for which the pressure drop was measured is distinct from the heated section numerically considered, it was not possible to compare in non-isothermal conditions either Δp, for obvious reasons, or f, since Re is changing along the tube and f depends on it. However, isothermal conditions turns Re constant throughout the tube (and so does f), allowing a comparison independent from the considered length.

Results for f in laminar and turbulent regimes, for the three considered inlet temperatures, are available in figure 3.10, as well as the theoretical laws of Hagen-Poiseuille (equation 2.21) for laminar flow and Colebrook (equation 2.26) for turbulent flow, considering a roughness $e = 3\mu m$ [61]. There can be seen that laminar predictions follow almost perfectly the theoretical law and that this agreement is independent of the inlet temperature. Only for Re above 2150 the experimental measurements get away from the predicted ones, value around which the transition onset for pure isopropanol flow is observed in [61]. When turbulence is present, predictions at low Re are substantially superior than measured values and also than Colebrook equation, meaning a possible overestimation of the Δp effectively developed. Nevertheless, we also see that such over-prediction tends to diminish as Re increases, revealing that turbulence models are definitely more suited for developed turbulence conditions, characteristic of higher Re.

In the end, we conclude that despite not being perfect, our simulations provide very satisfactory results, with all trends being confirmed via experimentation and/or theory.

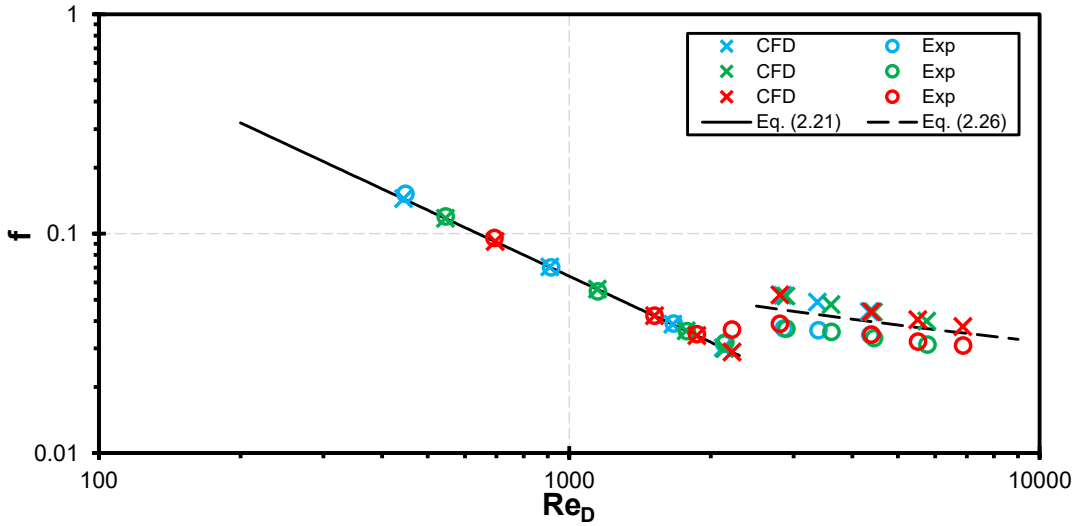

Figure 3.10: Isopropanol friction factor predictions and experiments. Blue data - $T_{in} = 15^{o}C$; Green data - $T_{in} = 25^{o}C$; Red data - $T_{in} = 35^{o}C$.

Chapter 4

Results and discussion

4.1 Data acquisition and treatment

During the model characterization process, several quantities that are not a direct output of the numerical solution have been presented to justify some decisions taken in the time of this work. We can point the obvious case of h which is strongly dependent on T_m, or f, function of u_m (or U_m). The central question here is that neither of them can be extracted from the solver without any algebraic manipulation, since they represent a weighted average of their respective radial profiles. Thus, becomes important to clarify the mathematical process behind these intermediate calculations, in order to demystify any possible confusion about the way numerical data was treated in the present work.

The core of the question here is to find $T_m(x)$, for every discrete position, since we will built on its local computation the axial evolutions of h and Nu, for instance. Looking to equation 2.34, we see that a c_p is needed, so we decided to compute it via model equation 2.53 using as temperature the value of $T_m(x)$, which is effectively our goal. This iterative process can be solved using the widely known *Newton-Raphson method*, with a second order convergence rate.

Also in $T_m(x)$ computation are involved some integrals that must be numerically computed. Considering the grid nodes as the integration points for those numerical values are available, such integrations over the radial coordinate can be performed employing a *trapezoidal rule*, since it allows different spacing among two consecutive nodes (useful in turbulent simulations) and it is easily implemented. This procedure was followed for mass flow rate in $u_m(x)$ computation and for $\overline{h}$ and f calculations, which requires axial integrations too. Such routines have been numerically implemented in Fluent® via UDF.

4.2 Predictions vs. experiments

In this section, the performance of the model is assessed by comparing predictions with experimental values of the heat transfer coefficient and the friction factor for the nanofluid.

4.2.1 Heat transfer coefficient

Figure 4.1 presents four sets of plots of the convective heat transfer coefficient, h, each one characterized by nanoparticles mass fraction and inlet temperature, for laminar regime. Numerical results, in every case shown, behave as expected and according to the theory of laminar heated flow, showing also that as long as the mass flow increases (and Re), the thermal developing zone gets larger, as well as h. Experiments, despite always slightly higher than predictions, in most cases follow very well the numerical trends up to more that half the tube length, but in the last two experimental points the slight rising trend already identified and discussed in section 3.5 is present again.

The discrepancy seen comes, again, from the distinct numerical and experimental temperature differences. Still, the reason for such discrepancy is unclear, apart from computational/experimental errors, once buoyancy effects were considered in [61] and revealed to be insignificant. Certain is the lack of influence of particles addition on the thermal development of the flow, since the present model is able to predict within 15% error the experimental data, excluding the last two experimental points.

A similar comparison was carried out in turbulent regime, as shown in figure 4.2. This time, due to a weaker experimental evidence, only three cases per inlet temperature/particle loading case were simulated. A wall roughness $e = 3\mu m$ was assumed again. At a first view, we can observe that predictions do not match as well as they did in laminar flow, but some trends can be identified. Firstly, the model exhibits a propensity to overestimate h when 15^oC is the inlet temperature, but the contrary happens when 35^oC is considered. For 25^oC, the trend is not uniform. It is also common to all conditions that, as $\dot{m}$ and q'' increase, predicted h tend to be smaller relatively to experimental measurements. These effects led to good matches in some circumstances, but to large differences in others, as the cases plotted in figure 4.2 (f), where a difference of nearly 1.2ºC in ΔT yields h around 30% smaller. The respective temperature plots and simulation parameters regarding figures 4.1 and 4.2 are available in appendix A.

In fact, these trends are not totally new, as a look back over figure 3.9 allows us to infer. In figures (b) and (d) it is clearly perceptible that Nu is over and underestimated for inlet temperatures of 15^oC and 35^oC, respectively. The rough oscillations and the last two points always out of trend, two characteristics of the measured Nu evolutions of figure 3.9, are clearly present on the h measurements of figure 4.2, which means they are not a direct consequence of the nanoparticles addition.

We cannot ignore the differences as they exist and are quite significant in terms of h, but, again, considering figure 3.9 where small differences of less than 0.5ºC between numerical and measured ΔT produce relative errors of around 20% in Nu, we are encouraged to believe that the majority of the error related to h came from the same effect, even though some trends might not be so sharp or so flat as they were predicted. Still, we believe the model continues to produce reliable results, since from the total 35 simulated cases, only in 20% of them there were local h predicted 20% above their measured value, not accounting again with the two highest axial coordinates measurements. The good agreement exhibited for most cases with inlet temperatures of 15^oC and 25^oC is real, which make us to wonder about what physical reason stands behind the large differences found for 35^oC, besides experimental errors.

To add more evidence and corroborate these conclusions, figure 4.3 shows a direct comparison between predicted and experimental average coefficients, $\overline{h}$, which can be seen as a good indicator of

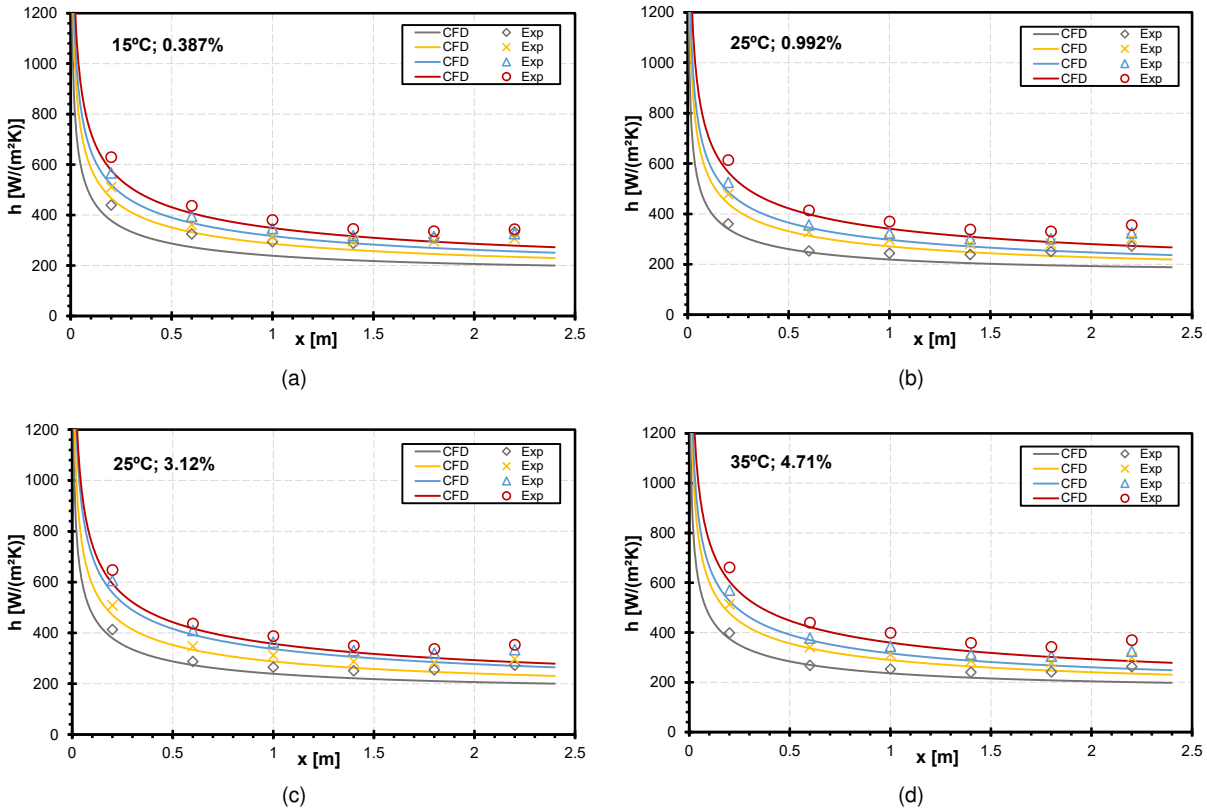

Figure 4.1: Examples of predicted and experimental local heat transfer coefficients of Al_2O_3-isopropanol in laminar regime, for several particle loadings and inlet temperatures.

the h axial evolution. Both laminar and turbulent regimes were considered and each point represents a simulation of an experimental situation similar to those of figures 4.1 and 4.2, considered here too.

Laminar case shows, again, a very good agreement among predictions and measurements, considering that only in four cases the error exceeds 10%. This is really demonstrative of the accuracy of laminar predictions, even considering that in experimental $\overline{h}$ are included the measurements at the last two axial locations that contribute to slightly higher values. For turbulent flow, as expected, the error magnitude involved is higher, especially for the $T_{in} = 35ºC$ case, but only five cases exhibit errors over 20%. The already mentioned overestimation when $T_{in} = 15ºC$ is again noted and confirmed, as well as the most accurate predictions attributed to $T_{in} = 15ºC$ and $T_{in} = 25ºC$. What is easier to check now is the increased growing rate of experimental data over predictions as long as higher $\overline{h}$ are obtained (consequence of higher $\dot{m}$ and q''). This is especially noticed for the largest T_{in} and ω and our model reveals to be incapable to reproduce such tendency. However, and based on the reasons presented before, errors in experimental data should not be ignored.

4.2.2 Friction factor

With the aim of seeking for any possible influence of inlet temperature and particle loading on the nanofluid hydrodynamic characteristics, only isothermal conditions have been simulated to calculate the friction factor, for the same reasons explained in section 3.5. Numerical results for f were gath-

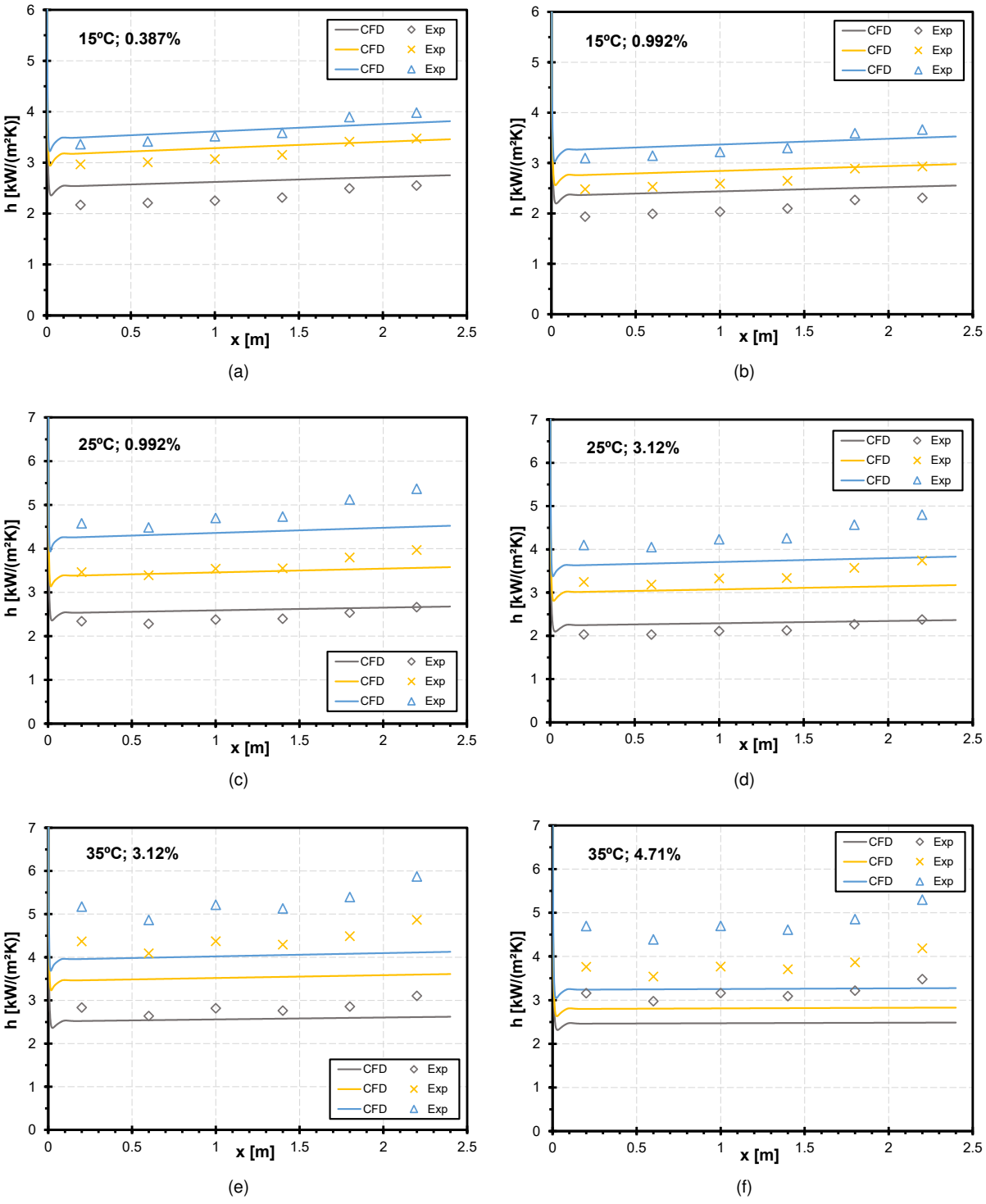

Figure 4.2: Examples of predicted and experimental local heat transfer coefficients of Al_2O_3-isopropanol in turbulent regime, for several particle loadings and inlet temperatures.

ered and compared with experimental measurements and the theoretical laws of Hagen-Poiseuille and Colebrook, as illustrated in figure 4.4. A roughness of $e = 3\mu m$ was considered either in the numerical solving procedure or in Colebrook equation.

For laminar regime, in line with the previous tests already seen, the plot shows excellent agreement between theoretical, experimental and numerical data for the entire range of laminar Re. The only

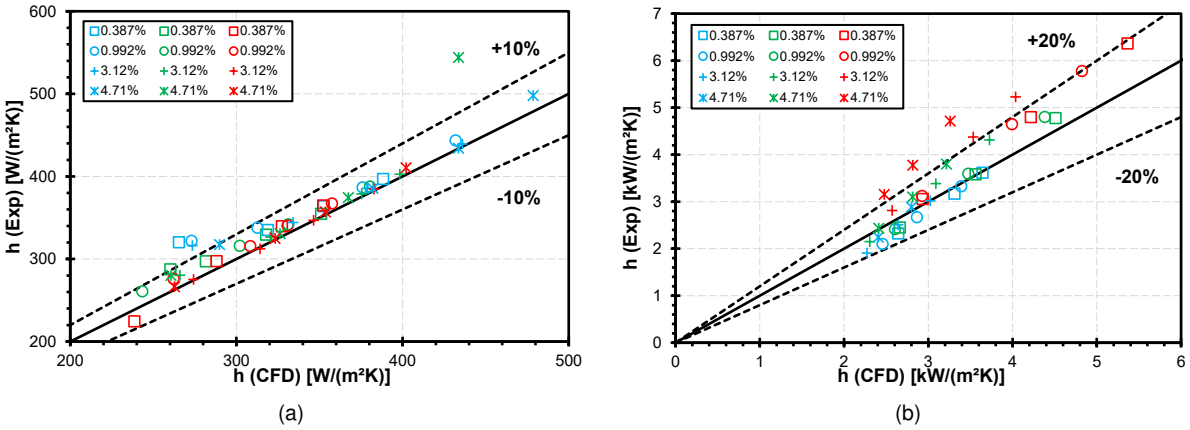

Figure 4.3: Comparison between numerical and experimental average heat transfer coefficients for (a) laminar regime and (b) turbulent regime. Blue data - $T_{in} = 15^oC$; Green data - $T_{in} = 25^oC$; Red data - $T_{in} = 35^oC$.

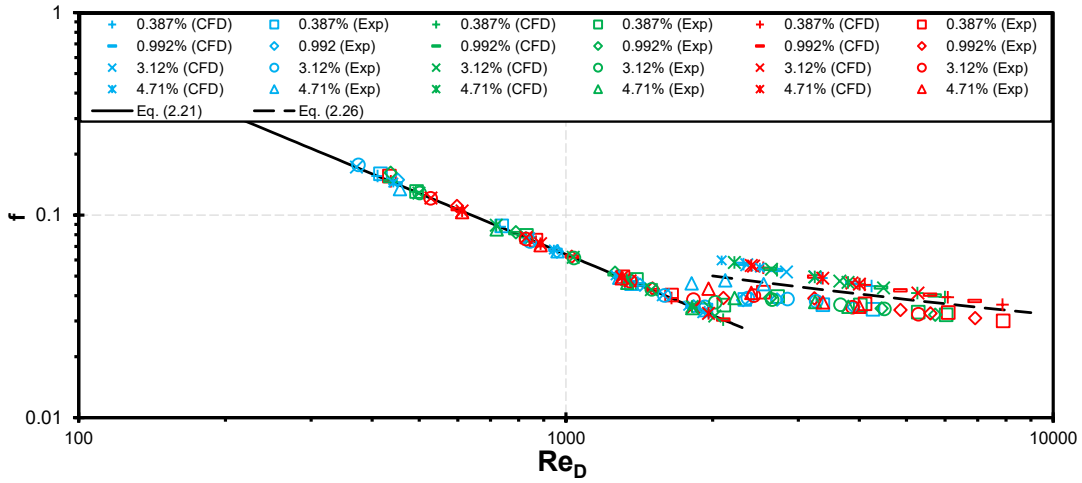

Figure 4.4: Al_2O_3-isopropanol friction factor predictions and experiments. Blue data - $T_{in} = 15^oC$; Green data - $T_{in} = 25^oC$; Red data - $T_{in} = 35^oC$.

exception is the onset of the transition zone, where the laminar version of our model is totally unsuited, since has no way to predict it and, consequently, to account the extra contribution to f due to turbulence. For that zone, the model continues to follow the theoretical law, as it did for base fluid in section 3.5.

With respect to turbulent flow, not much can be added to what was already concluded when base fluid was investigated in order to validate the model. For low turbulent Re, turbulence is in a state far away from developed and the model, through turbulence modeling, over-predicts the friction factor typically overestimating the pressure drop of the flow. This difference, one more time, tends to vanish as the Re increases and fully developed turbulence is more prone to be attained, as revealed by the agreement between numerical data and Colebrook equation. Nevertheless, experimental data is always below these two lines, indicating a possible overestimation even for larger Re than what really happens.

No influence of temperature or particle addition was noted in the numerical results for both flow regimes, corroborating the experimental verification of Newtonian behavior for the Al_2O_3-isopropanol nanofluid.

4.3 Parametric analysis

Due to the way the experimental investigation was structured, is was not possible to explore the influence that a single one controlling parameter has on the heat transfer coefficient and on pressure drop. Thus, we performed a sensitive analysis to study the influence of, individually, change mass flow rate, wall heat flux, inlet temperature and particle mass fraction. Here the main goal is not a rigorous quantification of possible enhancements or deteriorations, since the imposed conditions do not have any specific application. Instead, we will try to find some tendencies and favorable modifications to extract the most profit possible from the use of nanofluids.

4.3.1 Laminar flow

Firstly we will investigate h and Δp in laminar flow conditions. Two different inlet temperatures were considered ($15^{o}C$ and $35^{o}C$), as well as all the particle loadings studied during the last section. As thermal properties are strongly influenced by temperature and particle concentration, the computed Re, for a given $\dot{m}$, could belong to laminar or turbulent regime, according to the conjugation of these two outer factors. This effect made impossible to cover a sufficient large range of Re in both temperatures with one single $\dot{m}$ variation range, so this is the reason supporting the smaller $\dot{m}$ considered for $35^{o}C$, in comparison to those selected to $15^{o}C$.

Figure 4.5 presents the separate influence that $\dot{m}$ and q'' has on the average heat transfer coefficient, $\overline{h}$. Its choice over $h(x)$ is quite obvious, since it globally represents the performance of the system. Figure 4.5 (a) clearly shows that $\overline{h}$ increases with $\dot{m}$. It makes sense, since mass flow rate powers the fluid bulk motion, a basic request of forced convection to exist. Also a higher T_{in} enhances $\overline{h}$, for a fixed $\dot{m}$ and q''. We attribute this increase to the c_p augmentation together with a ρ reduction due to the greater temperatures, which allows the fluid to absorb more energy per °C raised and accelerate by continuity, respectively.

A curious fact of figure 4.5 (a) is the improvement (or lack of it) powered by nanoparticles addition. With exception of $T_{in} = 15^{o}C$ and $\omega = 4.71\%$ which claims some attention with its nearly 3% increase respectively to pure fluid, the heat transfer enhancement is almost unnoticed and irrelevant, especially for higher temperatures. We know that following a single-phase numerical approach, the possible heat transfer enhancement is obtained purely thanks to altered thermal properties, but what is seen here is that, when $\dot{m}$ is maintained, the k improvement given by nanoparticles and responsible to promote the heat flow into the fluid is not enough to compensate in a large proportion the adverse contributions of ρ intensification and c_p decrease. Such observations agree very well with the data presented in [61] regarding the $\dot{m}c_p$ comparison basis.

The q'' influence on $\overline{h}$ is presented in figure 4.5 (b). It is important to remember that $\dot{m}$ between the two temperatures is different, being this the reason of the major discrepancy seen in $\overline{h}$ from the two temperatures. A greater heat flux yields higher heat transfer rates, as expected. Still, the results for $\omega = 4.71\%$ are curious since, as long as q'' increases, the $\overline{h}$ growing rate deteriorates, reaching at $35^{o}C$ worse performances that those of pure fluid when submitted to maximum q'' considered.

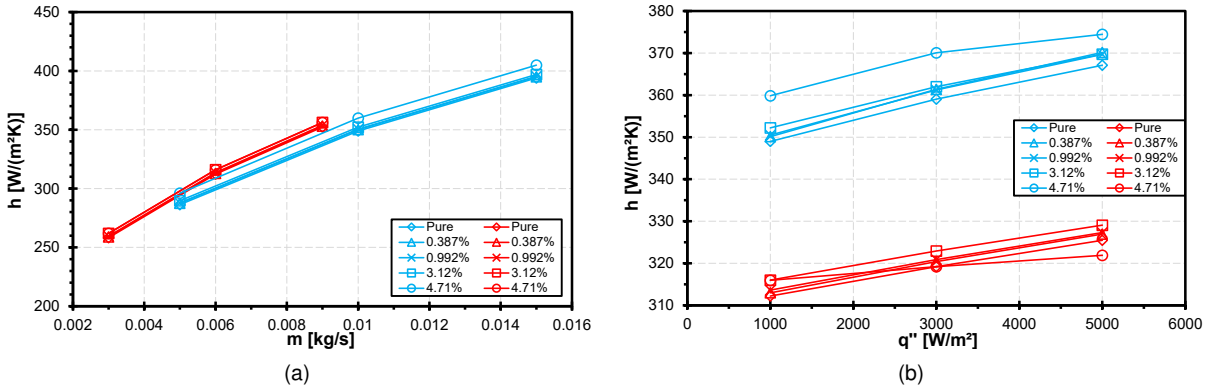

Figure 4.5: Influence of (a) mass flow rate ($q'' = 1000W/m^2$) and (b) wall heat flux ($\dot{m} = 0.01kg/s$ and $\dot{m} = 0.006kg/s$ for $T_{in} = 15^oC$ and $T_{in} = 35^oC$, respectively) on average heat transfer coefficient, for laminar flow conditions. Blue data - $T_{in} = 15^oC$; Red data - $T_{in} = 35^oC$.

The effect of $\dot{m}$ and q'' on pressure drop, Δp, is well documented in figure 4.6, which shows the increase of Δp with $\dot{m}$ and the reduction with q''. Δp quantifies the energy dissipated by friction at the wall, which is directly related to the fluid viscosity. If the viscosity of the nanofluid is reduced by temperature, but expanded by particles concentration, we should expect a Δp evolving in a similar manner, and figure 4.6 (a) proves such expected trends.

The linear relationship of Δp with $\dot{m}$ can be explained using the theoretical results available for a fully developed laminar flow in circular tubes. From this theory, it is known that Δp grows linearly with the mean velocity through the following law

$$\Delta p = \frac{32\mu L u_m}{D^2} \tag{4.1}$$

Therefore, since $\dot{m}$ is directly proportional to u_m, it is easy to conclude that Δp increases linearly with $\dot{m}$, as shown in figure 4.6 (a). The inclusion of nanoparticles led to a maximum intensification of Δp quantified around 60% for 15^oC and 80% for 35^oC, when compared to base fluid performance.

The influence of the thermal load on Δp can be explained taking into account, one more time, the influence that more energy brought into the system has on the nanofluid viscosity. Note again that despite higher temperatures were responsible for reduced pressure drops, the lower Δp present in 4.6 (b) has also a contribution from the reduced flow rate considered for $T_{in} = 35^oC$. Δp tends, effectively, to decrease with q'', being this reduction more accentuated for $T_{in} = 15^oC$. The reason behind such behavior relies on the asymptotic decreasing evolution of $\mu(T)$ for every single ω, meaning that a temperature augmentation nearly 15^oC has a more accentuated reduction of μ than nearly 35^oC. Consequently, such occurrence would also be observed in terms of Δp, explaining the decreasing evolutions detected for $T_{in} = 15^oC$ and the almost flat ones for $T_{in} = 35^oC$ with increasing thermal loads.

4.3.2 Turbulent flow

In the line of the previous analysis, a sensitive study focusing on the influence of the controlling parameters on the heat transfer performance and pressure losses was performed for turbulent flow conditions. The restriction in terms of flow rate was identical, namely to ensure turbulent conditions, but due to a

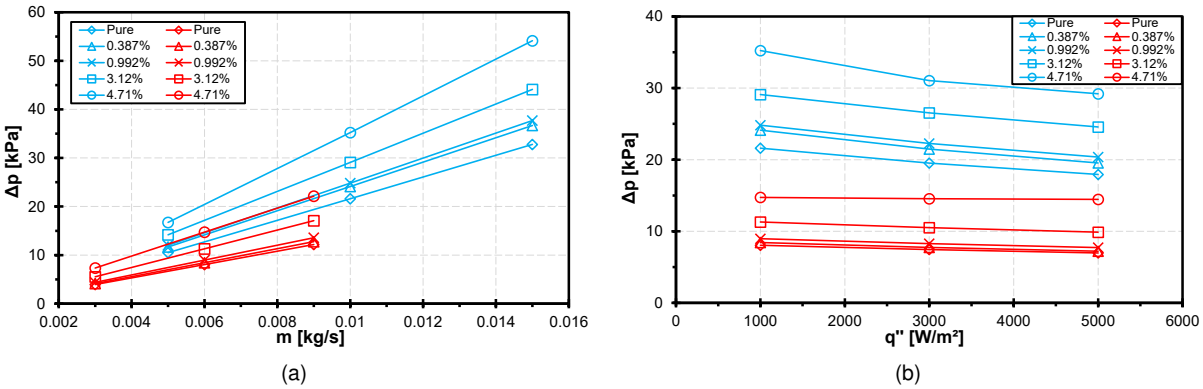

Figure 4.6: Influence of (a) mass flow rate ($q'' = 1000W/m^2$) and (b) wall heat flux ($\dot{m} = 0.01kg/s$ and $\dot{m} = 0.006kg/s$ for $T_{in} = 15^oC$ and $T_{in} = 35^oC$, respectively) on pressure drop, for laminar flow conditions. Blue data - $T_{in} = 15^oC$; Red data - $T_{in} = 35^oC$.

much wider range of flow rates compared with laminar flow, this time it was possible to choose and preserve the same flow rates for the two inlet temperatures studied, 15^oC and 35^oC. The principal benefit of this fact is to allow a direct comparison among every one of the presented cases, which represents an improved capacity in respect to laminar study, especially when discussing the q'' influence.

The influence of $\dot{m}$ and q'' on $\overline{h}$ is shown in figure 4.7. Figure (a) presents how $\dot{m}$ influences the heat transfer performance of the nanofluid, for the range of temperatures and particle loadings tested. As expected, and following the laminar tendency, we note that this performance is powered by the $\dot{m}$ augmentation, justified by the increased fluid bulk motion.

Also in line with laminar results is the temperature influence on $\overline{h}$ under the presence of turbulence. For a given ω and $\dot{m}$, a higher temperature continues to represent an improved nanofluid thermal performance. However, the mechanisms supporting such improvement are not the same. This does not deny the discussion presented in section 4.3.1 regarding this topic, but instead, it points out that turbulent transport has more importance on the flow dynamics than the variation of the properties. What might be surprising a priori is the decrease of the heat transfer coefficient with the addition of nanoparticles, reaching a maximum deterioration of around 30% in comparison to the base fluid performance when $\omega = 4.71\%$ was considered. This represents the opposite of what was desired, but is in accordance with the data presented by [61] concerning the $\dot{m}c_p$ comparison basis.

Such results motivated a more detailed research of the turbulent characteristics of the flow. In order to find some relationships between modifications in turbulent quantities and the respective $\overline{h}$ variation, figure 4.8 shows radial profiles of turbulent kinetic energy, κ, and its dissipation rate, ε, as a function of temperature and particle loading, while keeping constant mass flow rate and heat flux. In fact, an interesting correlation was found among ε, temperature and particle concentration. It has been noticed that the peak of ε is greater when temperature increases, but it is reduced with the addition of nanoparticles. In terms of $\overline{h}$, its higher values are always consistent with the larger peaks of ε, which led us to think that they might be somehow related. Additionally, both $\overline{h}$ and ε are affected in the same way by temperature and particle loading, reinforcing this idea.

The dissipation rate is associated to the end of the energy cascade, where viscous effects become

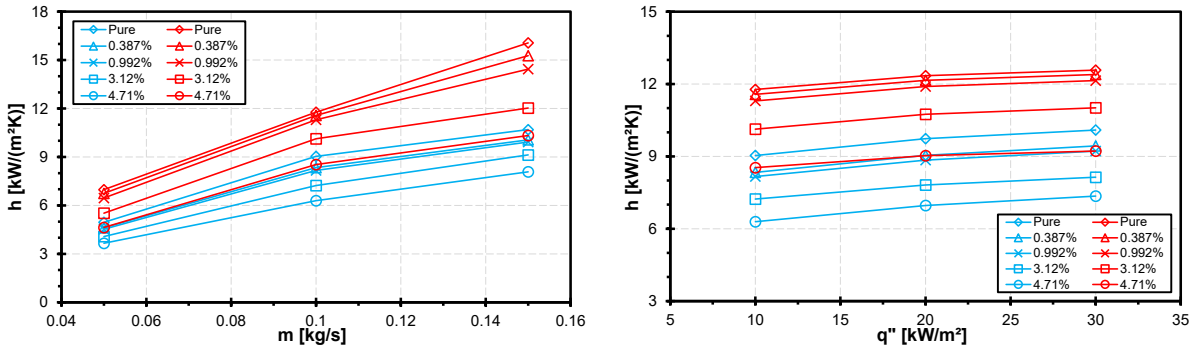

Figure 4.7: Influence of (a) mass flow rate ($q'' = 10kW/m^2$) and (b) wall heat flux ($\dot{m} = 0.1kg/s$) on average heat transfer coefficient, for turbulent flow conditions. Blue data - $T_{in} = 15^oC$; Red data - $T_{in} = 35^oC$.

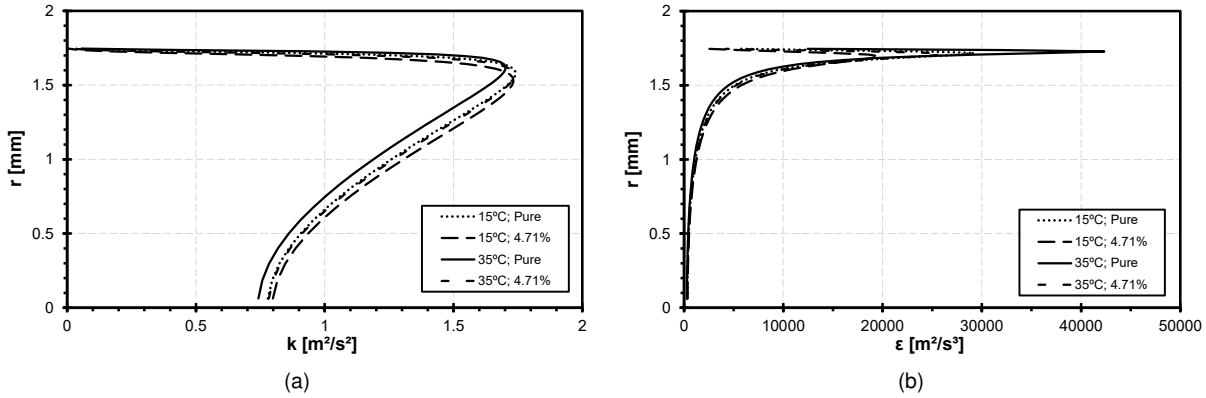

Figure 4.8: Radial profiles of (a) turbulent kinetic energy and (b) dissipation rate for several temperatures and particle loadings, conserving $\dot{m} = 0.1kg/s$ and $q'' = 20kW/m^2$.

relevant over inertial effects, promoting κ destruction. Such dissipation, associated to the smallest eddies, is more accentuated in zones where the mean velocity field has higher gradients, which explains its peak near the wall. Looking at the definition of ε

$$\varepsilon = 2\nu \mathbf{S} \cdot \mathbf{S} \tag{4.2}$$

it is observed its dependency on kinematic viscosity and, logically, on the magnitude of mean velocity gradients, represented here by the mean strain rate. Temperature contributes to increase ε, but since it has the opposite effect on the kinematic viscosity, ν, this improvement must be due to an augmented strain rate. Regarding particle addition, the effect is the opposite but the reasoning is the same. In fact, ν increases with particle concentration but ε decreases, as a direct consequence of a lower strain rate.

In conclusion, a larger strain rate, indicating sharper velocity gradients within the boundary layer, is synonym of a better thermal performance. Temperature promotes this effect, while the addition of nanoparticles do not, revealing poorer results on a $\dot{m}$ comparison basis. This outcome is further supported by figure 4.7 (b), which reveals that greater thermal loads have a positive effect on $\overline{h}$, for a constant $\dot{m}$. Higher q'' supplies more energy to the system, and therefore larger temperatures are reached. Since temperature has a positive effect on $\overline{h}$ as proved before, the observed raising tendency confirms

the expectations.

To close this section, Δp was also investigated in turbulent regime and the results can be seen in figure 4.9. Following the same methodology, several temperatures and particle loading were tested, keeping constant in (a) q'' and in (b) $\dot{m}$. If we compare these figures with those of the laminar test, we can notice that the evolution trends are the same, but the increase of Δp with $\dot{m}$ has not a linear shape. It can be explained looking at equation 2.23 and observing the quadratic dependence on u_m revealed by Δp. This, consequently, corresponds to a quadratic evolution of Δp with $\dot{m}$, which is closer to what is present in figure 4.9 (a) than the linear growing rate hypothesis.

These observations might indicate that the phenomena ruling pressure losses are the same, independently of the flow regime, and in fact they are. Even though in presence of turbulence, pressure losses are still related with wall friction, which continues to be ruled by the molecular viscosity effects. This can be proven considering that wall friction occurs within the viscous sub-layer of a turbulent boundary layer, where viscous dissipation is dominant over turbulent motion. Thus, Δp continues being ruled by the variation of the molecular viscosity and therefore, the discussion presented in section 4.3.1 concerning this topic remains valid.

Comparatively to the base fluid, a lower relative penalty due to particles addition was noticed, with no more than 17% augmentation of Δp for the smallest $\dot{m}$ and around 10% when the largest ones are considered, independently of the temperature set.

4.4 Influence of the comparison basis

In the previous section we saw how each controlling parameter affected, separately, the heat transfer performance and the pressure losses of the system. But those influences, if looked through other perspectives, can mean different things. This is basically what was said in the end of section 1.2.2 about the variety of comparison basis used to evaluate nanofluid performances and the influence that they had on possible final conclusions. A particular example of this problem is, for instance, to evaluate the impact in $\overline{h}$ by changing $\dot{m}$ through three different comparison basis: mean velocity, Reynolds number and pumping power required. Using the same data presented before appropriately transformed to the referred comparison basis, the aim of this section is to identify the ideal conditions in which a basis should be selected and what conclusions could be taken, misleading or not, from their use.

4.4.1 Mean velocity

From the mass flow rate it is easy to obtain our first comparison basis: the mean velocity. Looking at equation 2.18, the only quantity which is sensible to T and ω variation is the density, ρ, so it is through this quantity that some variation will be introduced. It is known that ρ reduces for higher T but increases as more particles are added, which implies opposite effects on the velocity, for a given $\dot{m}$. However, as ρ does not change much in the range of T and ω studied, we expect that mean velocities exhibit a small variation range, for an equal $\dot{m}$.

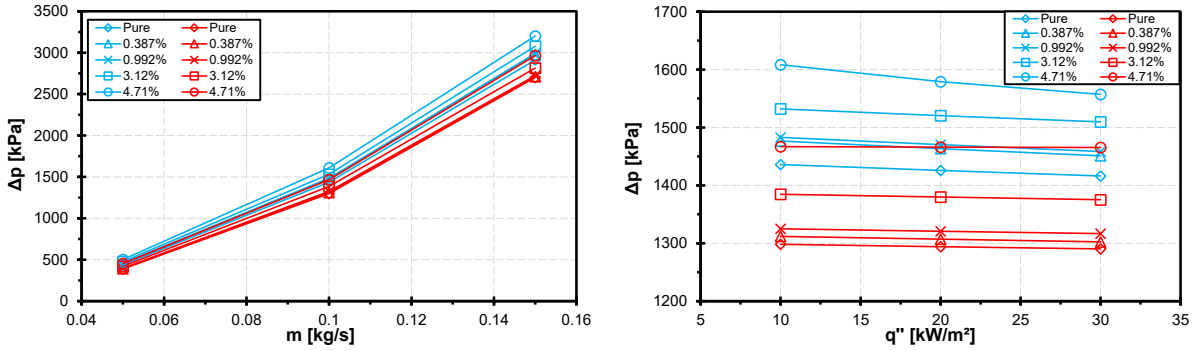

Figure 4.9: Influence of (a) mass flow rate ($q'' = 10kW/m^2$) and (b) wall heat flux ($\dot{m} = 0.1kg/s$) on pressure drop, for turbulent flow conditions. Blue data - $T_{in} = 15^oC$; Red data - $T_{in} = 35^oC$.

Data presented in section 4.3 were plotted according to what was explained before and is now available in figure 4.10, for both flow regimes and the same temperatures and particle loadings. The comparison with the corresponding charts in section 4.3 shows that no significant differences exist between the two considered basis. The trends are quite similar as expected, with exception to the laminar case, where the small reduction in velocity due to ω allows a slight separation among the ω-constant lines of each temperate that can be seen as an enhancement. Still, one should be aware that, for a constant velocity basis, we are not considering equal mass flow rates.

4.4.2 Reynolds number

Due to its popularity in the fluid dynamics field, Re is a very appreciated basis used to compare nanofluids' performance. However, when comparing two nanofluid flows with equal Re, we are ignoring the effect of nanoparticles on the thermal properties, which led to a comparison between two totally distinct dynamics. This was, basically, what led Yu et al. [17], in their review work, to advise against the use of Re as a comparative basis in nanofluid's research. Still, we continue interested in investigate its use, since we would like to evaluate the conclusions it allows us to draw.

To adapt the data produced before to a constant Re comparison basis, we need to relate $\dot{m}$ to Re values. This is achieved through the use of following expression

$$Re = \frac{4\dot{m}}{\pi\mu D} \tag{4.3}$$

By looking at equation 4.3, it is easy to conclude that the T and ω variation will affect Re by the way they influence μ, for a case of constant $\dot{m}$. Considering this, Re will rise as long as T increases and decreases if more particles are added. By definition, Re is seen as the ratio of inertia to viscous forces and, since a constant flow rate is considered, no alteration on inertia forces was introduced. Viscous forces, in its turn, are totally dependent on μ magnitude, so they will change in consonance with μ variation, being then reduced as T increases and powered as ω rises. This justifies the way Re reacts to these two important variables.

Results for a constant Re comparison basis are available in figure 4.11 for every temperature and

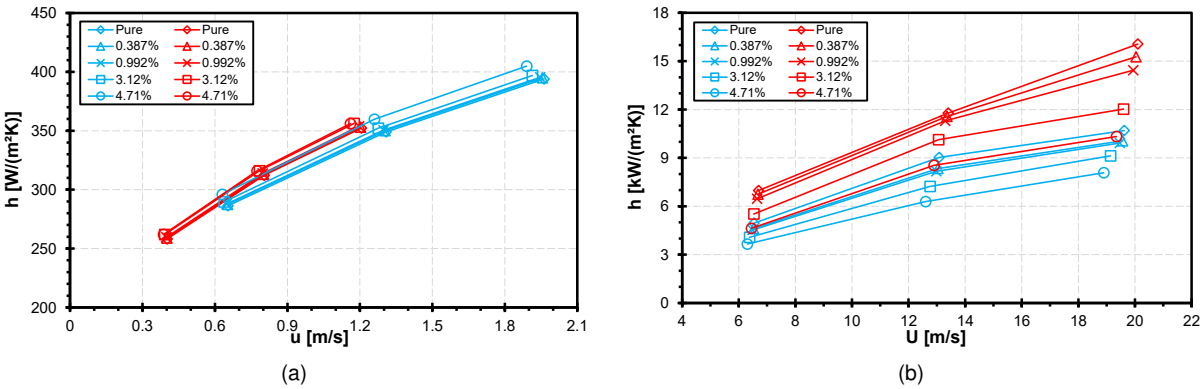

Figure 4.10: Average heat transfer coefficient compared under constant mean velocity basis. (a) laminar and (b) turbulent flow conditions.

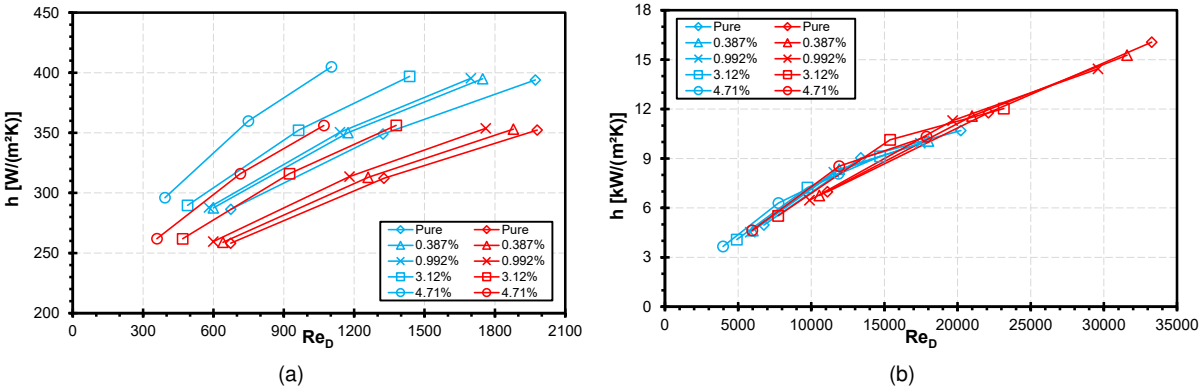

Figure 4.11: Average heat transfer coefficient compared under constant Reynolds number basis. (a) laminar and (b) turbulent flow conditions.

particle loading considered during this study. Taking into account the substantial Re variation along the tube length due to temperature, each test was characterized by a computed Re based on thermal properties evaluated at an average *fluid temperature*, T_f, given by

$$T_f = \frac{T_{m,in} + T_{m,out}}{2} \tag{4.4}$$

Comparing the laminar predictions of figure 4.11 with those presented before for other comparison basis, some differences are clearly noticed. The first one that goes against what was previously concluded is that $\overline{h}$ is enhanced by a temperature reduction. This happens because μ is powered by a temperature decrease, and equation 4.3 shows that keeping the same Re will only be achieved thanks to a $\dot{m}$ augmentation. Considering that for $T_{in} = 15^{o}C$ the $\dot{m}$ are in fact higher than for $T_{in} = 35^{o}C$, this $\overline{h}$ enhancement of about 10 to 14% in comparison with the base fluid and is in fact a consequence $\dot{m}$ augmentation rather than T reduction.

For a constant T and $\dot{m}$, Re is significantly reduced when ω is augmented from 0% to 4.71%, reaching almost half of its initial value for the largest ω. What succeeds is that such reduction allows a separation of the ω-constant lines, which reflects a supposed improvement of $\overline{h}$. For $\omega = 4.71\%$ and considering the same Re, an enhancement superior to 20% in $\overline{h}$ was verified when compared to the base fluid. This

suggests that a nanofluid is prone to have a superior thermal performance as long as it contains more nanoparticles, which was already proved in section 4.3.1 but in totally different proportions. Moreover, these qualitative improvement tendencies agree with the majority of the laminar investigations given in section 1.3, where both Re and ω were identified as sources of improvement for $\overline{h}$ for several nanofluids, and also with [61], confirming what has been presented and discussed until now.

Figure 4.11 (b) exhibits the results of this comparative study concerning turbulent regime. In line with laminar observations, they do not present the same trends seen before in section 4.3, demonstrating one more time the influence that a comparison basis could have. Both temperature and particle concentration affect Re in turbulent regime as they do in laminar and the discussion presented in the previous paragraphs regarding that remains valid. So, looking to the figure, we see overlapped data, indicating that from a constant Re point of view, there is no great influence on the heat transfer coefficient either from temperature or particle addition. This contrasts with the information presented before since it indicated a clear deterioration of the thermal performance mainly due to nanoparticles in turbulent regime, while this one simply indicates they do are neither beneficial nor unfavorable.

Trying to find a justification for such fact, we searched on the literature some possible examples where other researchers got similar results regarding Al_2O_3 nanofluids. We found that not many teams looked directly to h as a function of Re. Instead, they prefer to plot Nu vs. Re, like [43]. However, we found that [39] reported enhancements on h vs. Re when more particles were added. In fact, both teams announced improvements regarding nanoparticles addition, but they have studied particle concentrations up to 6% in volume. Comparing with our highest mass fraction, $\omega = 4.71\%$, which barely means 1% in volume, it gives the idea that for such small quantities of added particles, any possibly enhancement goes unnoticed. This is also corroborated by the study of [35] which used concentrations up to 0.9% in volume and reported no significant enhancement verified. If we compare this evidence with those from [61], it qualitatively agrees well for the smallest ω, but not for the largest ones, for which they reported enhancements. Nevertheless, this disagreement was expected since our model cannot match some experimental measurements, as seen in section 4.2.1.

Δp was also investigated under constant Re basis in order to perform a qualitative comparison with the data available in [61]. Figure 4.12 shows that, for the same Re, Δp more than doubled for $15^{\circ}C$ in comparison to $35^{\circ}C$. This augmentation has to do with the increased μ and $\dot{m}$ for smaller temperatures. The increase with Re satisfies the $\Delta p(\dot{m})$ trends found in section 4.3, being the growing rate sharper for higher particle concentrations. Since Re is a quotient, the relative variations of μ are much more accentuated in a Re basis than in a $\dot{m}$ one, reason why the ω-constant lines are more distant here than in figures 4.6 and 4.9. The sharper slopes verified and barely quadratic curves from turbulent data relatively to the linear laminar data seemed to be in good qualitative agreement with the plots of [61].

4.4.3 Pumping power

Recognized in [17] as the "most conservative criteria for a beneficial nanofluid" evaluation, the constant pumping power comparison basis allow us to measure how much energy we have to supply while pump-

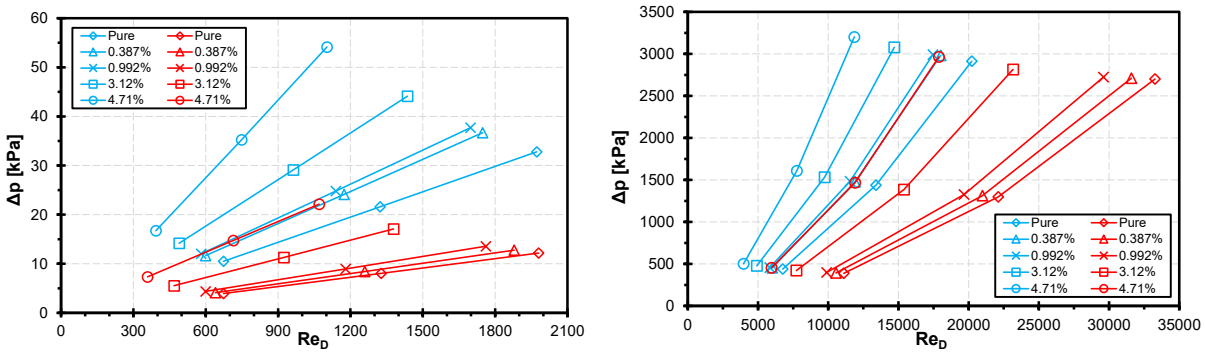

Figure 4.12: Pressure drop compared under constant Reynolds number basis. (a) laminar and (b) turbulent flow conditions.

ing a more viscous nanofluid. Therefore, the intention of this comparison basis is to understand if the additional cost of pumping a nanofluid worths to be paid or not.

The power required to pump the fluid is given by the the following relation

$$P_{pump} = \frac{\dot{m}\Delta p}{\rho} \tag{4.5}$$

and it represents the energy per unit time that a pump must supply to the fluid in order to move it along the system. Results for this comparison are displayed in figure 4.13. Imagining we have a fixed amount of power available (for instance through the use of the same pump independently of the fluid), the best thermal performance is always achieved by the base fluid. This happens due to a smaller $\dot{m}$ that is possible to pump when more nanoparticles are added to the base fluid because of the increased viscous effects. Higher temperatures promote the thermal performance from this point of view due to its viscosity reducing effect, allowing to pump a greater $\dot{m}$ compared to a colder fluid.

It is also interesting as well is to see that the greatest improvement in $\overline{h}$ is achieved in virtue of a small pumping power increase, being this rate shortened as long as higher $\overline{h}$ were required. This means that if we intend the same heat transfer rates for different particle concentrations, we have to supply much more energy to the system in the cases where higher particle loadings are involved.

To conclude, the pumping power magnitude for laminar flow is so reduced that in most cases it is definitely worth to pay around 40% more energy pumping the fluid. For turbulent flow, the amounts involved are definitely higher. Still, it is not worth to pay it, since no improvement in thermal performance is attained in turbulent conditions.

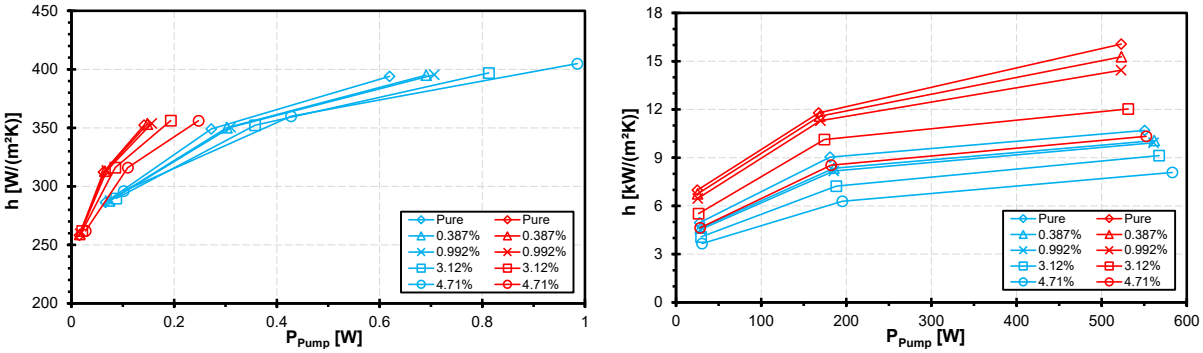

Figure 4.13: Average heat transfer coefficient compared under constant pumping power basis. (a) laminar and (b) turbulent flow conditions.

Chapter 5

Conclusions

5.1 Main achievements

The main motivation supporting this work was to provide a numerical tool able to accurately predict the thermal performance and the hydrodynamic characteristics reported by [61] of an Al_2O_3-isopropanol flow. To attain our objective, in virtue of the nonexistence of a general theory about nanofluids, they have to be modeled using current techniques. The simplest way available to model the flow using CFD was proposed here: assume a nanofluid as a single-phase fluid with altered properties. Some other assumptions were also used to support this major one, as described in section 2.1, but what is implicit here is that the possible success of this work would corroborate the good approximation level of these assumptions about nanofluids behavior, something that has been already noticed in [17] and more recently in [18]. So, this thesis has not only a comparative nature, but a confirmatory one too.

The performance of the CFD model regarding laminar flow conditions is very good. The measured local convective heat transfer coefficients (CHTCs) always exhibited a tendency to be superior to their respective predictions, still they do not deviate more that 10% in majority, if we consider the average CHTC. This percentage increases to 15% if local CHTC were contemplated. Predictions of the friction factor follow perfectly the theoretical and experimental trends, independently from the temperature set, proving the nanofluid Newtonian dynamics.

During the sensitivity tests, it was noticed a stronger influence of the mass flow rate than the thermal load on heat transfer performance enhancement. Also, the inlet temperature was a source of improvement, as well as particle mass fraction. However, the improvement due to the increase of the particle mass fraction was barely noticed. For a constant mass flow rate, a maximum 3% enhancement was verified for a nanofluid at $15^{o}C$ and loaded with 4.71% in mass, in comparison to its base fluid.

For turbulent flow conditions, the match between predicted and measured data was not so good. Some experimental data expressed trends that were not replicated in the predicted local CHTC. Overestimations were mostly found for the lower temperatures considered, while under-predictions appeared among the high temperature cases, where the longest discrepancies have been found. In the worst case, a predicted wall temperature 1.2^{o}C higher than the respective measurement gave rise to a local

CHTC around 30% smaller than the experimental value. Still, the majority of the simulation led to local and average CHTCs among a 20% error margin relatively to its measured value. We found that the trends presented on local CHTC measurements were the same already seen when the local Nu was studied for the base fluid during the model validation, as well as the type of discrepancies verified. This fact suggests that such differences were not directly caused by the presence of nanoparticles in the flow.

The computed friction factor in turbulent conditions was always higher than the measured ones, particularly for the smallest Re. With Re augmentation, the flow tends to be in a fully developed turbulence regime and the model predicts f in better agreement with theory and experiments, confirming the conviction that turbulence models do not perform so well for developing turbulence conditions.

The sensitive analysis for turbulent flow conditions revealed one more time the mass flow rate increase as the best way to promote the heat transfer performance of the system. Temperature and the thermal load were also seen as improvement sources, but the most important conclusion is the deterioration of CHTC with particle addition. This is totally the opposite of what was desired and represents a clear drawback against the use of this nanofluid in turbulent conditions. For the maximum particle loading simulated, decreases in the order of 30% have been found for both temperatures studied, for a given mass flow rate.

On the other hand, by analyzing the turbulent flow quantities, we found that the best thermal performance was achieved for the highest dissipation rate. Such optimal conditions are attained when the mean velocity gradients reach their highest value in the turbulent boundary layer. From the turbulence theory, these mean velocity gradients are responsible for supplying the energy necessary to the production of turbulence and, consequently, to promote turbulent transport. So, the more turbulence produced, the better the thermal performance and, while temperature promotes this phenomenon, the addition of nanoparticles has a negative contribution on it. This conclusion is corroborated by the reduced degree of turbulence reported by [61] regarding the nanoparticles effect on CHTC in turbulent flow conditions.

The pressure drop depends on the fluid viscosity in both flow regimes and the way temperature and particle concentration affect it is reflected in terms of pressure losses. The addition of nanoparticles promoted pressure drop from 60% to 80% in laminar regime, being these values reduced to between 17% - 10% for turbulent conditions, in spite of the much higher magnitudes involved.

The influence of different comparison basis on the interpretation of the results was also addressed. The constant velocity basis was the one that allows the closer agreement with the conclusions taken via constant mass flow rate comparison. Since between the two bases there is only the influence of density, both produce almost indistinguishable results. Expected results were also found for a constant pumping power basis. If more particles are added to the fluid, more energy is required to pump it and reach the same thermal performance, due to the viscosity increase. For the cases where the pumping power is a constraint of the project, the designer must do this comparison to estimate how much energy will cost the possible enhancement of CHTC, specially for turbulent flow conditions.

The most controversial results came from the constant Re comparison basis analysis, reflecting trends unseen until here. Contrarily to what was proved before, the enhancements due to particles addition appear in a much larger proportion for constant Re than for constant mass flow rate or constant

velocity bases, and higher temperatures do not produce any beneficial effect. The aforementioned conclusions came essentially from the fact that an equal Re computed for flows with different temperatures and particle concentrations simply ensures the same ratio of inertia to viscous forces among themselves, and not the same dynamic conditions, since a viscosity variation imposed by exterior factors will imply a velocity change too. For turbulent flow conditions, constant Re basis has revealed a curious insensitivity of the CHTC on temperature and particle concentration variations, clearly contrasting with the decrease of CHTC observed through the remaining comparison bases powered by particles addition, and the favorable effect of temperature augmentation.

In conclusion, the model performs well while predicting the heat transfer conditions of a laminar Al_2O_3-isopropanol flow, as demonstrated by the good match between predictions and experimental data. Based on that, we can confirm that this nanofluid follows very well the hypothesis of being correctly represented as a homogeneous fluid with altered properties. Predictions for turbulent flow revealed an inferior degree of agreement in relation to laminar case, still the differences in the majority of simulations were kept within an acceptable error level, validating the hypothesis when turbulence is present, as well.

Improvements in CHTC directly related to Al_2O_3 nanoparticles addition were only found in laminar flow conditions. However, those percentages are quite small and possibly do not justify their use replacing the base fluid alone, since their manufacture requires additional economical effort and they might suffer from long stability problems. Even though, if these are considered minor problems, as well as the extra pumping power, it is possible to attain a better performance using this nanofluid in laminar forced convection applications. Nevertheless, one should not blindly trust on the quantification of the enhancements resultant from a constant Re comparison basis, since the realities compared are not really the same. No advantage was seen from the use of Al_2O_3-isopropanol nanofluids in turbulent flow conditions.

5.2 Suggestions for future work

During this work we noted that the highest particle mass fraction considered, $\omega = 4.71\%$, represents in fact a particle volume concentration, $\phi \approx 1\%$, which compared to other studies available, is manifestly low. Also the Re variation range of this study was quite limited, all within the turbulence developing zone. Based on that, we suggest that higher particle quantities could be considered in future experimental studies, as well as larger mass flow rates, in order to investigate possible and higher enhancements due to particles addition and to provide a vaster characterization of this nanofluid, at least for turbulent flow conditions.

About the numerical aspect of nanofluids investigation, it seems always interesting when an introductory work like ours, based on the homogeneous fluid approach, could be compared with other where the interaction of solid and fluid particles is separately modeled in a two-phase approach. Also an improved turbulence model might be tested, so it could improve the pressure drop predictions.

Bibliography

[1] World Energy Outlook 2017. International Energy Agency. https://www.iea.org/weo2017/#section-6, last access in October 2018.

[2] A. E. Bergles. ExHFT for fourth generation heat transfer technology. *Experimental Thermal and Fluid Science*, 26:335–344, 2002. PII: S08 9 4-1 7 77(02)001 4 5- 0.

[3] S. U. S. Choi and J. Eastman. Enhancing thermal conductivity of fluids with nanoparticles. In *Proceedings of the ASME International Mechanical Engineering Congress and Exposition*, volume 66, January 1995.

[4] W. Yu, D. M. France, J. L. Routbort, and S. U. S. Choi. Review and comparison of nanofluid thermal conductivity and heat transfer enhancements. *Heat Transfer Engineering*, 29(5):432–460, 2008. doi: 10.1080/01457630701850851.

[5] A. K. Sharma, A. K. Tiwari, and A. R. Dixit. Rheological behaviour of nanofluids: A review. *Renewable and Sustainable Energy Reviews*, 53:779–791, January 2016. doi: 10.1016/j.rser.2015.09.033.

[6] A. Ghadimi, R. Saidur, and H. S. C. Metselaar. A review of nanofluid stability properties and characterization in stationary conditions. *International Journal of Heat and Mass Transfer*, 54:4051–4068, August 2011. doi:10.1016/j.ijheatmasstransfer.2011.04.014.

[7] W. Yu and H. Xie. A review on nanofluids: Preparation, stability mechanisms, and applications. *Journal of Nanomaterials*, Volume 2012:17 pages, 2012. doi:10.1155/2012/435873.

[8] K. H. Solangi, S. N. Kazi, M. R. Luhur, A. Badarudin, A. Amiri, R. Sadri, M. N. M. Zubir, S. Gharahkhani, and K. Teng. A comprehensive review of thermo-physical properties and convective heat transfer to nanofluids. *Energy*, 89:1065–1086, September 2015. doi: 10.1016/j.energy.2015.06.105.

[9] S. Kakaç and A. Pramuanjaroenkij. Review of convective heat transfer enhancement with nanofluids. *International Journal of Heat and Mass Transfer*, 52:3187–3196, June 2009. doi:10.1016/j.ijheatmasstransfer.2009.02.006.

[10] J. Fan and L. Wang. Review of heat conduction in nanofluids. *Journal of Heat Transfer*, 133, April 2011. doi: 10.1115/1.4002633.

[11] J. A. Eastman, S. R. Phillpot, S. U. S. Choi, and P. Keblinski. Thermal transport in nanofluids. *Annu. Rev. Mater. Res.*, 34:219–46, March 2004. doi: 10.1146/annurev.matsci.34.052803.090621.

[12] W. Yu, D. M. France, D. Singh, E. V. Timofeeva, D. S. Smith, and J. L. Routbort. Mechanisms and models of effective thermal conductivities of nanofluids. *Journal of Nanoscience and Nanotechnology*, 10:4824–4849, 2010. doi:10.1166/jnn.2010.2413.

[13] J. J. Wang, R. T. Zheng, J. W. Gao, and G. Chen. Heat conduction mechanisms in nanofluids and suspensions. *Nano Today*, 7:124–136, 2012. doi:10.1016/j.nantod.2012.02.007.

[14] J. Buongiorno. Convective transport in nanofluids. *Journal of Heat Transfer*, 128, March 2006. doi: 10.1115/1.2150834.

[15] X.-Q. Wang and A. S. Mujumdar. A review on nanofluids - part i: Theoretical and numerical investigations. *Brazilian Journal of Chemical Engineering*, 25(04):613 – 630, 2008. ISSN 0104-6632.

[16] S. Kakaç and A. Pramuanjaroenkij. Single-phase and two-phase treatments of convective heat transfer enhancement with nanofluids - a state-of-the-art review. *International Journal of Thermal Sciences*, 100:75–97, February 2016. doi: 10.1016/j.ijthermalsci.2015.09.021.

[17] W. Yu, D. M. France, E. V. Timofeeva, D. Singh, and J. L. Routbort. Comparative review of turbulent heat transfer of nanofluids. *International Journal of Heat and Mass Transfer*, 55:5380–5396, October 2012. doi: 10.1016/j.ijheatmasstransfer.2012.06.034.

[18] M. Buschmann, R. Azizian, T. Kempe, J. Juliá, R. Martínez-Cuenca, B. Sundén, Z. Wu, A. Seppälä, and T. Ala-Nissila. Correct interpretation of nanofluid convective heat transfer. *International Journal of Thermal Sciences*, 129:504–531, July 2018. doi: 10.1016/j.ijthermalsci.2017.11.003.

[19] M. Bahiraei. A comprehensive review on different numerical approaches for simulation in nanofluids: Traditional and novel techniques. *Journal of Dispersion Science and Technology*, 35(7):984–996, 2014. doi: 10.1080/01932691.2013.825210.

[20] S. M. Vanaki, P. Ganesan, and H. A. Mohammed. Numerical study of convective heat transfer of nanofluids: A review. *Renewable and Sustainable Energy Reviews*, 54:1212–1239, February 2016. do: 10.1016/j.rser.2015.10.042.

[21] Y. Xuan and W. Roetzel. Conceptions for heat transfer correlation of nanofluids. *International Journal of Heat and Mass Transfer*, 43:3701–3707, 2000. PII: S00 1 7- 93 1 0(99)0 03 6 9- 5.

[22] *ANSYS Fluent Theory Guide, Release 18.0*. ANSYS, Inc., January 2017.

[23] Y. Xuan and Z. Yao. Lattice boltzmann model for nanofluids. *Heat Mass Transfer*, 41:199–205, 2005. doi: 10.1007/s00231-004-0539-z.

[24] B. C. Pak and Y. I. Cho. Hydrodynamic and heat transfer study of dispersed fluids with submicron metallic oxide particles. *Experimental Heat Transfer*, 11:151–170, April 1998. doi: 10.1080/08916159808946559.

[25] Y. Xuan and Q. Li. Investigation on convective heat transfer and flow features of nanofluids. *Journal of Heat Transfer*, 125:151–155, February 2003. doi: 10.1115/1.1532008.

[26] D. Kim, Y. Kwon, Y. Cho, C. Li, S. Cheong, Y. Hwang, J. Lee, D. Hong, and S. Moon. Convective heat transfer characteristics of nanofluids under laminar and turbulent flow conditions. *Current Applied Physics*, 9:119–123, 2009. doi:10.1016/j.cap.2008.12.047.

[27] W. H. Azmi, K. V. Sharma, P. K. Sarma, R. Mamat, and G. Najafi. Heat transfer and friction factor of water based TiO_2 and SiO_2 nanofluids under turbulent flow in a tube. *International Communications in Heat and Mass Transfer*, 59:30–38, December 2014. doi: 10.1016/j.icheatmasstransfer.2014.10.007.

[28] R. Martínez-Cuenca, R. Mondragón, L. Hernández, C. Segarra, J. C. Jarque, T. Hibiki, and J. E. Juliá. Forced-convective heat-transfer coefficient and pressure drop of water-based nanofluids in a horizontal pipe. *Applied Thermal Engineering*, 98:841–849, April 2016. doi: 10.1016/j.applthermaleng.2015.11.050.

[29] R. B. Mansour, N. Galanis, and C. T. Nguyen. Effect of uncertainties in physical properties on forced convection heat transfer with nanofluids. *Applied Thermal Engineering*, 27:240–249, January 2007. doi:10.1016/j.applthermaleng.2006.04.011.

[30] W. Duangthongsuk and S. Wongwises. Effect of thermophysical properties models on the predicting of the convective heat transfer coefficient for low concentration nanofluid. *International Communications in Heat and Mass Transfer*, 35:1320–1326, December 2008. doi:10.1016/j.icheatmasstransfer.2008.07.015.

[31] D. Wen and Y. Ding. Experimental investigation into convective heat transfer of nanofluids at the entrance region under laminar flow conditions. *International Journal of Heat and Mass Transfer*, 47: 5181–5188, 2004. doi:10.1016/j.ijheatmasstransfer.2004.07.012.

[32] W. Y. Lai, B. Duculescu, P. E. Phelan, and R. Prasher. Convective heat transfer with nanofluids in a single 1.02-mm tube. In *Proceedings of the ASME International Mechanical Engineering Congress and Exposition*, 2006.

[33] K. S. Hwang, S. P. Jang, and S. U. S. Choi. Flow and convective heat transfer characteristics of water-based Al_2O_3 nanofluids in fully developed laminar flow regime. *International Journal of Heat and Mass Transfer*, 52:193–199, January 2009. doi: 10.1016/j.ijheatmasstransfer.2008.06.032.

[34] B. Ilhan and H. Ertürk. Experimental characterization of laminar forced convection of hbn-water nanofluid in circular pipe. *International Journal of Heat and Mass Transfer*, 111:500–507, August 2017. doi: 10.1016/j.ijheatmasstransfer.2017.03.040.

[35] W. Williams, J. Buongiorno, and L.-W. Hu. Experimental investigation of turbulent convective heat transfer and pressure loss of alumina/water and zirconia/water nanoparticle colloids (nanofluids) in horizontal tubes. *Journal of Heat Transfer*, 130(042412), April 2008. doi: 10.1115/1.2818775.

[36] M. Piratheepan and T. N. Anderson. An experimental investigation of turbulent forced convection heat transfer by a multi-walled carbon-nanotube nanofluid. *International Communications in Heat and Mass Transfer*, 57:286–290, October 2014. doi: 10.1016/j.icheatmasstransfer.2014.08.010.

[37] S. E. B. Maïga, C. T. Nguyen, N. Galanis, and G. Roy. Heat transfer behaviours of nanofluids in a uniformly heated tube. *Superlattices and Microstructures*, 35:543–557, 2004. doi: 10.1016/j.spmi.2003.09.012.

[38] S. E. B. Maïga, S. J. Palm, C. T. Nguyen, N. Galanis, and G. Roy. Heat transfer enhancement by using nanofluids in forced convection flows. *International Journal of Heat and Fluid Flow*, 26: 530–546, 2005. doi: 10.1016/j.ijheatfluidflow.2005.02.004.

[39] P. K. Namburu, D. K. Das, K. M. Tanguturi, and R. S. Vajjha. Numerical study of turbulent flow and heat transfer characteristics of nanofluids considering variable properties. *International Journal of Thermal Sciences*, 48:290–302, 2009. doi: 10.1016/j.ijthermalsci.2008.01.001.

[40] Y. He, Y. Men, Y. Zhao, H. Lu, and Y. Ding. Numerical investigation into the convective heat transfer of TiO_2 nanofluids flowing through a straight tube under the laminar flow conditions. *Applied Thermal Engineering*, 29:1965–1972, July 2009. doi: 10.1016/j.applthermaleng.2008.09.020.

[41] V. Bianco, F. Chiacchio, O. Manca, and S. Nardini. Numerical investigation of nanofluids forced convection in circular tubes. *Applied Thermal Engineering*, 29:3632–3642, July 2009. doi: 10.1016/j.applthermaleng.2009.06.019.

[42] V. Bianco, O. Manca, and S. Nardini. Numerical investigation on nanofluids turbulent convection heat transfer inside a circular tube. *International Journal of Thermal Sciences*, 50:341–349, March 2011. doi: 10.1016/j.ijthermalsci.2010.03.008.

[43] G. Saha and M. C. Paul. Numerical analysis of the heat transfer behaviour of water based Al_2O_3 and TiO_2 nanofluids in a circular pipe under the turbulent flow condition. *International Communications in Heat and Mass Transfer*, 56:96–108, August 2014. doi: 10.1016/j.icheatmasstransfer.2014.06.008.

[44] E. Sadeghinezhad, H. Togun, M. Mehrali, P. S. Nejad, S. T. Latibari, T. Abdulrazzaq, S. N. Kazi, and H. S. C. Metselaar. An experimental and numerical investigation of heat transfer enhancement for graphene nanoplatelets nanofluids in turbulent flow conditions. *International Journal of Heat and Mass Transfer*, 81:41–51, February 2015. doi: 10.1016/j.ijheatmasstransfer.2014.10.006.

[45] R. Saidur, K. Y. Leong, and H. A. Mohammad. A review on applications and challenges of nanofluids. *Renewable and Sustainable Energy Reviews*, 15:1646–1668, April 2011. doi: 10.1016/j.rser.2010.11.035.

[46] R. Taylor, S. Coulombe, T. Otanicar, P. Phelan, A. Gunawan, W. Lv, G. Rosengarten, R. Prasher, and H. Tyagi. Small particles, big impacts: A review of the diverse applications of nanofluids. *Journal of Applied Physics*, 113, 2013. doi: 10.1063/1.4754271.

[47] S. M. S. Murshed and C. A. N. de Castro. A critical review of traditional and emerging techniques and fluids for electronics cooling. *Renewable and Sustainable Energy Reviews*, 78:821–833, October 2017. doi: 10.1016/j.rser.2017.04.112.

[48] J. Qu, H. ying Wu, and P. Cheng. Thermal performance of an oscillating heat pipe with Al_2O_3 and TiO_2–water nanofluids. *International Communications in Heat and Mass Transfer*, 37:111–115, February 2010. doi: 10.1016/j.icheatmasstransfer.2009.10.001.

[49] K. H. Do, H. J. Ha, and S. P. Jang. Thermal resistance of screen mesh wick heat pipes using the water-based Al_2O_3 and TiO_2 nanofluids. *International Journal of Heat and Mass Transfer*, 53: 5888–5894, December 2010. doi: 10.1016/j.ijheatmasstransfer.2010.07.050.

[50] W. Escher, T. Brunschwiler, N. Shalkevich, A. Shalkevich, T. Burgi, B. Michel, and D. Poulikakos. On the cooling of electronics with nanofluids. *Journal of Heat Transfer*, 133, May 2011. doi: 10.1115/1.4003283.

[51] M. Kalteh, A. Abbassi, M. Saffar-Avval, A. Frijns, A. Darhuber, and J. Harting. Experimental and numerical investigation of nanofluid forced convection inside a wide microchannel heat sink. *Applied Thermal Engineering*, 36:260–268, April 2012. doi: 10.1016/j.applthermaleng.2011.10.023.

[52] C. T. Nguyen, G. Roy, C. Gauthier, and N. Galanis. Heat transfer enhancement using Al_2O_3 and TiO_2–water nanofluid for an electronic liquid cooling system. *Applied Thermal Engineering*, 27: 1501–1506, 2007. doi: 10.1016/j.applthermaleng.2006.09.028.

[53] M. Rafati, A. A. Hamidi, and M. S. Niaser. Application of nanofluids in computer cooling systems (heat transfer performance of nanofluids). *Applied Thermal Engineering*, 45-46:9–14, December 2012. doi: 10.1016/j.applthermaleng.2012.03.028.

[54] N. A. C. Sidik, M. N. A. W. M. Yazid, and R. Mamat. A review on the application of nanofluids in vehicle engine cooling system. *International Communications in Heat and Mass Transfer*, 68: 85–90, November 2015. doi: 10.1016/j.icheatmasstransfer.2015.08.017.

[55] S. Z. Heris, M. Shokrgozar, S. Poorpharhang, M. Shanbedi, and S. H. Noie. Experimental study of heat transfer of a car radiator with cuo/ethylene glycol-water as a coolant. *Journal of Dispersion Science and Technology*, 35(5):677–684, July 2013. doi: 10.1080/01932691.2013.805301.

[56] A. M. Hussein, R. A. Bakar, K. Kadirgama, and K. V. Sharma. Heat transfer enhancement using nanofluids in an automotive cooling system. *International Communications in Heat and Mass Transfer*, 53:195–202, April 2014. doi: 10.1016/j.icheatmasstransfer.2014.01.003.

[57] S. C. Tzeng, C. W. Lin, and K. D. Huang. Heat transfer enhancement of nanofluids in rotary blade coupling of four-wheel-drive vehicles. *Acta Mechanica*, 179:11–23, 2005. doi: 10.1007/s00707-005-0248-9.

[58] T. P. Otanicar, P. E. Phelan, and J. S. Golden. Optical properties of liquids for direct absorption solar thermal energy systems. *Solar Energy*, 83:969–977, 2009. doi: 10.1016/j.solener.2008.12.009.

[59] T. Otanicar, P. E. Phelan, R. S. Prasher, G. Rosengarten, and R. A. Taylor. Nanofluid-based direct absorption solar collector. *Journal of Renewable and Sustainable Energy*, 2(3), 2010. doi: 10.1063/1.3429737.

[60] O. Mahian, A. Kianifar, S. A. Kalogirou, I. Pop, and S. Wongwises. A review of the applications of nanofluids in solar energy. *International Journal of Heat and Mass Transfer*, 57:582–594, February 2013. doi: 10.1016/j.ijheatmasstransfer.2012.10.037.

[61] A. Nikulin, A. S. Moita, A. L. N. Moreira, S. M. S. Murshed, A. Huminic, Y. Grosu, A. Faik, J. Nieto-Maestre, and O. Khliyeva. Effect of Al_2O_3 nanoparticles on laminar, transient and turbulent flow of isopropyl alcohol. *International Journal of Heat and Mass Transfer*, 130:1032–1044, March 2019. doi: 10.1016/j.ijheatmasstransfer.2018.10.114.

[62] F. M. White. *Fluid Mechanics*. McGraw-Hill Education, 8th edition, 2016. ISBN: 978-0-07-339827-3.

[63] F. Moukalled, L. Mangani, and M. Darwish. *The Finite Volume Method in Computational Fluid Dynamics*. Springer, 2016. ISBN: 978-3-319-16873-9.

[64] T. G. Myers, H. Ribera, and V. Cregan. Does mathematics contribute to the nanofluid debate? *International Journal of Heat and Mass Transfer*, 111:279–288, August 2017. doi: 10.1016/j.ijheatmasstransfer.2017.03.118.

[65] T. L. Bergman, A. S. Lavine, F. P. Incropera, and D. P. Dewitt. *Fundamentals of Heat and Mass Transfer*. John Wiley & Sons, Inc., 7th edition, 2011. ISBN: 978-0470-50197-9.

[66] W. M. Kays and M. E. Crawford. *Convective Heat and Mass Transfer*. McGraw-Hill, Inc., 3rd edition, 1993. ISBN: 0-07-033721-7.

[67] A. Bejan. *Convection Heat Transfer*. John Wiley & Sons, Inc., 4th edition, 2013. ISBN: 978-0-470-90037-6.

[68] H. K. Versteeg and W. Malalasekera. *An Introduction to Computational Fluid Dynamics*. Pearson Education Limited, 2nd edition, 2007. ISBN: 978-0-13-127498-3.

[69] A. Nikulin. Personal communication. 2019.

[70] *ANSYS Fluent Customization Manual Guide, Release 18.0*. ANSYS, Inc., January 2017.

[71] S. V. Patankar. *Numerical Heat Transfer and Fluid Flow*. Hemisphere Publishing Corporation, 1980. ISBN: 0-89116-522-3.

[72] *ANSYS Fluent User's Guide, Release 18.1*. ANSYS, Inc., April 2017.

Appendix A

Data and temperature plots for figures 4.1 and 4.2

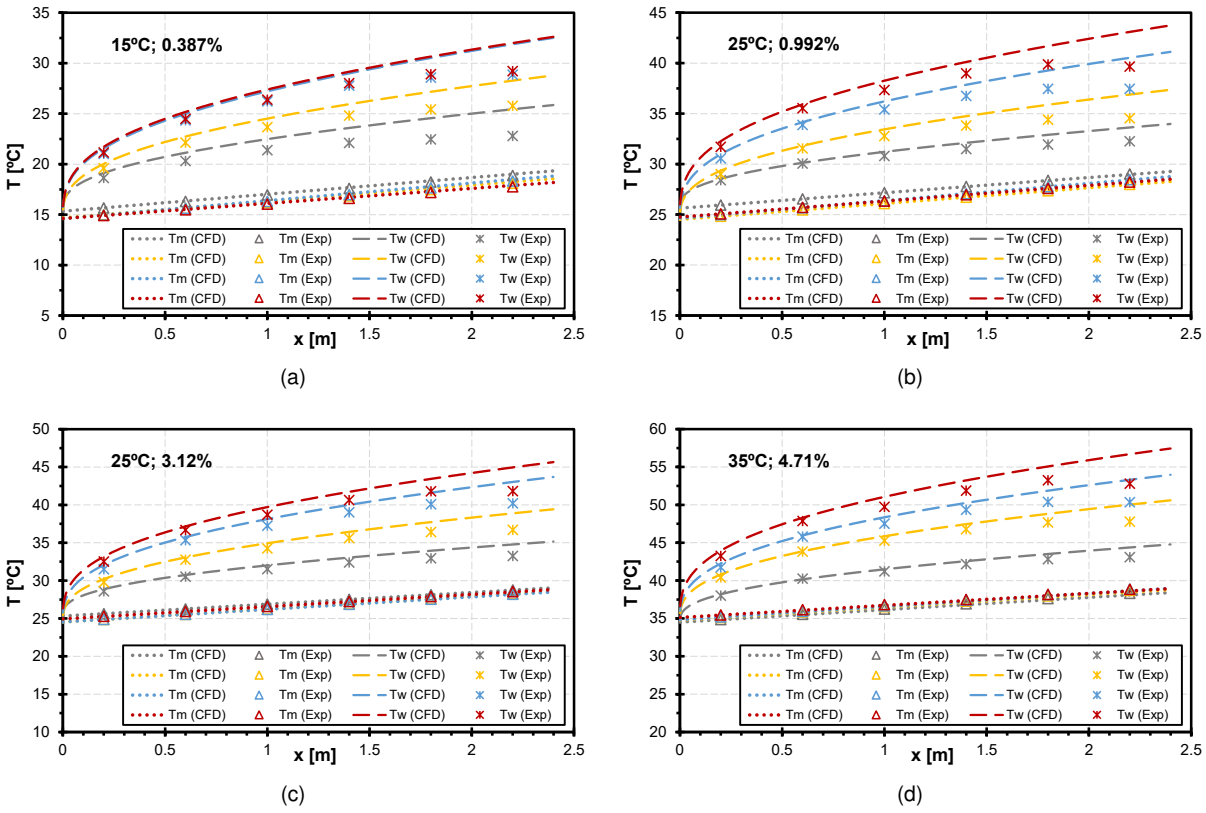

Figure A.1: Axial evolutions of T_m and T_w for the simulations presented in figure 4.1 (the color code is kept unaltered to allow a direct comparison with figure 4.1).

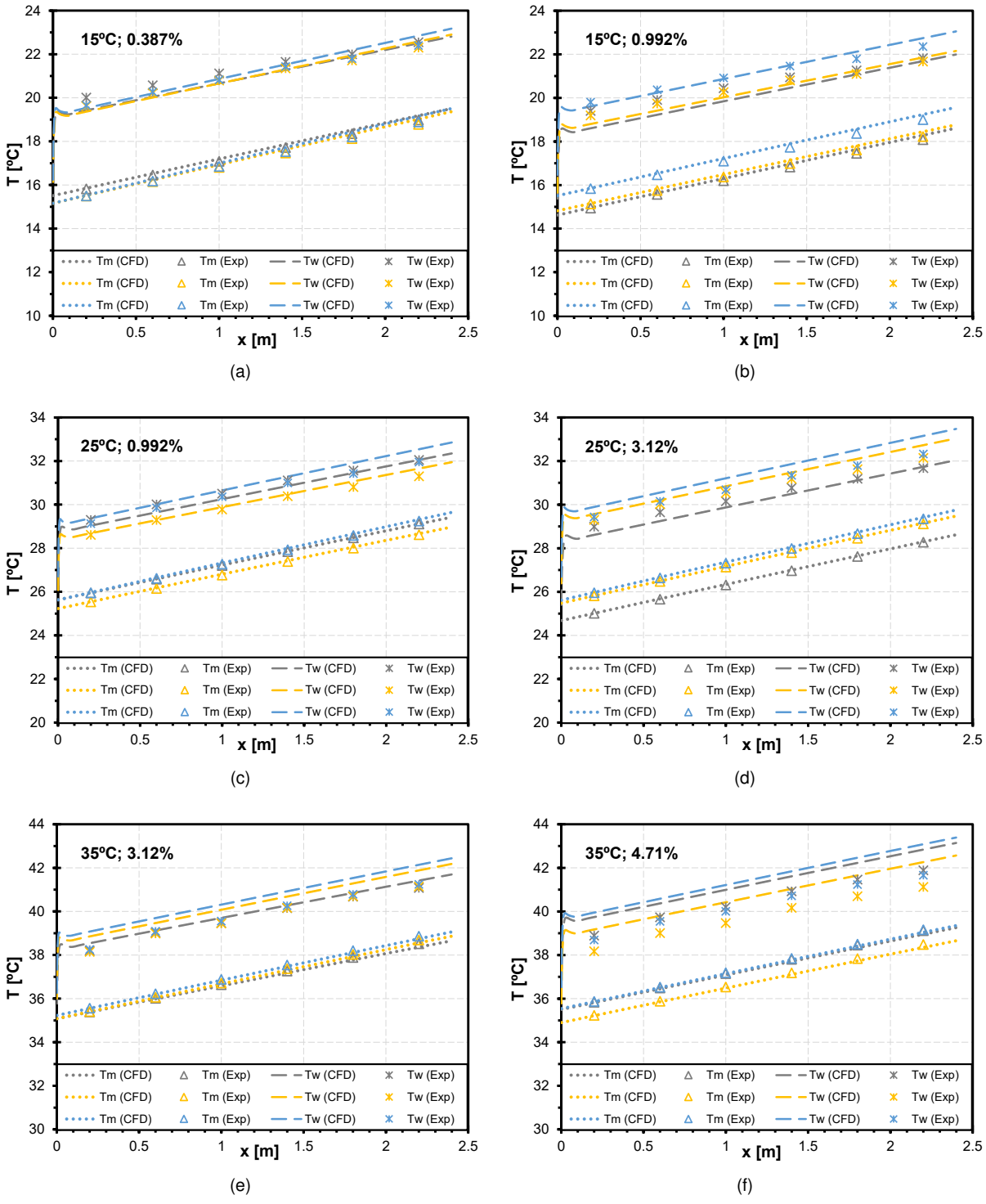

Figure A.2: Axial evolutions of T_m and T_w for the simulations presented in figure 4.2 (the color code is kept unaltered to allow a direct comparison with figure 4.2).

Table A.1: Data used for the simulations presented in figure 4.1 (the color identifies each case in each image of figure 4.1).

	Figure (a)			Figure (b)		
	T_{in} [ºC]	$\dot{m}$ $[kg/s]$	$q''[W/m^2]$	T_{in} [ºC]	$\dot{m}$ $[kg/s]$	$q''[W/m^2]$
$Gray$	15.34	0.00359	1303.91	25.63	0.00538	887.74
$Yellow$	14.68	0.00670	2350.21	24.52	0.00245	1991.16
$Blue$	14.62	0.00903	3433.09	24.64	0.00715	2924.89
$Dark\ red$	14.62	0.01226	3935.01	24.76	0.01098	4071.12
	Figure (c)			Figure (d)		
	T_{in} [ºC]	$\dot{m}$ $[kg/s]$	$q''[W/m^2]$	T_{in} [ºC]	$\dot{m}$ $[kg/s]$	$q''[W/m^2]$
$Gray$	25.32	0.00336	1225.17	34.51	0.00303	1257.81
$Yellow$	24.53	0.00637	2502.41	34.77	0.00631	2716.42
$Blue$	24.54	0.01041	4014.61	34.82	0.00843	3729.11
$Dark\ red$	24.95	0.01240	4695.60	35.13	0.01263	5148.81

Table A.2: Data used for the simulations presented in figure 4.2 (the color identifies each case in each image of figure 4.2).

	Figure (a)			Figure (b)		
	T_{in} [ºC]	$\dot{m}$ $[kg/s]$	$q''[W/m^2]$	T_{in} [ºC]	$\dot{m}$ $[kg/s]$	$q''[W/m^2]$
$Gray$	15.51	0.02542	9087.34	14.62	0.02447	8631.31
$Yellow$	15.17	0.03289	12234.42	14.82	0.02901	10075.06
$Blue$	15.16	0.03647	13980.99	15.51	0.03443	12286.87
	Figure (c)			Figure (d)		
	T_{in} [ºC]	$\dot{m}$ $[kg/s]$	$q''[W/m^2]$	T_{in} [ºC]	$\dot{m}$ $[kg/s]$	$q''[W/m^2]$
$Gray$	25.63	0.02094	7830.39	24.68	0.02140	8088.87
$Yellow$	25.23	0.02922	10635.46	25.48	0.02945	11296.88
$Blue$	25.63	0.03730	14508.63	25.62	0.03616	14258.52
	Figure (e)			Figure (f)		
	T_{in} [ºC]	$\dot{m}$ $[kg/s]$	$q''[W/m^2]$	T_{in} [ºC]	$\dot{m}$ $[kg/s]$	$q''[W/m^2]$
$Gray$	35.08	0.02093	7974.00	35.50	0.02437	9652.97
$Yellow$	35.08	0.02988	11965.76	34.90	0.02828	11066.15
$Blue$	35.23	0.03453	13940.09	35.54	0.03329	13233.31